Numerical Methods for Steady Viscous Free-Surface Flows

Harald van Brummelen

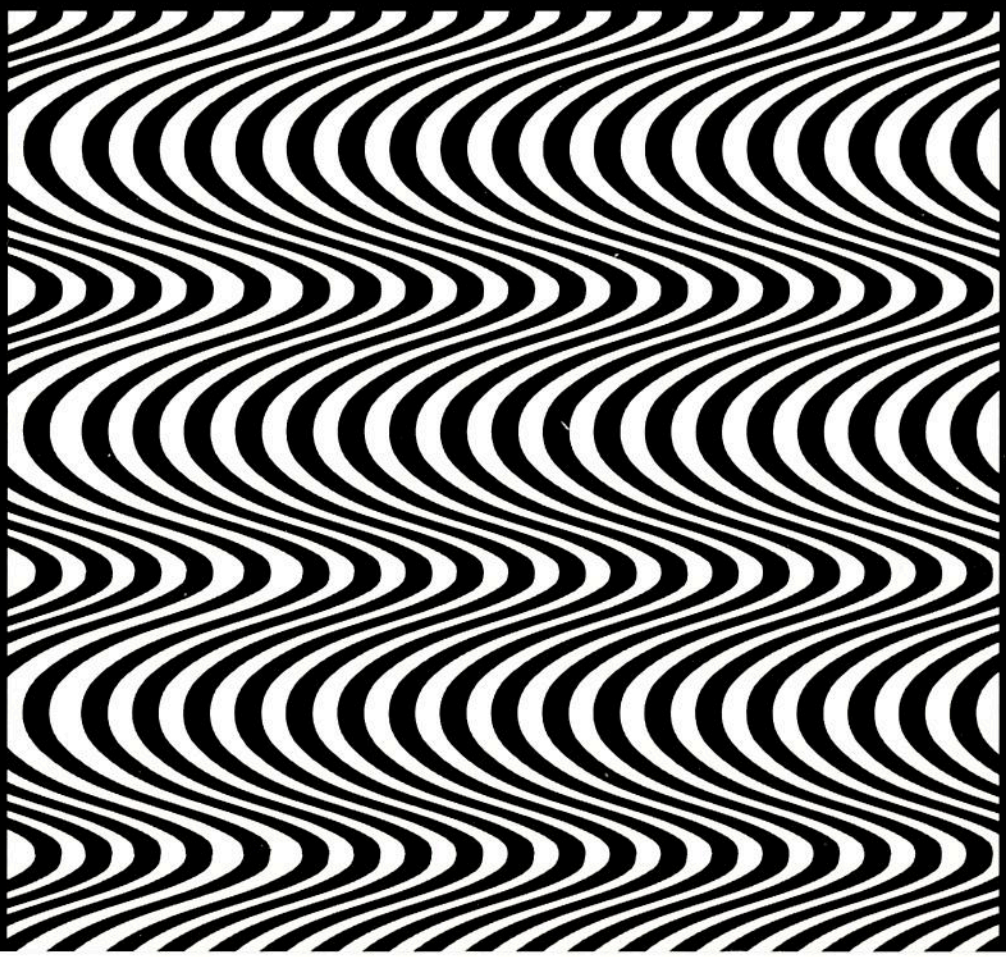

Numerical Methods for Steady Viscous Free-Surface Flows

Numerical Methods for Steady Viscous Free-Surface Flows

ACADEMISCH PROEFSCHRIFT

ter verkrijging van de graad van doctor
aan de Universiteit van Amsterdam
op gezag van de Rector Magnificus
prof. mr. P.F. van der Heijden
ten overstaan van een door
het college voor promoties ingestelde commissie,
in het openbaar te verdedigen in de Aula der Universiteit
op vrijdag 8 februari 2002, te 10:00 uur

door

Einar Harald van Brummelen

geboren te Soest

Promotor:	prof. dr. P.W. Hemker
Co-promotor:	dr. ir. H.C. Raven
Faculteit:	Natuurwetenschappen, Wiskunde en Informatica

Contents

Preface

This thesis records the research that I conducted between 1997 and 2001, as a member of the Modelling, Analysis and Simulation group at the Centre of Mathematics and Computer Science (CWI) in Amsterdam. The research presented in this thesis was financially supported by the Maritime Research Institute Netherlands (MARIN) and was performed in a collaboration between CWI and MARIN.

Many people have contributed to the realization of this thesis. I would like to thank my promotor Piet Hemker for his helpful critique and for his stimulating zest for work. My supervisor Barry Koren has been very supportive, and I thank him for his understanding as well as our pleasant collaboration. I am grateful to Hoyte Raven of MARIN for his patience in forging our different perspectives into synergy, and the resulting fruitful collaboration.

I thankfully acknowledge Guus Segal's help in performing the numerical experiments of Chapter 5. Due to his efforts, the experiments were smooth sailing.

My former and present room mates deserve credits for making my stay at CWI a pleasant one, and for the many enlightening discussions: Walter Stortelder, Jaap Noordmans, Jason Frank, Mervyn Lewis and Menno Genseberger. Jaap's struggle has left a deep impression on me, and the sadness of his death is beyond words.

I am indebted to the members of the *Resistance and Propulsion Research* group at MARIN. They provided valuable help when I adapted their codes for my purposes. Moreover, I found their interest in my work encouraging.

A pleasant distraction from the investigations was the organization of the PhDays meetings for Dutch and Flemish Ph.D. students in the field of numerical mathematics. I would like to thank my co-organizers and, in particular, my consorts of the memorable first edition: Debby Lanser, Martijn Anthonissen and Serge Goossens.

I enjoyed the company of many of my colleagues at CWI, in particular, Simone van der Wolff and Michaël Smeding.

The efforts underlying this thesis would have been meaningless without my parents, my sister, my friends and, most of all, my Debby.

Chapter 1
Introduction

1.1 Motivation

Flows of two distinct adjacent fluids occur in a wide variety of physical systems and engineering applications. The interaction of the fluids at their mutual interface gives rise to a multitude of complex phenomena. In many cases, however, one of the fluids exerts negligible stress on the interface, so that the other fluid can be considered separately. The interface then acts as a free surface, i.e., a boundary of which the position depends on the behavior of the enclosed flow. A specific instance of such a free-surface flow, that is of great practical relevance, is the flow of water underlying air. Accurate prediction of the behavior of free-surface flows is therefore important, e.g., in the assessment and design of immersed structures and vessels, such as ships.

Predictions of the behavior of free-surface flows are made on the basis of models. These models can be constructed at various levels of approximation. A particularly reliable mathematical model of fluid flow is a system of nonlinear partial differential equations, referred to as the Navier–Stokes equations. These equations were formulated independently by Navier (1822) and Stokes (1845). Unfortunately, these equations are too complicated to explicitly extract their solution. It is, however, possible to construct discrete approximations to the solution. The discretization of the differential equations yields a system of nonlinear algebraic equations. The solution of the algebraic system can be formulated in terms of recurrence relations, which are ideally suited to treatment by computers. Consequently, the prosperous development of computers has made it possible to consider increasingly complex flow problems. The investigation of flow problems by means of a computer is called Computational Fluid Dynamics (CFD). Figure 1.1 on the following page displays the steps in the solution of a flow problem by CFD, including some examples.

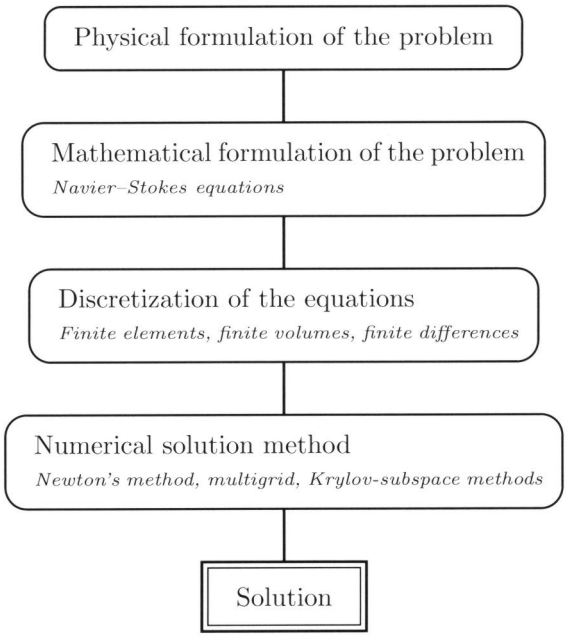

Figure 1.1: Steps in the solution of a flow problem by means of CFD.

The numerical solution of the Navier–Stokes equations with a free boundary has only recently become tractable. Previously, one had to revert to simpler models, for instance, the free-surface potential-flow equations. The free-surface potential flow equations already describe many of the prominent features of free-surface flow. The numerical techniques for these potential-flow equations are well developed, and they are routinely used in the investigation of practical flow problems. However, to include viscous effects, e.g., the interaction between the viscous boundary layer and the free surface near a surface-penetrating object, it is necessary to progress to the Navier–Stokes equations. Unfortunately, many of the numerical techniques for free-surface potential flow cannot be extended straightforwardly to the free-surface Navier–Stokes equations.

An important class of problems for which efficient numerical techniques are available for the potential-flow equations, but not for the Navier–Stokes equations, are *steady* free-surface flows. An example of such a steady free-surface flow is the wave pattern carried by a ship at forward speed in still water. In the field of ship hydrodynamics, dedicated techniques have been developed for solving the steady free-surface potential-flow equations. In contrast, methods for the Navier–Stokes equations typically continue a transient process until a steady state is reached. This time-integration method is often computationally inefficient, due to the specific transient behavior of free-surface flows. Alternative solution methods for

the steady free-surface Navier–Stokes equations exist. However, the performance of these methods usually depends sensitively on the parameters in the problem, or their applicability is too restricted. In general, the numerical solution of the steady free-surface Navier–Stokes equations by current computational methods is prohibitively expensive in actual design processes.

The need for efficient numerical techniques for the steady free-surface Navier–Stokes equations in practical applications, and the inadequacy of available methods, provide the motivation for the research presented in this thesis.

1.2 Outline

The contents of this thesis are organized as follows:

In Chapter 2 we present the mathematical formulation of free-surface flow. The Navier–Stokes equations are introduced. In addition, we discuss boundary conditions and initial conditions and their relevance for well-posedness of the corresponding initial boundary value problem. Furthermore, we state the interface conditions for two contiguous fluids and we derive the free-surface conditions as a special case.

Chapter 3 contains an analysis of the free-surface Navier–Stokes equations in primitive variables, by means of perturbation methods and Fourier techniques. In contrast to the classical analyses of free-surface flows (e.g., Refs. [37, 44, 63]), we adhere to a formulation of the equations in primitive variables, instead of a vorticity-based formulation. By virtue of the formulation in primitive variables, the analysis can serve in the investigation of numerical methods for the free-surface Navier–Stokes equations, if the differential operators in the continuum equations are replaced by their difference approximation. Moreover, the formulation in primitive variables permits a convenient treatment of the practically relevant case of three spatial dimensions, whereas the classical analyses are restricted to two spatial dimensions due to the properties of the vorticity formulation. The analysis yields important information on the properties of viscous free-surface flows in two and three spatial dimensions, e.g., on the dispersive behavior of surface gravity waves, the asymptotic temporal behavior of wave groups and the structure of the free-surface boundary layer.

In Chapter 4 we propose a novel iterative solution method for solving the steady free-surface Navier–Stokes equations. Moreover, we prove that the usual time-integration approach is generally inappropriate for solving steady free-surface flows. The proposed iterative solution method is analogous to methods for solving steady free-surface potential-flow problems. The method alternatingly solves the steady Navier–Stokes equations with a so-called quasi free-surface condition imposed at the free surface, and adjusts the free surface on the basis of the computed solution. The quasi free-surface condition ensures that the disturbance induced by the subsequent displacement of the boundary is negligible. Each surface adjustment then yields an improved approximation to the actual free-boundary position.

To establish the efficiency of the method, we show that its convergence behavior is asymptotically independent of the mesh width of the applied grid. The asymptotic computational complexity (computational cost per grid point) of the method deteriorates only moderately with decreasing mesh width. Mesh width independence of the computational complexity can be achieved by means of nested iteration. Numerical experiments and results are presented for a two-dimensional test case.

In Chapter 5 we consider an alternative approach to solving steady free-surface flow problems, viz., the optimal shape design method. A general characteristic of free-boundary problems is that the number of free-boundary conditions is one more than the number of boundary conditions required by the governing boundary value problem. A free-boundary problem can therefore be reformulated into the equivalent shape optimization problem of finding the boundary that minimizes a norm of the residual of one of the free-surface conditions, subject to the boundary value problem with the remaining free-surface conditions imposed. Such optimal shape design problems can in principle be solved efficiently by means of the adjoint method. Chapter 5 investigates the suitability of the adjoint shape optimization method for solving steady free-surface flow problems. Because inviscid, irrotational flow adequately describes the prominent features of free-surface flow, we base our investigation on the free-surface potential-flow equations. The adjoint shape optimization method is equally applicable to the free-surface Navier–Stokes equations, but the specifics of the method are in that case much more involved. Our investigation serves as an indication of the properties of the adjoint shape optimization method for steady free-surface flows. We formulate the optimal shape design problem associated with steady free-surface potential flow, and we examine the properties of the optimization problem. In addition, we analyze the convergence behavior of the adjoint method, by means of Fourier techniques. Motivated by the results of the analysis, we address preconditioning for the optimization problem. Numerical experiments and results are presented for a two-dimensional model problem.

Chapter 6 presents a preliminary investigation of the interface capturing approach to solving free-surface flow problems. Free-surface flows form a specific class of two-fluid flow. If the objective is the numerical solution of a free-surface flow problem, then it can be attractive to adhere to the underlying two-fluid flow formulation. In the absence of viscosity, two-fluid flow is described by a system of hyperbolic conservation laws. The numerical techniques for such systems of hyperbolic conservation laws are well developed and, in particular, efficient algorithms are available for solving steady hyperbolic problems. In Chapter 6 we present the prerequisites for a Godunov-type interface capturing method. We consider an Osher-type approximate Riemann solver and we elaborate its application to two-fluid flows. Moreover, we address the spurious pressure oscillations that are commonly incurred by conservative discretizations of two-fluid flows, and we construct a non-oscillatory conservative discretization. The implementation of the interface capturing approach with efficient techniques for steady problems is deferred to future research.

Chapters 7 and 8 contain concluding remarks and suggestions for future research, respectively.

Parts of the Chapters 3 to 6 have been published before. Chapter 3 is based on:

> E.H. van Brummelen, *Analysis of the incompressible Navier–Stokes equations with a quasi free-surface condition*, Tech. Report MAS-R9922, ISSN 1386-3703, CWI, 1999, Available at `http://www.cwi.nl/ftp/CWIreports/MAS/MAS-R9922.ps.Z`.

Chapter 4 has appeared as:

> E.H. van Brummelen, H.C. Raven, and B. Koren, *Efficient numerical solution of steady free-surface Navier–Stokes flow*, J. Comput. Phys. **174** (2001), no. 1, 120–137.

A condensed form was also published as:

> E.H. van Brummelen, H.C. Raven, and B. Koren, *Numerical solution of steady free-surface Navier–Stokes flow*, Computational Fluid Dynamics 2000: Proceedings of the First International Conference on Computational Fluid Dynamics (Kyoto, Japan, 10-14 July, 2000) (N. Satofuka, ed.), Springer, Berlin, 2001, pp. 305–310.

Chapter 5 will appear as:

> E.H. van Brummelen and A. Segal, *Numerical solution of steady free-surface flows by the adjoint optimal shape design method*, Int. J. Num. Meth. Fluids,

and has been published in condensed form as:

> E.H. van Brummelen and A. Segal, *Adjoint shape optimization for steady free-surface flows*, Numerical Methods for Fluid Dynamics VII: Proceedings of the Seventh ICFD Conference on Numerical Methods for Fluid Dynamics (Oxford, U.K., 16-19 March, 2001) (M.J. Baines, ed.), ICFD, Oxford University Computing Laboratory, Oxford, pp. 549–556.

Sections of Chapter 6 appeared as:

> E.H. van Brummelen and B. Koren, *A level-set method and an approximate Riemann solver for capturing free-surface water waves*, Proceedings of the AMIF-ESF Workshop Computing Methods for Two Phase-Flow (Aussois, 12-14 January, 2000) (H. Paillère, ed.), CEA, Saclay, 2000, (Paper 23 from CD-ROM),

as:

> E.H. van Brummelen and B. Koren, *A Godunov-type scheme for capturing water waves*, Proceedings of: Godunov Methods, Theory and Applications (Oxford, 12-22 October, 1999) (E.F. Toro, ed.), Kluwer (to appear),

and as:

E.H. VAN BRUMMELEN, *A Godunov-type scheme with applications in hydrodynamics*, Tech. Report MAS-R9829, ISSN 1386-3703, CWI, 1997, Available at `http://www.cwi.nl/ftp/CWIreports/MAS/MAS-R9829.ps.Z`.

Chapter 2
Mathematical Description of Free-Surface Flow

2.1 Introduction

Flows of two distinct, contiguous fluids are encountered in many practical applications. A free-surface flow is a particular instance of such a two-fluid flow, in which the properties of the fluids are such that one fluid exerts negligible stress on the other. A model for free-surface flow is therefore included in a model for two-fluid flow. The mathematical model for two-fluid flow comprises governing equations for fluid flow and interface conditions, which describe the interaction of contiguous fluids at their interface. In this chapter we present the governing equations for fluid flow and the interface conditions for two-fluid flow, and we derive the free-surface conditions from the general interface conditions.

2.2 Governing Equations for Fluid Flow

2.2.1 Conservation Laws

Fluid flows are presumed to be governed by *conservation laws*. These conservation laws state that mass, momentum and energy are conserved during the motion of the fluid. To model a fluid flow, the state of the flow is described by a set of designated fluid-properties called the *state variables*, e.g., velocity, pressure, density, etc. The conserved quantities can be expressed in these state variables. The mathematical description of the conservation laws for the derived quantities is a system of partial differential equations for the state variables.

To present the governing equations for fluid flow, we consider a volume of fluid. The fluid occupies an open domain $\mathcal{V} \subset \mathbb{R}^d$ $(d = 2, 3)$. Positions in $\mathcal{V}$ are identified by spatial coordinates $(x_1, \ldots, x_d)$ relative to the horizontal Cartesian base vectors $\mathbf{e}_1, \ldots, \mathbf{e}_{d-1}$ and the vertical Cartesian base vector $\mathbf{e}_d$. The gravi-

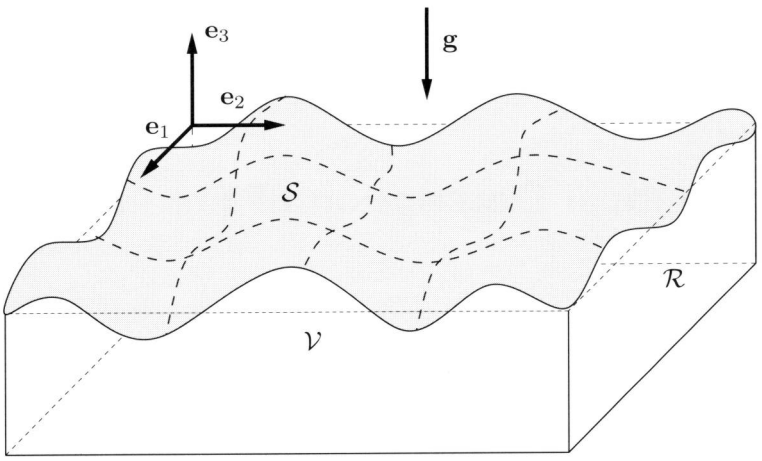

Figure 2.1: Schematic illustration of the free-surface flow problem.

tational acceleration, $\mathbf{g}$, is constant and vertically downward, i.e., $\mathbf{g} = -g\mathbf{e}_d$ for some constant $g \geq 0$. See Figure 2.1 for an illustration.

Suitable state variables for a viscous, compressible fluid are the velocity, the pressure, the density, the temperature and the internal energy of the fluid. Denoting time by $t \geq 0$, we identify the velocity by $\mathbf{v}(\mathbf{x}, t)$, the pressure by $p(\mathbf{x}, t)$, the density by $\rho(\mathbf{x}, t)$, the temperature by $T(\mathbf{x}, t)$ and the internal energy per unit mass by $e(\mathbf{x}, t)$. The total energy is defined by $E := \rho(e + |\mathbf{v}|^2/2)$. Conservation of mass, momentum and energy is then expressed by, respectively,

$$\frac{\partial}{\partial t}\rho + \operatorname{div}\left(\rho\mathbf{v}\right) = 0\,, \qquad \mathbf{x} \in \mathcal{V}, t > 0\,, \tag{2.1a}$$

$$\frac{\partial}{\partial t}\rho\mathbf{v} + \operatorname{div}\left(\rho\mathbf{v}\mathbf{v} + p\mathbf{I} - \boldsymbol{\tau}\right) - \rho\mathbf{g} = 0\,, \qquad \mathbf{x} \in \mathcal{V}, t > 0\,, \tag{2.1b}$$

$$\frac{\partial}{\partial t}E + \operatorname{div}\left((E+p)\mathbf{v} - \mathbf{v}\cdot\boldsymbol{\tau} - k\boldsymbol{\nabla}T\right) - \rho\mathbf{v}\cdot\mathbf{g} = 0\,, \qquad \mathbf{x} \in \mathcal{V}, t > 0\,, \tag{2.1c}$$

with k the thermal conductivity of the fluid. The tensor $\boldsymbol{\tau}$ in (2.1b) is called the *viscous stress tensor*. In the absence of $\boldsymbol{\tau}$ and k, the equations (2.1) are called the *Euler equations*.

The velocity vector can be represented by d Cartesian components $v_j := \mathbf{v}\cdot\mathbf{e}_j$. Similarly, the viscous stress tensor has d^2 Cartesian components τ_{ij}. Hence, the unknowns in (2.1) are ρ, v_j $(j = 1, \ldots, d)$, p, T, e and τ_{ij} $(i, j = 1, \ldots, d)$, and their number is $d^2 + d + 4$. The momentum equations (2.1b) can be separated into d independent conditions. Hence, (2.1) specifies $d + 2$ relations. Closure of the system of equations therefore requires $d^2 + 2$ supplementary relations. These relations are provided by a *constitutive relation*, which relates the viscous stress

tensor to the state variables, and two additional *equations of state*, which give a mutual relation between the state variables; see also [77].

A common constitutive relation for the viscous stress tensor is (see, for instance, Ref. [5])

$$\boldsymbol{\tau} := \mu \left((\boldsymbol{\nabla}\mathbf{v}) + (\boldsymbol{\nabla}\mathbf{v})^T - \tfrac{2}{3}(\operatorname{div}\mathbf{v})\,\mathbf{I} \right), \tag{2.1d}$$

where μ is the dynamic viscosity of the fluid. A fluid with constitutive relation (2.1d) for the viscous stress tensor is called a *Newtonian fluid*. The momentum equations (2.1b) with $\boldsymbol{\tau}$ according to (2.1d) are called the *Navier–Stokes equations*.

The flows considered in the sequel have a constant temperature and internal energy. The considered fluid either satisfies a barotropic equation of state $p := p(\rho)$, or it is homogeneous and incompressible, i.e., ρ is constant and $\mathbf{v}$ is solenoidal. In both cases, conservation of mass and momentum implies conservation of energy, and (2.1c) is redundant.

2.2.2 Dimensionless Equations

It is often convenient to express the quantities that are used to describe the flow problem on scales that are relevant for the considered problem. For example, an appropriate reference length for flow around a ship hull is the length of the hull. For the considered fluid flows, three independent reference scales can be assigned, viz., a reference length L_0, a reference velocity V_0 and a reference density ρ_0. All other scales in the problem are then implicitly defined, e.g., the implied time scale is L_0/U_0.

Let L_0, U_0 and ρ_0 denote a suitable reference length, velocity and density, respectively. We introduce the dimensionless variables

$$\mathbf{x}' := \mathbf{x}/L_0, \quad t' := t\,U_0/L_0, \quad \mathbf{v}' := \mathbf{v}/V_0, \quad \rho' := \rho/\rho_0 \quad p' := (p - p_0)/\rho_0 V_0^2, \tag{2.2}$$

with p_0 a reference pressure, typically, the atmospheric pressure. The dimensionless form of the Navier–Stokes equations is obtained by inserting (2.2) into (2.1b), (2.1d). Upon omitting the primes, we obtain

$$\frac{\partial}{\partial t}\rho\mathbf{v} + \operatorname{div}\left(\rho\mathbf{v}\mathbf{v} + p\mathbf{I} - \boldsymbol{\tau}\right) + \rho\mathrm{Fr}^{-2}\mathbf{e}_d = 0, \qquad \mathbf{x} \in \mathcal{V}, t > 0\,, \tag{2.3a}$$

with $\boldsymbol{\tau}$ the dimensionless viscous stress tensor,

$$\boldsymbol{\tau} := \mathrm{Re}^{-1}\left((\boldsymbol{\nabla}\mathbf{v}) + (\boldsymbol{\nabla}\mathbf{v})^T - \tfrac{2}{3}(\operatorname{div}\,\mathbf{v})\,\mathbf{I} \right), \tag{2.3b}$$

and

$$\mathrm{Re} := \frac{\rho_0 V_0 L_0}{\mu}\,, \qquad \mathrm{Fr} := \frac{V_0}{\sqrt{g L_0}}\,. \tag{2.3c}$$

The dimensionless numbers Re and Fr are called the *Reynolds number* and the *Froude number*, respectively. The Reynolds number is the ratio of inertial and

viscous forces in the flow. The Froude number is the ratio of the reference velocity over the velocity of a particular gravity wave, viz., a sinusoidal wave with dimensionless wave-number one in a fluid of infinite depth. In the absence of free-surface stresses, such as surface tension, the parameters Re and Fr are the distinguishing parameters for a viscous flow subject to gravity.

2.2.3 Additional Conditions and Well-Posedness

To complete the description of a flow problem, the governing equations (2.1) must be provided with additional conditions. The additional conditions specify conditions which the state variables must satisfy at the boundaries of the considered space–time domain. In general, we can distinguish *initial conditions* and *boundary conditions*. The partial differential equations (2.1) and the additional conditions form an *initial boundary value problem*.

The properties of an initial boundary value problem depend critically on the additional conditions. In particular, the additional conditions determine whether a boundary value problem is well posed or ill posed. An initial boundary value problem is said to be well posed if it possesses the following properties:

Existence: a solution exists,

Uniqueness: the solution is unique,

Stability: the solution is stable,

and ill posed otherwise. The stability requirement implies that the solution can be bounded in terms of the right-hand side of the differential equations and of the additional conditions (in some appropriate sense).

Only in specific cases has it been established that initial boundary value problems from fluid dynamics are well posed. A detailed discussion of additional conditions and of existence, uniqueness and stability of initial boundary value problems is beyond the scope of our research. Relevant references on the subject of additional conditions and posedness include, e.g.: [69, 70] for homogeneous, incompressible fluids, [59] for non-homogeneous incompressible fluids, [36] for boundary conditions for hyperbolic systems with constant or variable coefficients, and [16] for absorbing boundary conditions on truncated spatial domains.

2.3 Interface Conditions

2.3.1 Two-Fluid Flow Interface Conditions

We consider a flow of two distinct contiguous fluids, separated by an interface. Equations (2.1) describe the behavior of the flow in each of the fluids. At the interface, the state variables must comply with interface conditions. These interface conditions provide a relation between the state variables of the contiguous fluids.

The interface conditions consist of kinematic and dynamic conditions. The kinematic conditions are related to the continuity of velocity of the fluids at the interface. The dynamic conditions express conservation of momentum at the interface. A detailed model for the behavior of fluid interfaces and the corresponding interface conditions are presented in [4, 57]. Without additional assumptions on the properties of the interface, the dynamic conditions depend in a complicated manner on the geometry of the interface. To simplify the dynamic interface conditions, we assume that the contributions of interface viscosity, interface tension and interface density to the dynamic conditions are negligible. These assumptions are valid in many practical applications.

To present the interface conditions, we consider an interface $\mathcal{S}$ between the two contiguous fluids. One fluid is designated the primary fluid and the other fluid the secondary fluid. Denoting the unit normal vector to $\mathcal{S}$ from the primary to the secondary fluid by $\mathbf{n}(\mathbf{x}, t)$, we define

$$\mathbf{x}^{\pm} := \lim_{\epsilon \downarrow 0} \mathbf{x} \pm \epsilon \mathbf{n} \,, \tag{2.4}$$

i.e., $\mathbf{x}^+$ and $\mathbf{x}^-$ are at the interface in the primary and secondary fluid, respectively. Under the aforementioned assumptions, the stresses exerted on the interface by the primary and secondary fluid must cancel:

$$-\mathbf{n} \cdot (p\mathbf{I} - \boldsymbol{\tau})\Big|_{\mathbf{x}^-}^{\mathbf{x}^+} = 0 \,. \tag{2.5}$$

Conditions (2.5) are called the *dynamic interface conditions*. In equation (2.5), we can distinguish d separate conditions. If $\mathbf{t}_j(\mathbf{x}, t)$ $(j = 1, \ldots, d-1)$ are orthogonal tangent vectors to $\mathcal{S}$, the inner product of (2.5) and $\mathbf{t}_j$ yields $d-1$ conditions:

$$\mathbf{t}_j \cdot \boldsymbol{\tau} \cdot \mathbf{n}\Big|_{\mathbf{x}^-}^{\mathbf{x}^+} = 0 \,, \qquad j = 1, \ldots, d-1. \tag{2.6a}$$

Conditions (2.6a) prescribe continuity of shear stresses across the interface. These conditions are called the tangential dynamic conditions. The inner product of (2.5) and $\mathbf{n}$ yields:

$$-(p - \boldsymbol{\tau} : \mathbf{nn})\Big|_{\mathbf{x}^-}^{\mathbf{x}^+} = 0 \,. \tag{2.6b}$$

This condition is called the normal dynamic condition.

The kinematic conditions for the interface prescribe that the flow velocity is continuous across the interface:

$$\mathbf{v}\Big|_{\mathbf{x}^-}^{\mathbf{x}^+} = 0 \,, \tag{2.7a}$$

and that the interface moves with the local flow velocity. The latter implies that if the interface position is written in parametric form as

$$\mathcal{S} := \{\mathbf{x} \in \mathbb{R}^d : \mathbf{x} = \mathbf{X}(\mathbf{y}, t)\}$$

Table 2.1: Appropriate number of interface conditions n, for different combinations of the contiguous fluids in a two-fluid flow in $\mathbb{R}^d$.

combination	n
viscous /viscous	$2d+1$
viscous /inviscid	$d+2$
inviscid/inviscid	3

with $\mathbf{y} \in \mathbb{R}^{d-1}$, then

$$\frac{\partial \mathbf{X}(\mathbf{y},t)}{\partial t} = \mathbf{v}(\mathbf{X}(\mathbf{y},t),t)\,. \tag{2.7b}$$

Note that the velocity at the interface is uniquely defined by virtue of (2.7a).

The interface conditions (2.6) and (2.7) are only valid if both fluids are viscous. If either of the fluids is inviscid, the kinematic conditions (2.7) must be modified. The continuity condition (2.7a) then only applies in the direction normal to the interface, i.e.,

$$\mathbf{n}\cdot\mathbf{v}\Big|_{\mathbf{x}^-}^{\mathbf{x}^+} = 0\,, \tag{2.8a}$$

and only the normal velocity of the interface is prescribed:

$$\mathbf{n}\cdot\frac{\partial \mathbf{X}}{\partial t} = \mathbf{n}\cdot\mathbf{v}\,. \tag{2.8b}$$

Moreover, the tangential dynamic conditions then imply that the shear stress of the viscous fluid must vanish at the interface.

If both fluids are inviscid, the dynamic conditions are modified as well. In that case, the tangential dynamic conditions (2.6a) are discarded and the normal dynamic condition reduces to:

$$-p\Big|_{\mathbf{x}^-}^{\mathbf{x}^+} = 0\,. \tag{2.9}$$

Condition (2.9) states that the pressure is continuous across the interface.

The above implies that the number of interface conditions depends on the properties of the contiguous fluids. Table 2.1 lists the appropriate number of interface conditions for different combinations of the contiguous fluids.

2.3.2 Free-Surface Conditions

A free surface can be regarded as a particular instance of an interface, in which the stresses exerted on the interface by one fluid are negligible on a reference scale that is appropriate for the other. This occurs if the difference in densities of the contiguous fluids is large.

In order to derive the free-surface conditions from the general interface conditions, we consider a flow of two adjacent fluids with different densities. Let ρ_0^- and

ρ_0^+ denote the reference densities for the primary and secondary fluid, respectively, and let V_0 be a suitable reference velocity for the flow. The derived reference stress $\rho_0^+ V_0^2$ is suitable for the secondary fluid if moderate constants $\underline{c}_j$ and $\overline{c}_j$ $(j = 1, 2)$ exist such that

$$\underline{c}_1 \leq \frac{\|p - p_0\|}{\rho_0^+ V_0^2} \leq \overline{c}_1 \,, \qquad \underline{c}_2 \leq \frac{\|\boldsymbol{\tau}\|}{\rho_0^+ V_0^2} \leq \overline{c}_2 \,, \tag{2.10}$$

with $\|\cdot\|$ the maximum norm of $\cdot$ in the secondary fluid for all $t > 0$. Equation (2.10) is expressed with respect to the reference stress $\rho_0^- V_0^2$, which is suitable for the primary fluid, by

$$\underline{c}_1\left(\frac{\rho_0^+}{\rho_0^-}\right) \leq \frac{\|p - p_0\|}{\rho_0^- V_0^2} \leq \overline{c}_1\left(\frac{\rho_0^+}{\rho_0^-}\right) , \qquad \underline{c}_2\left(\frac{\rho_0^+}{\rho_0^-}\right) \leq \frac{\|\boldsymbol{\tau}\|}{\rho_0^- V_0^2} \leq \overline{c}_2\left(\frac{\rho_0^+}{\rho_0^-}\right) . \tag{2.11}$$

This implies that if the density ratio ρ_0^+/ρ_0^- is small, the deviation from $p_0\mathbf{n}$ of the stress exerted on the interface by the secondary flow is insignificant for the primary flow. The primary flow is then independent of the secondary flow and, moreover, the motion of the interface depends exclusively on the primary flow. In this case, the interface is called a free surface (or free boundary) of the primary flow.

The free-surface conditions follow from the general interface conditions under the assumption that the secondary flow is inviscid and exerts a constant pressure on the interface. The dynamic free-surface conditions follow immediately from (2.5): in dimensionless form,

$$\mathbf{n} \cdot (p\mathbf{I} - \boldsymbol{\tau}) = 0 \,, \qquad \mathbf{x} \in \mathcal{S}, t > 0 \,, \tag{2.12}$$

with p and $\boldsymbol{\tau}$ the dimensionless pressure and viscous stress tensor, respectively. The kinematic condition (2.8b) describes the motion of the free surface. Condition (2.8b) can be recast into a convenient form, if the free surface is represented as a level set:

$$S := \{\mathbf{x} \in \mathbb{R}^d : \psi(\mathbf{x}, t) = 0\} \,. \tag{2.13}$$

The kinematic free-surface condition can then be recast into

$$\frac{\partial \psi}{\partial t} + \mathbf{v} \cdot \boldsymbol{\nabla} \psi = 0 \,, \qquad \mathbf{x} \in \mathcal{S}, t > 0 \,. \tag{2.14}$$

In the absence of overturning waves, the free surface is often represented by a height function of the horizontal coordinates. If $\eta(x_1, \ldots, x_{d-1}, t)$ denotes the height of the surface with respect to some fixed reference surface, then the corresponding level set is $\psi(\mathbf{x}, t) = \eta(x_1, \ldots, x_{d-1}, t) - x_d$. The kinematic condition then assumes the familiar form:

$$\frac{\partial \eta}{\partial t} + \sum_{j=1}^{d-1} v_j \frac{\partial \eta}{\partial x_j} - v_d = 0 \,, \qquad \mathbf{x} \in \mathcal{S}, t > 0 \,. \tag{2.15}$$

Equations (2.8b), (2.14) and (2.15) are different formulations of the condition that the free surface moves in its normal direction with the normal component of the local flow velocity.

2.4 Problem Statement

We are concerned with the steady flow of water underlying air. The ratio of the density of air to the density of water is sufficiently small to treat the water–air interface as a free surface. Moreover, for our purposes, water can be treated as a homogeneous, incompressible, viscous fluid.

To formulate the free-surface flow problem, let $\mathcal{V}$ denote the volume occupied by the water, $\partial\mathcal{V}$ its boundary, $\mathcal{S}$ the free surface and $\mathcal{R} = \partial\mathcal{V} \setminus \mathcal{S}$ the rigid boundary; see Figure 2.1 on page 8. The steady free-surface flow problem is described by the aforementioned equations with the partial derivatives with respect to t omitted. Because the water is assumed to be homogeneous and incompressible, the density can be removed from the dimensionless governing equations. The steady free-surface flow problem is then stated as: Given the rigid boundary $\mathcal{R}$, find $\mathcal{S}$ and $\mathbf{v} : \overline{\mathcal{V}} \mapsto \mathbb{R}^d$ and $p : \overline{\mathcal{V}} \mapsto \mathbb{R}$ such that:

$$\operatorname{div}\left(\mathbf{v}\mathbf{v} + p\mathbf{I} - \boldsymbol{\tau}\right) = -\mathrm{Fr}^{-2}\mathbf{e}_d\,, \qquad \mathbf{x} \in \mathcal{V}\,, \tag{2.16a}$$

$$\operatorname{div}\mathbf{v} = 0\,, \qquad \mathbf{x} \in \mathcal{V}\,, \tag{2.16b}$$

with the viscous stress tensor $\boldsymbol{\tau}$ according to (2.3b), subject to the free-surface conditions

$$\mathbf{n}\cdot(p\mathbf{I} - \mathbf{n}\cdot\boldsymbol{\tau}) = 0\,, \qquad \mathbf{x} \in \mathcal{S}\,, \tag{2.17a}$$

$$\mathbf{n}\cdot\mathbf{v} = 0\,, \qquad \mathbf{x} \in \mathcal{S}\,, \tag{2.17b}$$

and the *rigid-boundary conditions* on $\mathcal{R}$.

The above problem statement contains the envisaged problem. However, to facilitate the investigation of numerical techniques, in the ensuing sections we will also consider closely related problems, e.g., the two-fluid compressible Euler equations or the steady free-surface potential flow equations.

Chapter 3

Analysis of Viscous Free-Surface Flow in Primitive Variables

3.1 Introduction

Flows that are partially bounded by a freely moving boundary occur in many practical applications, for instance, ship hydrodynamics, hydraulics and coating technology. Classically, free-surface flow problems have been examined by means of perturbation methods and Fourier techniques; see, e.g., Refs. [37, 44, 63]. These analyses are restricted to generic problems, such as perturbations of a uniform flow. However, these generic problems already contain important information on the general properties of free-surface flow problems. Presently, computational methods play an important role in the analysis of free-surface flow problems that occur in actual engineering applications.

The analysis of numerical methods for (initial) boundary value problems generally proceeds in the same manner as the classical analyses based on perturbation methods and Fourier techniques. The differential operators in the continuum problem are then replaced by their difference approximation. The familiar von Neumann stability analysis (see, for instance, Refs. [25, 52, 77]) is in fact an application of perturbation methods and Fourier techniques to difference equations. The analyses are important in the assessment of the stability of discretizations and of the convergence behavior of numerical solution methods.

It appears that an analysis of viscous free-surface flow problems in primitive variables, i.e., velocity and pressure, is not available. The classical analyses of viscous free-surface flows [37] and, in a more general context, stratified flows [26] adopt a vorticity-based formulation of the flow equations. Recent investigations of viscous free-surface flows (e.g., Ref. [15]) maintain this formulation. This outset has two disadvantages. Firstly, these analyses are generally inappropriate for the investigation of numerical methods, because most numerical methods for viscous free-surface flow problems treat the flow equations in primitive variables. Secondly,

the analyses are restricted to two spatial dimensions and, due to the properties of the vorticity formulation (see, e.g., Ref. [19]), cannot be straightforwardly extended to include the practically relevant case of three spatial dimensions.

In this chapter we present an analysis of the viscous free-surface flow equations in primitive variables. We consider the generic problem of perturbations in a uniform horizontal flow of finite depth in two- and three spatial dimensions. Only first-order perturbations are considered. Our primary interest is in the application of the analysis to the assessment of numerical methods for the viscous free-surface flow problem. However, this application is not currently presented. The presented analysis has *raison d'être* independently, as it yields important information on the properties of viscous free-surface flows in three spatial dimensions. Classical results in two spatial dimensions are included as a special case. The results concern the dispersive behavior of surface gravity waves, the asymptotic temporal behavior of wave groups, and the structure and properties of the free-surface boundary layer.

3.2 Statement of Objectives

We consider the dimensionless Navier–Stokes equations for an incompressible homogeneous fluid subject to gravity. The velocity being solenoidal, $\operatorname{div}\boldsymbol{\tau} = \mu\Delta\mathbf{v}$, with $\mu := 1/\mathrm{Re}$. Hence, we consider

$$\mathbf{v}_t + \operatorname{div}\mathbf{v}\mathbf{v} + \boldsymbol{\nabla}p - \mu\Delta\mathbf{v} = -\mathrm{Fr}^{-2}\mathbf{e}_d\,, \qquad \mathbf{x}\in\mathcal{V}_\eta, t>0\,, \tag{3.1a}$$

$$\operatorname{div}\mathbf{v} = 0\,, \qquad \mathbf{x}\in\mathcal{V}_\eta, t>0\,. \tag{3.1b}$$

The considered spatial domain $\mathcal{V}_\eta$ is defined by

$$\mathcal{V}_\eta := \{\mathbf{x}\in\mathbb{R}^d : -\infty < x_1,\ldots,x_{d-1} < +\infty, -1 < x_d < \eta\}, \tag{3.2}$$

with $\eta := \eta(x_1,\ldots,x_{d-1},t)$. The domain $\mathcal{V}_\eta$ is bounded by the moving boundary $\mathcal{S}_\eta := \{x_d = \eta\}$ and the rigid boundary $\mathcal{R} := \{x_d = -1\}$.

At the boundary $\mathcal{R}$ we impose the free-slip boundary conditions:

$$\mathbf{e}_d\cdot\mathbf{v} = 0\,, \qquad \mathbf{e}_d\cdot\big((\boldsymbol{\nabla}\mathbf{v}) + (\boldsymbol{\nabla}\mathbf{v})^T\big)\cdot\mathbf{e}_j = 0\,, \qquad \mathbf{x}\in\mathcal{R}, t>0\,, \tag{3.3}$$

with $j = 1,\ldots,d-1$. At $\mathcal{S}_\eta$ the dynamic free-surface conditions are imposed:

$$p - 2\mu\,\mathbf{n}\cdot\boldsymbol{\nabla}\mathbf{v}\cdot\mathbf{n} = 0\,, \qquad \mathbf{n}\cdot\big((\boldsymbol{\nabla}\mathbf{v}) + (\boldsymbol{\nabla}\mathbf{v})^T\big)\cdot\mathbf{t}_j = 0\,, \qquad \mathbf{x}\in\mathcal{S}_\eta, t>0\,, \tag{3.4}$$

with $\mathbf{n}$ the unit normal vector to $\mathcal{S}_\eta$ and $\mathbf{t}_j$, $j = 1,\ldots,d-1$, orthogonal unit tangential vectors to $\mathcal{S}_\eta$. Moreover, the vertical displacement η of the moving boundary $\mathcal{S}_\eta$ is related to the velocity of the underlying fluid flow by the kinematic condition

$$\eta_t + \mathbf{v}\cdot\boldsymbol{\nabla}\eta - v_d = 0\,, \qquad \mathbf{x}\in\mathcal{S}_\eta, t>0\,. \tag{3.5}$$

The moving boundary $\mathcal{S}_\eta$ is then a free surface.

Equations (3.1)–(3.5) must be supplemented with suitable initial conditions

$$\mathbf{v}(\mathbf{x},0) = \mathbf{v}_0(\mathbf{x})\,, \qquad p(\mathbf{x},0) = p_0(\mathbf{x})\,, \qquad \mathbf{x} \in \overline{\mathcal{V}}_\eta\,, \tag{3.6a}$$

with $\overline{\mathcal{V}}_\eta$ the closure of $\mathcal{V}_\eta$, and

$$\eta(\mathbf{x},0) = \eta_0(\mathbf{x})\,, \qquad \mathbf{x} \in \mathcal{S}_0\,, \tag{3.6b}$$

with $\mathbf{v}_0$, p_0 and η_0 given.

Our objective it to determine asymptotic solutions of (3.1)–(3.6) in the limit as $\|\eta\| \to 0$, i.e., for small displacements of the free surface. Moreover, we investigate the properties of such solutions.

3.3 Infinitesimal Solutions

3.3.1 Generating Solution

If the initial displacement of the free surface is specified

$$\eta(\mathbf{x},0) = 0\,, \qquad \mathbf{x} \in \mathcal{S}_0\,, \tag{3.7a}$$

and the initial conditions (3.6a) are specified

$$\mathbf{v}(\mathbf{x},0) = \mathbf{v}^{(0)}\,, \qquad p(\mathbf{x},0) = -\mathrm{Fr}^{-2}x_d\,, \qquad \mathbf{x} \in \overline{\mathcal{V}}_0\,, \tag{3.7b}$$

where $\mathbf{v}^{(0)} := (v_1^{(0)},\ldots,v_{d-1}^{(0)},0)$, with $v_1^{(0)},\ldots,v_{d-1}^{(0)}$ constant velocity components, and $\bar{\cdot}$ denotes closure, then the corresponding solution of (3.1)–(3.6) reads

$$\eta(\mathbf{x},t) = 0\,, \qquad \mathbf{x} \in \mathcal{S}_0, t \geq 0\,, \tag{3.8a}$$

and

$$\mathbf{v}(\mathbf{x},t) = \mathbf{v}^{(0)}\,, \qquad p(\mathbf{x},t) = -\mathrm{Fr}^{-2}x_d\,, \qquad \mathbf{x} \in \overline{\mathcal{V}}_0, t \geq 0\,. \tag{3.8b}$$

The above solution corresponds to a uniform horizontal flow. A uniform horizontal flow is indeed a (steady) solution of the considered free-surface flow problem.

If, instead, the initial displacement of the free surface is specified

$$\eta(\mathbf{x},0) = \epsilon h_0(\mathbf{x})\,, \qquad \mathbf{x} \in \mathcal{S}_0\,, \tag{3.9a}$$

with h_0 independent of ϵ, and, accordingly,

$$\mathbf{v}(\mathbf{x},0) = \mathbf{v}_0(\mathbf{x};\epsilon)\,, \qquad p(\mathbf{x},0) = p_0(\mathbf{x};\epsilon)\,, \qquad \mathbf{x} \in \overline{\mathcal{V}}_\eta\,, \tag{3.9b}$$

where $\mathbf{v}_0(\mathbf{x};\epsilon) \to \mathbf{v}^{(0)}$ and $p_0(\mathbf{x};\epsilon) \to -\mathrm{Fr}^{-2}x_d$ as $\epsilon \to 0$, then the corresponding solution of (3.1)–(3.5) approaches (3.8) as $\epsilon \to 0$. In this context, the solution (3.8) is called a *generating solution*.

3.3.2 Infinitesimal Conditions

We consider the free-surface flow problem (3.1)–(3.5), supplemented with the initial conditions (3.9). Motivated by §3.3.1, we assume that as $\epsilon \to 0$ the corresponding perturbed solution can be expanded asymptotically as

$$\eta(\mathbf{x},t;\epsilon) = \sum_{l=1}^{n} \chi_l(\epsilon)\,\eta^{(l)}(\mathbf{x},t) + o(\chi_n)\,, \tag{3.10a}$$

$$v_j(\mathbf{x},t;\epsilon) = v_j^{(0)} + \sum_{l=1}^{n} \psi_l^j(\epsilon)\,v_j^{(l)}(\mathbf{x},t) + o(\psi_n^j)\,, \qquad j=1,\ldots,d\,, \tag{3.10b}$$

$$p(\mathbf{x},t;\epsilon) = -\mathrm{Fr}^{-2}x_d + \sum_{l=1}^{n} \phi_l(\epsilon)\,p^{(l)}(\mathbf{x},t) + o(\phi_n)\,, \tag{3.10c}$$

for all $n = 1,2,\ldots$, with respect to certain uniform asymptotic sequences $\{\psi_l^j(\epsilon)\}$, $j=1,\ldots,d$, $\{\phi_l(\epsilon)\}$ and $\{\chi_l(\epsilon)\}$, with $l=1,2,\ldots$. For a definition of asymptotic sequences and the Landau symbols, o and O, used below, see, e.g., Ref. [35].

The condition that (3.10a) complies with (3.9a) implies that χ_1 must be of $O(\epsilon)$. We choose $\chi_1 = \epsilon$. The functions $\psi_1^j(\epsilon)$ and $\phi_1(\epsilon)$ are required to be of $o(1)$ as $\epsilon \to 0$. We assume that the expansion (3.10) is uniformly valid in $(\mathbf{x},t)$ for $\mathbf{x} \in \mathcal{V}_\eta$ and $t \geq 0$. The representation (3.10) of the solution as an asymptotic series is referred to as a *formal solution*. We refer to the first term in the series expansion as the *infinitesimal perturbation* or the *first-order perturbation*.

Upon inserting (3.10) in (3.1), we obtain

$$\sum_{l=1}^{n}\left(\psi_l^j\left[\frac{\partial v_j^{(l)}}{\partial t} + \sum_{k=1}^{d-1} v_k^{(0)}\frac{\partial v_j^{(l)}}{\partial x_k} - \mu\sum_{k=1}^{d}\frac{\partial^2 v_j^{(l)}}{\partial x_k^2}\right] + \phi_l\,\frac{\partial p^{(l)}}{\partial x_j}\right)$$
$$\sum_{l=1}^{n}\sum_{m=1}^{n}\sum_{k=1}^{d}\left(\psi_l^j\psi_m^k v_k^{(m)}\frac{\partial v_j^{(l)}}{\partial x_k}\right) + o(\psi_n^j) + o(\phi_n) = 0\,, \tag{3.11a}$$

and

$$\sum_{j=1}^{d}\left(\sum_{l=1}^{n}\psi_l^j\frac{\partial v_j^{(l)}}{\partial x_j} + o(\psi_n^j)\right) = 0\,, \tag{3.11b}$$

for all $\mathbf{x} \in \mathcal{V}_\eta, t \geq 0$. Because terms of different order in ϵ must vanish separately as $\epsilon \to 0$, (3.11a) implies: (1) that $\psi_l^j = O(\phi_l)$ to maintain a meaningful relation between $\mathbf{v}$ and p; (2) that $\phi_l = O(\phi_1\phi_{l-1}) = O(\phi_1^l)$ to maintain a meaningful relation between successive terms in the expansion. Based on (1), we choose $\psi_l^j = \phi_l$.

The requirement that (3.10) satisfies (3.1)–(3.5) and (3.9) imposes certain conditions on the successive terms in the expansion. The *infinitesimal conditions*, i.e., the conditions which the first-order perturbation must satisfy, are obtained

by inserting the expansion (3.10) in (3.1)–(3.5) and (3.9), and collecting terms of order $O(\phi_1)$.

Collecting terms of order $O(\phi_1)$ in (3.11):

$$\mathbf{v}_t^{(1)} + \mathbf{v}^{(0)} \cdot \boldsymbol{\nabla} \mathbf{v}^{(1)} + \boldsymbol{\nabla} p^{(1)} - \mu \Delta \mathbf{v}^{(1)} = 0 \,, \qquad \mathbf{x} \in \mathcal{V}_\eta, t > 0 \,, \tag{3.12a}$$

$$\operatorname{div} \mathbf{v}^{(1)} = 0 \,, \qquad \mathbf{x} \in \mathcal{V}_\eta, t > 0 \,. \tag{3.12b}$$

Inserting (3.10) in (3.3) and collecting terms of $O(\phi_1)$, the boundary conditions at the rigid boundary $\mathcal{R}$ yield

$$v_d^{(1)} = 0 \,, \qquad \mathbf{x} \in \mathcal{R},\ t > 0 \,, \tag{3.13a}$$

$$\frac{\partial v_j^{(1)}}{\partial x_d} + \frac{\partial v_d^{(1)}}{\partial x_j} = 0 \,, \qquad \mathbf{x} \in \mathcal{R},\ t > 0,\ j = 1, \ldots, d-1 \,. \tag{3.13b}$$

To obtain the free-surface conditions for the infinitesimal perturbation, an asymptotic expansion of the unit tangential and normal vectors to $\mathcal{S}_\eta$ is required. If the tangential and normal vectors to the undisturbed free surface $\mathcal{S}_0$ are $\mathbf{e}_j$ and $\mathbf{e}_d$, respectively, then the unit tangential and normal vectors to $\mathcal{S}_\eta$ can be expanded as

$$\mathbf{t}_j(\mathbf{x} + \eta(\mathbf{x}, t)\, \mathbf{e}_d) = \mathbf{e}_j + \big(\mathbf{e}_j \cdot \boldsymbol{\nabla} \eta(\mathbf{x}, t)\big)\, \mathbf{e}_d + O(\epsilon^2) \,, \tag{3.14a}$$

$$\mathbf{n}(\mathbf{x} + \eta(\mathbf{x}, t)\, \mathbf{e}_d) = \mathbf{e}_d - \sum_{j=1}^{d-1} \big(\mathbf{e}_j \cdot \boldsymbol{\nabla} \eta(\mathbf{x}, t)\big)\, \mathbf{e}_j + O(\epsilon^2) \,, \tag{3.14b}$$

with $\mathbf{x} \in \mathcal{S}_0$. The remainder is $O(\epsilon^2)$ because $\eta = O(\epsilon)$.

Taylor expansion of $\mathbf{v}(\mathbf{x}, t)$ around $\mathbf{x} \in \mathcal{S}_0$ yields

$$\mathbf{v}(\mathbf{x} + \eta(\mathbf{x})\, \mathbf{e}_d, t) = \mathbf{v}(\mathbf{x}, t) + \eta(\mathbf{x}, t)\, \mathbf{e}_d \cdot \boldsymbol{\nabla} \mathbf{v}(\mathbf{x}, t) + O(\epsilon^2) \,, \tag{3.15a}$$

$$\boldsymbol{\nabla} \mathbf{v}(\mathbf{x} + \eta(\mathbf{x})\, \mathbf{e}_d, t) = \boldsymbol{\nabla} \mathbf{v}(\mathbf{x}, t) + \eta(\mathbf{x}, t)\, \mathbf{e}_d \cdot \boldsymbol{\nabla} \boldsymbol{\nabla} \mathbf{v}(\mathbf{x}, t) + O(\epsilon^2) \,. \tag{3.15b}$$

Hence, by (3.10),

$$\mathbf{v}(\mathbf{x} + \eta(\mathbf{x})\, \mathbf{e}_d, t) = \mathbf{v}^{(0)} + \phi_1 \mathbf{v}^{(1)}(\mathbf{x}, t) + r(\epsilon) \,, \tag{3.16a}$$

$$\boldsymbol{\nabla} \mathbf{v}(\mathbf{x} + \eta(\mathbf{x})\, \mathbf{e}_d, t) = \phi_1 \boldsymbol{\nabla} \mathbf{v}^{(1)}(\mathbf{x}, t) + r(\epsilon) \,, \tag{3.16b}$$

with $\mathbf{x} \in \mathcal{S}_0$ and the remainder $r(\epsilon) = O(\epsilon^2) + O(\epsilon\phi_1) + O(\phi_1^2)$. Similarly, we obtain for the pressure

$$p(\mathbf{x} + \eta(\mathbf{x})\, \mathbf{e}_d, t) = \phi_1 p^{(1)}(\mathbf{x}, t) - \epsilon\, \mathrm{Fr}^{-2} \eta^{(1)}(\mathbf{x}, t) + \bar{r}(\epsilon) \,, \qquad \mathbf{x} \in \mathcal{S}_0 \,, \tag{3.17}$$

with $\bar{r}(\epsilon) = O(\phi_1^2) + O(\epsilon\phi_1) + O(\chi_2)$. Equation (3.17) yields a meaningful relation between p and η, provided $\phi_1 = O(\epsilon)$. We choose $\phi_1 = \epsilon$. From the remainder $\bar{r}$ we infer that a meaningful relation between successive terms in the approximation is only obtained if $\chi_l = O(\epsilon^l)$. Hence, the remainders r and $\bar{r}$ are both of $O(\epsilon^2)$.

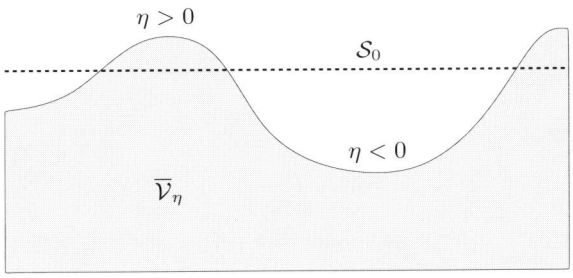

Figure 3.1: The spatial domain $\overline{\mathcal{V}}_\eta$ and the undisturbed free surface $\mathcal{S}_0$; $\mathcal{S}_0$ is not contained in $\overline{\mathcal{V}}_\eta$.

Inserting (3.10) and (3.14)–(3.17) in (3.4)–(3.5) and collecting terms of $O(\epsilon)$, we obtain the infinitesimal conditions

$$p^{(1)} - \mathrm{Fr}^{-2}\eta^{(1)} - 2\mu \frac{\partial v_d^{(1)}}{\partial x_d} = 0\,, \qquad \mathbf{x} \in \mathcal{S}_0, t > 0\,, \tag{3.18a}$$

$$\frac{\partial v_j^{(1)}}{\partial x_d} + \frac{\partial v_d^{(1)}}{\partial x_j} = 0\,, \qquad \mathbf{x} \in \mathcal{S}_0, t > 0\,, \tag{3.18b}$$

and

$$\frac{\partial \eta^{(1)}}{\partial t} + \sum_{j=1}^{d-1} v_j^{(0)} \frac{\partial \eta^{(1)}}{\partial x_j} - v_d^{(1)} = 0\,, \qquad \mathbf{x} \in \mathcal{S}_0, t > 0\,. \tag{3.18c}$$

Observe that (3.18) must be satisfied on the undisturbed free surface $\mathcal{S}_0$. However, $\mathbf{v}^{(1)}$ and $p^{(1)}$ are defined on the spatial domain $\overline{\mathcal{V}}_\eta$. Because $\mathcal{S}_0$ is not necessarily contained in $\overline{\mathcal{V}}_\eta$, it can occur that $\mathbf{v}^{(1)}$ and $p^{(1)}$ in (3.18) are not properly defined; see Figure 3.1. To avoid this, we assume that $\mathbf{v}^{(1)}$ and $p^{(1)}$ can be extended smoothly beyond the boundary $\mathcal{S}_\eta$ in such a manner that they are well defined in a neighborhood of $\mathcal{S}_\eta$ including $\mathcal{S}_0$. For $\mathbf{x} \in \mathcal{S}_0, \mathbf{x} \notin \overline{\mathcal{V}}_\eta$, we then define $\mathbf{v}^{(1)}$ and $p^{(1)}$ in (3.18) by their smooth extension from $\mathcal{S}_\eta$.

Ignoring terms of $O(\epsilon^2)$, the initial conditions (3.9) yield

$$\epsilon\eta^{(1)}(\mathbf{x}, 0) = \epsilon h_0(\mathbf{x})\,, \qquad \mathbf{x} \in \mathcal{S}_0\,, \tag{3.19a}$$

$$\mathbf{v}^{(1)}(\mathbf{x}, 0) = \mathbf{v}_0(\mathbf{x}; \epsilon) - \mathbf{v}^{(0)}\,, \qquad \mathbf{x} \in \mathcal{V}_\eta\,, \tag{3.19b}$$

$$p^{(1)}(\mathbf{x}, 0) = p_0(\mathbf{x}; \epsilon) + \mathrm{Fr}^{-2} x_d\,, \qquad \mathbf{x} \in \mathcal{V}_\eta\,. \tag{3.19c}$$

Equation (3.19) specifies the infinitesimal initial conditions.

3.3.3 Generic Modes

To determine the infinitesimal perturbation, i.e., the solution of (3.12)–(3.13) and (3.18)–(3.19), we first determine generic modes in compliance with (3.12). Subsequently, we use these generic modes to form the infinitesimal perturbation.

For convenient notation, let $\mathbf{q}(\mathbf{x},t) := \big(v_1^{(1)},\dots,v_d^{(1)},p^{(1)}\big)(\mathbf{x},t)$ and $h(\mathbf{x},t) := \eta^{(1)}(\mathbf{x},t)$. To construct a Fourier representation of $\mathbf{q}(\mathbf{x},t)$, we first consider an isolated mode:

$$\mathbf{q}(\mathbf{x},t) := \hat{\mathbf{q}}(\mathbf{k},s,\omega)\exp\left(\mathrm{i}\mathbf{k}\cdot\mathbf{x} + sx_d + \mathrm{i}\omega t\right), \tag{3.20a}$$

$$h(\mathbf{x},t) := \hat{h}(\mathbf{k},\omega)\exp\left(\mathrm{i}\mathbf{k}\cdot\mathbf{x} + \mathrm{i}\omega t\right), \tag{3.20b}$$

with $\mathbf{k} := k_1\mathbf{e}_1 + \cdots + k_{d-1}\mathbf{e}_{d-1}$, $k_j \in \mathbb{R}$ the horizontal *wave number*, $\omega \in \mathbb{C}$ the *radian frequency* and $s \in \mathbb{C}$. Note that the product $\mathbf{k}\cdot\mathbf{x}$ yields $k_1x_1+\ldots+k_{d-1}x_{d-1}$. Inserting (3.20a) into (3.12), we obtain

$$\hat{\mathbf{P}}(\mathbf{k},s,\omega)\cdot\hat{\mathbf{q}}(\mathbf{k},s,\omega)\exp\left(\mathrm{i}\mathbf{k}\cdot\mathbf{x} + sx_d + \mathrm{i}\omega t\right) = 0, \tag{3.21}$$

with the *Fourier symbol* $\hat{\mathbf{P}}(\mathbf{k},s,\omega)$ according to

$$\hat{\mathbf{P}}(\mathbf{k},s,\omega) := \begin{pmatrix} \hat{H}(\mathbf{k},s,\omega) & 0 & \dots & 0 & \mathrm{i}k_1 \\ 0 & \hat{H}(\mathbf{k},s,\omega) & \dots & 0 & \mathrm{i}k_2 \\ \vdots & \vdots & \ddots & \vdots & \vdots \\ 0 & 0 & \dots & \hat{H}(\mathbf{k},s,\omega) & s \\ \mathrm{i}k_1 & \mathrm{i}k_2 & \dots & s & 0 \end{pmatrix}, \tag{3.22a}$$

where

$$\hat{H}(\mathbf{k},s,\omega) := \mathrm{i}\omega + \mathrm{i}\mathbf{v}^{(0)}\cdot\mathbf{k} + \mu\big(|\mathbf{k}|^2 - s^2\big). \tag{3.22b}$$

Hence, (3.20a) complies with (3.12) if

$$\hat{\mathbf{q}}(\mathbf{k},s,\omega) \in \mathrm{kernel}\big(\hat{\mathbf{P}}(\mathbf{k},s,\omega)\big). \tag{3.23}$$

Equation (3.23) only allows nontrivial $\hat{\mathbf{q}}(\mathbf{k},s,\omega)$ if $\hat{\mathbf{P}}(\mathbf{k},s,\omega)$ is rank-deficient. This requires that $\mathbf{k}$, s and ω satisfy

$$\det(\hat{\mathbf{P}}(\mathbf{k},\omega)) = \big(|\mathbf{k}|^2 - s^2\big)\left(\hat{H}(\mathbf{k},s,\omega)\right)^{d-1} = 0. \tag{3.24}$$

For $d = 2$, the kernels of $\hat{\mathbf{P}}(\mathbf{k},s,\omega)$ corresponding to the different roots of (3.24) are:

$$\mathrm{span}\left\{\begin{pmatrix}1\\0\\0\end{pmatrix}, \begin{pmatrix}0\\1\\0\end{pmatrix}, \begin{pmatrix}0\\0\\1\end{pmatrix}\right\}, \qquad \text{if } \mathbf{k},s,\omega = 0, \tag{3.25a}$$

or otherwise

$$\operatorname{span}\left\{\begin{pmatrix} \mathrm{i}k_1 \\ (-1)^j|\mathbf{k}| \\ -\mathrm{i}\big(\omega+\mathbf{v}^{(0)}\cdot\mathbf{k}\big)\end{pmatrix}\right\}, \qquad \text{if } s=(-1)^j|\mathbf{k}| \ (j=1,2)\,, \tag{3.25b}$$

$$\operatorname{span}\left\{\begin{pmatrix} s \\ -\mathrm{i}k_1 \\ 0\end{pmatrix}\right\}, \qquad \text{if } \hat{H}(\mathbf{k},s,\omega)=0\,. \tag{3.25c}$$

For $d=3$,

$$\operatorname{span}\left\{\begin{pmatrix}1\\0\\0\\0\end{pmatrix},\begin{pmatrix}0\\1\\0\\0\end{pmatrix},\begin{pmatrix}0\\0\\1\\0\end{pmatrix},\begin{pmatrix}0\\0\\0\\1\end{pmatrix}\right\}, \qquad \text{if } \mathbf{k},s,\omega=0\,, \tag{3.26a}$$

or otherwise

$$\operatorname{span}\left\{\begin{pmatrix} \mathrm{i}k_1 \\ \mathrm{i}k_2 \\ (-1)^j|\mathbf{k}| \\ -\mathrm{i}\big(\omega+\mathbf{v}^{(0)}\cdot\mathbf{k}\big)\end{pmatrix}\right\}, \qquad \text{if } s=(-1)^j|\mathbf{k}| \ (j=1,2)\,, \tag{3.26b}$$

$$\operatorname{span}\left\{\begin{pmatrix} s \\ 0 \\ -\mathrm{i}k_1 \\ 0\end{pmatrix},\begin{pmatrix} 0 \\ s \\ -\mathrm{i}k_2 \\ 0\end{pmatrix}\right\}, \qquad \text{if } \hat{H}(\mathbf{k},s,\omega)=0\,. \tag{3.26c}$$

Note that (3.25a) and (3.26a) correspond to *constant modes*. Because (3.25b) and (3.26b) are independent of μ, the associated modes are called *inviscid modes*. In contrast, the modes corresponding to (3.25c) and (3.26c) are *viscous modes*.

In view of the linearity of (3.12), a solution of (3.12) can be represented as a linear combination of the modes (3.25) or (3.26). Hence, a *generic inviscid mode* can be defined by

$$\mathbf{q}^i(\mathbf{k},\omega,\mathbf{x},t)=\sum_{j=1}^{2}\theta_j^i(\mathbf{k},\omega)\,\hat{\mathbf{q}}_j^i(\mathbf{k},\omega)\exp\big(\mathrm{i}\mathbf{k}\cdot\mathbf{x}+(-1)^j|\mathbf{k}|x_d+\mathrm{i}\omega t\big)\,, \tag{3.27a}$$

with $\theta_j^i:\mathbb{R}^{d-1}\times\mathbb{C}\mapsto\mathbb{C}$ $(j=1,2)$, and

$$\hat{\mathbf{q}}_j^i(\mathbf{k},\omega)=\begin{pmatrix} \mathrm{i}k_1 \\ \vdots \\ \mathrm{i}k_{d-1} \\ (-1)^j|\mathbf{k}| \\ -\mathrm{i}\big(\omega+\mathbf{v}^{(0)}\cdot\mathbf{k}\big)\end{pmatrix}. \tag{3.27b}$$

A *generic viscous mode* is

$$\mathbf{q}^v(\mathbf{k},\omega,\mathbf{x},t) = \sum_{l=1}^{d-1}\sum_{j=1}^{2} \theta^v_{l,j}(\mathbf{k},\omega)\,\hat{\mathbf{q}}^v_{l,j}(\mathbf{k},\omega)\exp\left(\mathrm{i}\mathbf{k}\cdot\mathbf{x}+(-1)^j\sigma x_d+\mathrm{i}\omega t\right), \quad (3.28a)$$

with $\theta^v_{l,j} : \mathbb{R}^{d-1}\times\mathbb{C}\mapsto\mathbb{C}$ $(l=1,\ldots,d-1,\ j=1,2)$,

$$\sigma := \sigma(\mathbf{k},\omega) = \sqrt{|\mathbf{k}|^2+\mathrm{i}\big(\omega+\mathbf{v}^{(0)}\cdot\mathbf{k}\big)/\mu}\,, \quad (3.28b)$$

and

$$\hat{\mathbf{q}}^v_{1,j}(\mathbf{k},\omega) = \begin{pmatrix}(-1)^j\sigma\\ -\mathrm{i}k_1\\ 0\end{pmatrix}, \qquad \text{if } d=2\,, \quad (3.28c)$$

and

$$\hat{\mathbf{q}}^v_{1,j}(\mathbf{k},\omega) = \begin{pmatrix}(-1)^j\sigma\\ 0\\ -\mathrm{i}k_1\\ 0\end{pmatrix}, \qquad \hat{\mathbf{q}}^v_{2,j}(\mathbf{k},\omega) = \begin{pmatrix}0\\ (-1)^j\sigma\\ -\mathrm{i}k_2\\ 0\end{pmatrix}, \qquad \text{if } d=3\,. \quad (3.28d)$$

3.3.4 Surface Gravity Waves

A solution of (3.12)–(3.13) and (3.18) can be formed by linear combination of the generic modes (3.27)–(3.28). The case $d=2$ can be treated as a particular case of $d=3$, with $\theta^v_{2,j}$ and k_2 set to 0, and will therefore not be considered separately.

To enforce the boundary conditions (3.13), we choose

$$\theta^i_j(\mathbf{k},\omega) = \theta^i(\mathbf{k},\omega)\exp\left((-1)^j|\mathbf{k}|\right), \qquad \theta^v_{l,j}(\mathbf{k},\omega) = \theta^v_l(\mathbf{k},\omega)\exp\left((-1)^j\sigma\right), \quad (3.29)$$

with $\theta^i(\mathbf{k},\omega) : \mathbb{R}^{d-1}\times\mathbb{C}\mapsto\mathbb{C}$ and $\theta^v_l(\mathbf{k},\omega) : \mathbb{R}^{d-1}\times\mathbb{C}\mapsto\mathbb{C}$, where $j=1,2$ and $l=1,2$. Equations (3.27) and (3.28) then yield

$$\mathbf{q}^i(\mathbf{k},\omega,\mathbf{x},t) \;=\; \theta^i(\mathbf{k},\omega)\begin{pmatrix}\mathrm{i}k_1\cosh\left(|\mathbf{k}|(1+x_d)\right)\\ \mathrm{i}k_2\cosh\left(|\mathbf{k}|(1+x_d)\right)\\ |\mathbf{k}|\sinh\left(|\mathbf{k}|(1+x_d)\right)\\ -\Omega\cosh\left(|\mathbf{k}|(1+x_d)\right)\end{pmatrix}\exp\left(\mathrm{i}\mathbf{k}\cdot\mathbf{x}\;+\;\mathrm{i}\omega t\right), \quad (3.30a)$$

with

$$\Omega := \Omega(\mathbf{k},\omega) = \mathrm{i}(\omega+\mathbf{v}^0\cdot\mathbf{k})\,, \quad (3.30b)$$

and

$$\mathbf{q}^v(\mathbf{k},\omega,\mathbf{x},t) = \theta_1^v(\mathbf{k},\omega)\begin{pmatrix}\sigma\cosh\big(\sigma(1+x_d)\big)\\ 0\\ -\mathrm{i}k_1\sinh\big(\sigma(1+x_d)\big)\\ 0\end{pmatrix}\exp\big(\mathrm{i}\mathbf{k}\cdot\mathbf{x}+\mathrm{i}\omega t\big)$$
$$+\,\theta_2^v(\mathbf{k},\omega)\begin{pmatrix}0\\ \sigma\cosh\big(\sigma(1+x_d)\big)\\ -\mathrm{i}k_2\sinh\big(\sigma(1+x_d)\big)\\ 0\end{pmatrix}\exp\big(\mathrm{i}\mathbf{k}\cdot\mathbf{x}+\mathrm{i}\omega t\big)\,, \quad (3.30c)$$

respectively.

The sum of the above inviscid and viscous modes, $\mathbf{q}^i+\mathbf{q}^v$, and the infinitesimal surface displacement (3.20b) satisfy the conditions (3.18) if the following conditions hold:

$$\theta^i\Omega\cosh|\mathbf{k}| + \mathrm{Fr}^{-2}\hat{h} + 2\mu(\theta^i|\mathbf{k}|^2\cosh|\mathbf{k}| - \mathrm{i}\sigma\cosh\sigma\,(\theta_1^v k_1+\theta_2^v k_2)) = 0\,, \quad (3.31a)$$
$$\Omega\hat{h} - (\theta^i|\mathbf{k}|\sinh|\mathbf{k}| - \mathrm{i}\sinh\sigma\,(\theta_1^v k_1+\theta_2^v k_2)) = 0\,, \quad (3.31b)$$
$$\theta^i\,2\mathrm{i}k_1|\mathbf{k}|\sinh|\mathbf{k}| + \theta_1^v(\sigma^2+k_1^2)\sinh\sigma = 0\,, \quad (3.31c)$$
$$\theta^i\,2\mathrm{i}k_2|\mathbf{k}|\sinh|\mathbf{k}| + \theta_2^v(\sigma^2+k_2^2)\sinh\sigma = 0\,, \quad (3.31d)$$

Eliminating the ratios $\hat{h}/\theta^i$, θ_1^v/θ^i and θ_2^v/θ^i from these equations, we obtain

$$\Big(k_1^2(\sigma^2+k_2^2)+k_2^2(\sigma^2+k_1^2)\Big)\Big(4\mu\Omega\sigma|\mathbf{k}|(\tanh|\mathbf{k}|/\tanh\sigma)+2\mathrm{Fr}^{-2}|\mathbf{k}|\tanh|\mathbf{k}|\Big)$$
$$-(\sigma^2+k_1^2)(\sigma^2+k_2^2)\Big(\Omega(\Omega+2\mu|\mathbf{k}|^2)+\mathrm{Fr}^{-2}|\mathbf{k}|\tanh|\mathbf{k}|\Big) = 0\,. \quad (3.32)$$

Recall that σ is defined by (3.28b). Hence, (3.32) specifies a relation between the radian frequency ω and the wave number $\mathbf{k}$. Such a relation is called a *dispersion relation*. Elimination of σ^2 from (3.32) by means of the definition (3.28b) yields the following implicit relation for the dispersion relation:

$$\Omega\big(\Omega+\mu|\mathbf{k}|^2\big)\Big(\big(\Omega+2\mu|\mathbf{k}|^2\big)^2+\mathrm{Fr}^{-2}|\mathbf{k}|\tanh|\mathbf{k}|\Big)$$
$$-\mu^2\Big(4\Omega\sigma|\mathbf{k}|(\tanh|\mathbf{k}|/\tanh\sigma)\Big(|\mathbf{k}|^2(\Omega+\mu|\mathbf{k}|^2)+2\mu k_1^2k_2^2\Big)$$
$$+k_1^2k_2^2\Big(3\mathrm{Fr}^{-2}|\mathbf{k}|\tanh|\mathbf{k}|-\Omega(\Omega+2\mu|\mathbf{k}|^2)\Big)\Big) = 0\,. \quad (3.33)$$

It appears impossible to explicitly extract the dispersion relation $\omega(\mathbf{k})$ from equation (3.33). However, an asymptotic expansion of the dispersion relation in the limit $\mu\to 0$ can be constructed. As $\mu\to 0$, (3.33) possesses two distinct roots

$$\omega_j(\mathbf{k};\mu) = -\mathbf{v}^{(0)}\cdot\mathbf{k} + (-1)^j\Phi(\mathbf{k}) + \mathrm{i}2\mu|\mathbf{k}|^2 + o(\mu)\,, \quad (3.34a)$$

with $j = 1, 2$ and

$$\Phi(\mathbf{k}) = \sqrt{\mathrm{Fr}^{-2}|\mathbf{k}|\tanh|\mathbf{k}|}\,. \tag{3.34b}$$

To construct the expansion (3.34), it is important to note that

$$\frac{\sigma}{\tanh\sigma} = \frac{\sqrt{\mu|\mathbf{k}|^2+\Omega}}{\sqrt{\mu}}\,\frac{\exp\big(2\sqrt{|\mathbf{k}|^2+\Omega/\mu}\big)+1}{\exp\big(2\sqrt{|\mathbf{k}|^2+\Omega/\mu}\big)-1} = O\big(1/\sqrt{\mu}\big)\,, \tag{3.35}$$

as $\mu \to 0$. Hence, the remainder in (3.34) is indeed $o(\mu)$.

If (3.34) is inserted in (3.20a) and terms of $o(\mu)$ are ignored, it follows that an isolated Fourier mode behaves in $x_1, \ldots, x_{d-1}$ and t as:

$$\exp\big(-2\mu|\mathbf{k}|^2 t\big)\exp\big(\mathrm{i}\mathbf{k}\cdot\mathbf{x} - \mathrm{i}\big(\mathbf{v}^{(0)}\cdot\mathbf{k} - (-1)^j\Phi(\mathbf{k})\big)t\big)\,. \tag{3.36}$$

Equation (3.36) associates a traveling wave with each root of the dispersion relation. These waves are called *surface gravity waves*. The surface gravity waves move with the *phase velocity*

$$\mathbf{c}(\mathbf{k}) = |\mathbf{k}|^{-2}\big(\mathbf{v}^{(0)}\cdot\mathbf{k} - (-1)^j\Phi(\mathbf{k})\big)\,\mathbf{k}\,, \qquad j = 1, 2\,, \tag{3.37}$$

(see, e.g., Ref. [78]) and attenuate as $\exp(-2\mu|\mathbf{k}|^2 t)$.

3.3.5 Constant Perturbations

A solution of (3.12)–(3.13) and (3.18) can also be formed by linear combination of the constant modes (3.26a). One can infer that for $d = 3$ any such *constant perturbation* can be represented as

$$\begin{pmatrix} v_1^{(1)} \\ v_2^{(1)} \\ v_3^{(1)} \\ p^{(1)} \end{pmatrix}(\mathbf{x}, t) = \bar{\mathbf{w}}\,, \quad \text{with} \quad \bar{\mathbf{w}} := \begin{pmatrix} \bar{v}_1 \\ \bar{v}_2 \\ 0 \\ \bar{p} \end{pmatrix}\,, \tag{3.38a}$$

and

$$h(\mathbf{x}, t) = \mathrm{Fr}^2\bar{w}_4\,, \tag{3.38b}$$

for arbitrary constants $\bar{v}_1, \bar{v}_2$ and $\bar{p}$. The case $d = 2$ can again be treated as a particular case of $d = 3$, with $\bar{v}_2$ set to 0, and will not be considered separately.

3.3.6 Compatibility of Initial Conditions

The surface gravity waves express the infinitesimal perturbation corresponding to a disturbance in the initial conditions in the form of an isolated Fourier mode. A general infinitesimal perturbation can be represented as a linear combination of the constant mode and the Fourier integral of these surface gravity waves, provided

that the perturbation in the initial conditions complies with certain compatibility conditions.

To facilitate the description of the compatibility conditions, we note that the conditions (3.31c)–(3.31d) specify an interdependence between the inviscid mode (3.30a) and the viscous mode (3.30c). For each root $\omega_j(\mathbf{k})$ of the dispersion relation (3.33), we can condense the corresponding surface gravity wave into

$$\hat{\mathbf{w}}_j(\mathbf{k}, x_d) \exp\left(\mathrm{i}\mathbf{k}\cdot\mathbf{x} + \mathrm{i}\omega_j(\mathbf{k})t\right), \tag{3.39a}$$

where

$$\hat{\mathbf{w}}_j(\mathbf{k}, x_d) := \hat{\mathbf{w}}_j^i(\mathbf{k}, x_d) - \mu\hat{\mathbf{w}}_j^v(\mathbf{k}, x_d), \tag{3.39b}$$

with

$$\hat{\mathbf{w}}_j^i(\mathbf{k}, x_d) := \begin{pmatrix} \mathrm{i}k_1 \cosh\big(|\mathbf{k}|(1+x_d)\big) \\ \mathrm{i}k_2 \cosh\big(|\mathbf{k}|(1+x_d)\big) \\ |\mathbf{k}| \sinh\big(|\mathbf{k}|(1+x_d)\big) \\ -\Omega_j \cosh\big(|\mathbf{k}|(1+x_d)\big) \end{pmatrix}, \tag{3.39c}$$

and

$$\begin{aligned} \hat{\mathbf{w}}_j^v(\mathbf{k}, x_d) := {} & \frac{2\mathrm{i}k_1|\mathbf{k}|\sinh|\mathbf{k}|}{\mu|\mathbf{k}|^2 + \Omega_j + \mu k_1^2} \begin{pmatrix} \sigma_j \cosh\big(\sigma_j(1+x_d)\big)/\sinh\sigma_j \\ 0 \\ -\mathrm{i}k_1 \sinh\big(\sigma_j(1+x_d)\big)/\sinh\sigma_j \\ 0 \end{pmatrix} \\ & + \frac{2\mathrm{i}k_2|\mathbf{k}|\sinh|\mathbf{k}|}{\mu|\mathbf{k}|^2 + \Omega_j + \mu k_2^2} \begin{pmatrix} 0 \\ \sigma_j \cosh\big(\sigma_j(1+x_d)\big)/\sinh\sigma_j \\ -\mathrm{i}k_2 \sinh\big(\sigma_j(1+x_d)\big)/\sinh\sigma_j \\ 0 \end{pmatrix}, \end{aligned} \tag{3.39d}$$

with $\Omega_j := \Omega(\mathbf{k}, \omega_j(\mathbf{k}))$ and $\sigma_j := \sigma(\mathbf{k}, \omega_j(\mathbf{k}))$ according to (3.30b) and (3.28b), respectively.

Moreover, from the conditions (3.31) it follows that the surface displacement carried by the surface gravity wave (3.39) is

$$\hat{h}_j(\mathbf{k}) \exp\left(\mathrm{i}\mathbf{k}\cdot\mathbf{x} + \omega_j(\mathbf{k})t\right), \tag{3.40a}$$

with

$$\begin{aligned} \hat{h}_j(\mathbf{k}) := -\mathrm{Fr}^2 \Bigg[& \Omega_j \cosh|\mathbf{k}| + 2\mu|\mathbf{k}|^2 \cosh|\mathbf{k}| \\ & - \frac{4\mu^2\sigma_j|\mathbf{k}|\sinh|\mathbf{k}|}{\tanh\sigma_j} \left(\frac{k_1^2}{\mu|\mathbf{k}|^2 + \Omega_j + \mu k_1^2} + \frac{k_2^2}{\mu|\mathbf{k}|^2 + \Omega_j + \mu k_2^2} \right) \Bigg]. \end{aligned} \tag{3.40b}$$

To specify the compatibility condition for the initial conditions (3.9), we define

$$\mathbf{q}_0(\mathbf{x}) := \lim_{\epsilon \to 0} \frac{1}{\epsilon} \begin{pmatrix} \mathbf{v}_0(\mathbf{x};\epsilon) - \mathbf{v}^{(0)} \\ p_0(\mathbf{x};\epsilon) + \mathrm{Fr}^{-2} x_d \end{pmatrix} . \tag{3.41}$$

Let m denote the number of roots of the dispersion relation (3.33). The initial conditions (3.9) are called *compatible* with (3.1)–(3.5) to $O(\epsilon^2)$ as $\epsilon \to 0$, if $\theta_j : \mathbb{R}^{d-1} \mapsto \mathbb{C}$ exist such that

$$\mathbf{q}_0(\mathbf{x}) = \bar{\mathbf{w}} + \int_{-\infty}^{\infty} \sum_{j=1}^{m} \theta_j(\mathbf{k})\, \hat{\mathbf{w}}_j(\mathbf{k}, x_d) \exp\left(\mathrm{i}\mathbf{k}\cdot\mathbf{x}\right) \mathrm{d}\mathbf{k} + O(\epsilon) , \tag{3.42a}$$

$$h_0(\mathbf{x}) = \mathrm{Fr}^2 \bar{w}_4 + \int_{-\infty}^{\infty} \sum_{j=1}^{m} \theta_j(\mathbf{k})\, \hat{h}_j(\mathbf{k}) \exp\left(\mathrm{i}\mathbf{k}\cdot\mathbf{x}\right) \mathrm{d}\mathbf{k} + O(\epsilon) . \tag{3.42b}$$

with $\bar{\mathbf{w}} \in \mathbb{R}^{d+1}$ a constant vector in accordance with (3.38a). The compatibility conditions (3.42) imply that the infinitesimal initial conditions (3.19) can be satisfied to $O(\epsilon^2)$ by a linear combination of the constant modes (3.38) and a Fourier integral of the surface gravity waves.

Existence of the integrals in (3.42) implies certain restrictions on the initial conditions, in addition to the compatibility conditions; see, e.g., Ref. [72]. However, many of these restrictions can be relaxed if θ_j is understood in a generalized sense [43].

3.3.7 General Infinitesimal Perturbations

The infinitesimal perturbation corresponding to an arbitrary compatible initial condition can be represented as

$$\mathbf{q}(\mathbf{x}, t) = \bar{\mathbf{w}} + \sum_{j=1}^{m} \int_{-\infty}^{\infty} \theta_j(\mathbf{k})\, \hat{\mathbf{w}}_j(\mathbf{k}, x_d) \exp\left(\mathrm{i}\mathbf{k}\cdot\mathbf{x} + \mathrm{i}\omega_j(\mathbf{k})t\right) \mathrm{d}\mathbf{k} , \tag{3.43a}$$

$$h(\mathbf{x}, t) = \mathrm{Fr}^2 \bar{w}_4 + \sum_{j=1}^{m} \int_{-\infty}^{\infty} \theta_j(\mathbf{k})\, \hat{h}_j(\mathbf{k}) \exp\left(\mathrm{i}\mathbf{k}\cdot\mathbf{x} + \mathrm{i}\omega_j(\mathbf{k})t\right) \mathrm{d}\mathbf{k} , \tag{3.43b}$$

for appropriate $\bar{\mathbf{w}}$ and $\theta_j(\mathbf{k})$. If $\theta_j(\mathbf{k})\, \hat{\mathbf{w}}_j(\mathbf{k}, x_d)$ and $\theta_j(\mathbf{k})\, \hat{h}_j(\mathbf{k})$ are analytic functions of $\mathbf{k}$ for all considered x_d, then the integrals describe the behavior of *wave groups*, i.e., a group of contiguous (in Fourier space) surface gravity waves.

Denoting the Fourier transforms of $\mathbf{q}_0(\mathbf{x})$ and $h_0(\mathbf{x})$ from $x_1, \ldots, x_{d-1}$ to $\mathbf{k}$ by $\hat{\mathbf{w}}_0(\mathbf{k}, x_d)$ and $\hat{h}_0(\mathbf{k})$, respectively, the infinitesimal initial conditions imply the

following conditions on $\bar{\mathbf{w}}$ and $\theta_j(\mathbf{k})$:

$$\hat{\mathbf{w}}_0(\mathbf{k}, x_d) = \bar{\mathbf{w}}\,\delta(\mathbf{k}) + \sum_{j=1}^{m} \theta_j(\mathbf{k})\hat{\mathbf{w}}_j(\mathbf{k}, x_d)\,, \tag{3.44a}$$

$$\hat{h}_0(\mathbf{k}) = \mathrm{Fr}^2 \bar{w}_4\,\delta(\mathbf{k}) + \sum_{j=1}^{m} \theta_j(\mathbf{k})\hat{h}_j(\mathbf{k})\,, \tag{3.44b}$$

with $\delta(\mathbf{k})$ the Dirac δ-function. If the conditions (3.44) uniquely determine $\bar{\mathbf{w}}$ and $\theta_j(\mathbf{k})$ for all $\mathbf{k}$ such that $\hat{\mathbf{w}}_j(\mathbf{k}, x_d) \neq 0$ or $\hat{k}_j(\mathbf{k}) \neq 0$, then the infinitesimal perturbation (3.43) is uniquely determined by (3.1)–(3.5) and the initial conditions (3.9). This is, of course, a prerequisite for well posedness of the problem defined by (3.1)–(3.5) and (3.9).

From (3.33) and (3.39)–(3.40) it follows that $\hat{\mathbf{w}}_j(\mathbf{k}, x_d) = 0$ and $\hat{h}_j(\mathbf{k}) = 0$ iff $\mathbf{k} = 0$. The conditions (3.44) with $\mathbf{k} = 0$ then uniquely determine $\bar{\mathbf{w}}$. For all $\mathbf{k} \neq 0$, the conditions (3.44) uniquely determine $\theta_j(\mathbf{k})$, provided that the pairs $(\hat{\mathbf{w}}_j(\mathbf{k}, x_d), \hat{h}_j(\mathbf{k}))$, $j = 1, \ldots, m$, are linearly independent for some $x_d \in [0, 1]$.

For sufficiently small μ, the infinitesimal perturbation is unique: From (3.34) and (3.39) it follows that the number of roots of the dispersion relation is $m = 2$ as $\mu \to 0$ and that the associated pairs $(\hat{\mathbf{w}}_j(\mathbf{k}, x_d), \hat{h}_j(\mathbf{k}))$, $j = 1, 2$, are linearly independent for all $\mathbf{k} \neq 0$.

3.4 Solution Behavior

In this section we summarize several characteristic features of surface gravity waves and of surface gravity wave groups.

3.4.1 Evolution of Local Disturbances

The dispersive behavior of the surface gravity waves implies that the velocity of the waves varies with the wave number. This is apparent from expression (3.37) for the phase velocity. Consequently, the Fourier modes that are present in an initially local disturbance in the flow appear later at different positions. This well-known phenomenon is also described in the classical references [37, 44].

To illustrate this behavior, we consider the evolution of the free-surface displacement for a stagnant inviscid free-surface flow in two spatial dimensions, i.e., $v_1^{(0)} = 0$, $\mu = 0$ and $d = 2$, in the case that the infinitesimal initial displacement of the free surface is given by

$$h_0(x) = \mathrm{e}^{-x^2}\,, \qquad -\infty < x < \infty\,. \tag{3.45}$$

The Fourier components of the initial displacement $h_0(x)$ are

$$\hat{h}_0(k) := \frac{1}{2\pi}\int_{-\infty}^{\infty} h_0(x)\,\mathrm{e}^{-\mathrm{i}kx}\,\mathrm{d}x = \frac{\mathrm{e}^{-k^2/4}}{2\sqrt{\pi}}\,. \tag{3.46}$$

The infinitesimal free-surface displacement is expressed by (3.43b). Considering the typical case $\theta_2(k) = 0$, we obtain that the infinitesimal free-surface displacement is given by the wave group

$$h(x,t) = \int_{-\infty}^{\infty} \frac{\mathrm{e}^{-k^2/4}}{2\sqrt{\pi}} \exp\left(\mathrm{i}kx + \mathrm{i}\sqrt{\mathrm{Fr}^{-2}|k|\tanh|k|}\, t\right) \mathrm{d}k \,. \tag{3.47}$$

Figure 3.2 plots the real part of $h(x,t)$ according to (3.47) for $\mathrm{Fr} = \frac{1}{2}$. The separation of the Fourier components with different wave numbers that occurs due to the dispersive behavior of the surface gravity waves is indeed apparent.

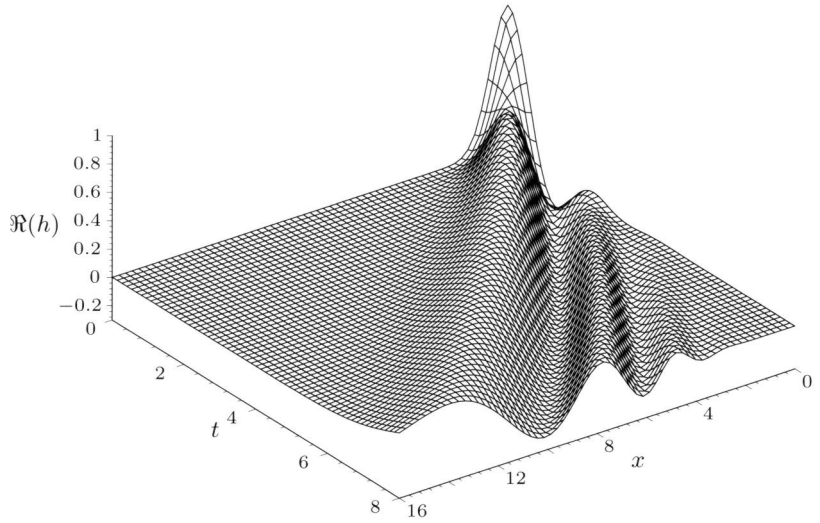

Figure 3.2: Evolution of a local disturbance in the free-surface position according to (3.47).

3.4.2 Steady Waves

Equations (3.39)–(3.40) imply that a surface gravity wave with wave number $\mathbf{k}$ is steady if the dispersion relation (3.33) has a root $\omega_j(\mathbf{k}) = 0$. For inviscid flows ($\mu = 0$), it follows from (3.34) that this occurs for $\mathbf{k}$ such that

$$\left(\mathbf{v}^{(0)} \cdot \mathbf{k}\right)^2 = \mathrm{Fr}^{-2}|\mathbf{k}|\tanh|\mathbf{k}| \,. \tag{3.48}$$

Without loss of generality, below we assume that the reference velocity is chosen such that $|\mathbf{v}^{(0)}| = 1$.

For $d = 2$, equation (3.48) yields a relation between the wave number and the Froude number:

$$|k|^{-1} \tanh |k| = \mathrm{Fr}^2 \,. \tag{3.49}$$

For subcritical flows, i.e., for $\mathrm{Fr} < 1$, equation (3.49) specifies a unique relation between the Froude number and the wave length $\lambda := 2\pi/k$. Figure 3.3 displays the relation between the wave length of the steady surface gravity wave and the Froude number, according to (3.49). For supercritical flows ($\mathrm{Fr} > 1$) a solution

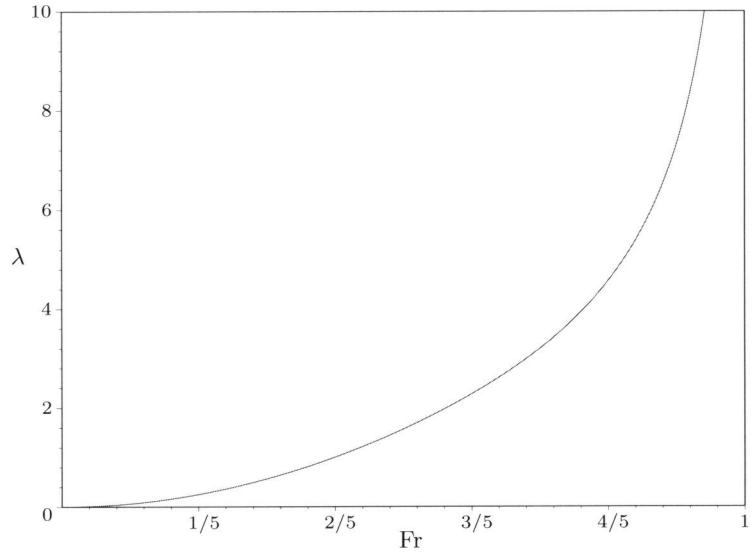

Figure 3.3: Relation between the wave length, λ, and the Froude number, Fr, for steady surface gravity waves in a channel of unit depth.

to (3.49) does not exists and, accordingly, a steady surface gravity wave does not occur.

To facilitate the derivation of the steady waves for $d = 3$, we assume, without loss of generality, that $\mathbf{v}^{(0)} = \mathbf{e}_1$, so that $\mathbf{v}^{(0)} \cdot \mathbf{k} = k_1$. Equation (3.48) then yields the following relation between k_1, k_2 and Fr:

$$\frac{k_1^2}{\sqrt{k_1^2 + k_2^2} \tanh \sqrt{k_1^2 + k_2^2}} = \mathrm{Fr}^{-2} \,. \tag{3.50}$$

Figure 3.4 on the next page displays curves in the (k_1, k_2)-plane on which the condition (3.50) is fulfilled for different values of Fr^{-2}. From Figure 3.4 it becomes apparent that for $d = 3$ the inviscid free-surface flow problem allows surface gravity waves with unbounded $|\mathbf{k}|$. From (3.36) it follows that these high wave number modes are effectively removed by viscosity.

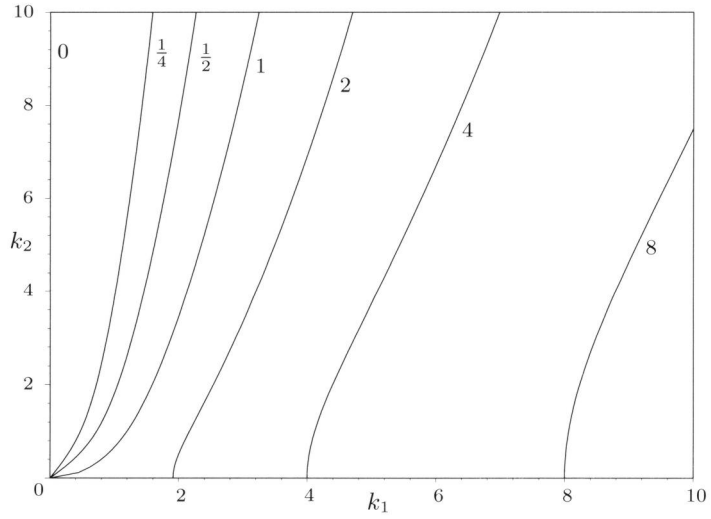

Figure 3.4: Wave-number curves of steady surface gravity waves in 3 dimensions for $\mathrm{Fr}^{-2} = 0, \frac{1}{4}, \frac{1}{2}, 1, 2, 4, 8$.

3.4.3 Asymptotic Temporal Behavior of Wave Groups

The asymptotic temporal behavior of a group of inviscid surface gravity waves is determined by the asymptotic properties of the inverse Fourier transforms in (3.43), with $\omega_j(\mathbf{k})$ by (3.34) and $\mu = 0$. The behavior of these integral transforms for $t \to \infty$ can be determined by means of the asymptotic expansion

$$\int_0^\infty \hat{f}(k) \exp\bigl(\mathrm{i}\xi(k)t\bigr)\,\mathrm{d}k = \hat{f}(k_0)\sqrt{\frac{2\pi}{|\xi''(k_0)|t}}\exp\bigl(\mathrm{i}[\xi(k_0)t + \tfrac{1}{4}\pi\,\mathrm{sign}\,\xi''(k_0)]\bigr) + O(e^{-\beta t}), \quad (3.51)$$

with β a positive constant, $\hat{f}(k)$ an analytic function and k_0 a stationary point of $\xi(k)$, i.e., $\xi'(k_0) = 0$. The expansion (3.51) requires that $\xi(k)$ is smooth in the neighborhood of stationary points in the sense that the ratio $\xi'''(k_0)/|\xi''(k_0)|^{3/2}$ is small; see Ref. [37]. The method of stationary phase (sometimes called method of steepest descent) can be used to prove (3.51); see, e.g., Refs. [44, 79].

The inverse Fourier transforms in (3.43) can be evaluated for $t \to \infty$ by introducing a suitable coordinate transformation for $\mathbf{k}$ and applying (3.51) recursively with respect to the transformed coordinates. The following asymptotic behavior

of the inverse Fourier transforms (3.43) is then obtained:

$$(2\pi/t)^{(d-1)/2}\big(\det \mathbf{H}(\mathbf{k}_0)\big)^{-1/2} \exp\big(\mathrm{i}\xi(\mathbf{k}_0)t + \mathrm{i}\zeta\big) + O(e^{-\beta t}), \tag{3.52a}$$

as $t \to \infty$, where

$$\xi(\mathbf{k}) := \mathbf{k}\cdot\mathbf{x}/t + \omega_j(\mathbf{k})\,, \tag{3.52b}$$

$\mathbf{H}(\mathbf{k})$ denotes its Hessian and ζ is a multiple of $\pi/4$ depending on the properties of the Hessian; see also Ref. [78].

If $\mu = 0$ in (3.34), then for fixed $\mathbf{x}$ and $t \to \infty$, a stationary point $\mathbf{k}_0$ of $\xi(\mathbf{k})$ occurs when

$$\frac{\partial\Phi(\mathbf{k})}{\partial k_j} = \mathrm{Fr}^{-1}\frac{\tanh|\mathbf{k}| + |\mathbf{k}|(1-\tanh^2|\mathbf{k}|)}{2\sqrt{|\mathbf{k}|\tanh|\mathbf{k}|}}\frac{k_j}{|\mathbf{k}|} = v_j^{(0)}, \qquad j = 1,\ldots,d-1. \tag{3.53}$$

Without loss of generality, we assume that $\mathbf{v}^{(0)}$ is scaled such that $|\mathbf{v}^{(0)}| = 1$. A necessary and sufficient condition for a stationary point to exist is $\mathrm{Fr}^{-2}\Lambda(|\mathbf{k}|) = 1$, with

$$\Lambda(|\mathbf{k}|) := \frac{(\tanh|\mathbf{k}| + |\mathbf{k}|(1-\tanh^2|\mathbf{k}|))^2}{4\,|\mathbf{k}|\tanh|\mathbf{k}|}. \tag{3.54}$$

One can show that $\Lambda(|\mathbf{k}|)$ is a bijection from $\mathbb{R}_+$ to $(0,1]$. Therefore, a stationary point exists iff $\mathrm{Fr} \le 1$, i.e., for subcritical flows. This stationary point corresponds to a wave of which the group velocity (see, e.g., [44, 78]) equals the flow-velocity. Consequently, the energy associated with this wave remains at a fixed position and decays only due to dispersion.

By (3.52a), at subcritical Froude numbers the asymptotic temporal behavior of the wave groups in (3.43) in $\mathbb{R}^d$ is $O(t^{(1-d)/2})$ as $t \to \infty$. In particular, the wave groups attenuate as $1/\sqrt{t}$ in $\mathbb{R}^2$ and as $1/t$ in $\mathbb{R}^3$. At supercritical Froude numbers, a stationary point of $\xi(\mathbf{k})$ does not exist and the first term in (3.52a) disappears. The wave groups then vanish exponentially as $t \to \infty$.

3.4.4 Free-Surface Boundary Layer

A particular feature of viscous free-surface flows is the boundary layer that is present in the vicinity of the free surface. The boundary layer of a surface gravity wave (3.39) is contained in the viscous contribution (3.39d). From (3.39d) it follows that the typical structure of the free-surface boundary layer is

$$\frac{\cosh\big(\sigma_j(1+x_d)\big)}{\sinh\sigma_j}\,, \tag{3.55a}$$

and

$$\frac{\sinh\big(\sigma_j(1+x_d)\big)}{\sinh\sigma_j}\,, \tag{3.55b}$$

for the horizontal and vertical velocity components, respectively. The pressure does not exhibit a free surface boundary layer.

Figure 3.5 plots the modulus of (3.55a) versus the vertical coordinate for several values of μ. The modulus of (3.55b) behaves similarly. The setting of the remaining parameters is $\mathrm{Fr} = \sqrt{\tanh 1}$, $k_1 = 1$ and $k_2 = 0$. In the absence of viscosity, this setting corresponds to a steady surface gravity wave with $d = 2$; cf. (3.49). To create Fig. 3.5, for each value of μ we extracted the Ω closest to $-\mathrm{i}$ from (3.33) and, subsequently, we obtained the corresponding σ from (3.28b). The free-surface boundary layer structure is apparent in Figure 3.5.

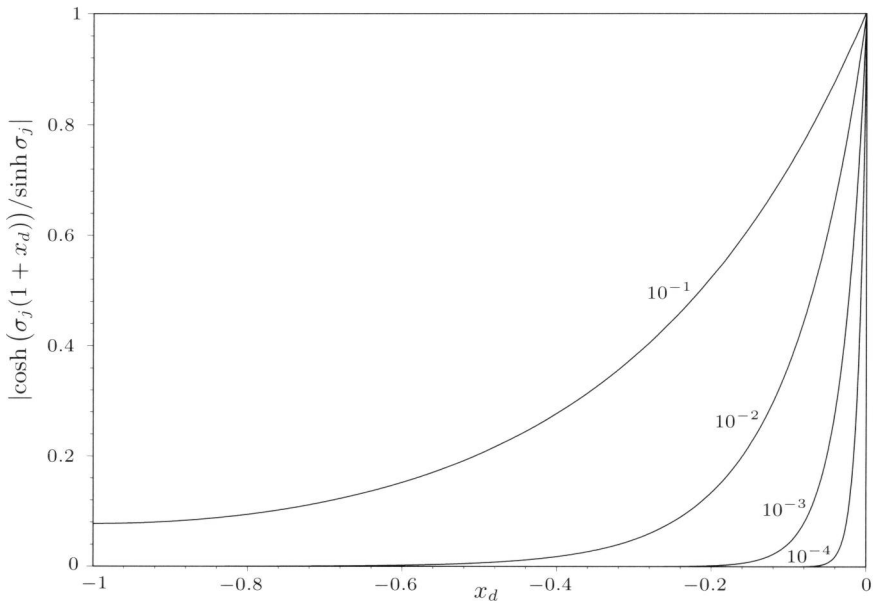

Figure 3.5: Structure of the free-surface boundary layer according to (3.55a) for $\mu = 10^{-1}, 10^{-2}, 10^{-3}, 10^{-4}$, with $\mathrm{Fr} = \sqrt{\tanh 1}$, $k_1 = 1$ and $k_2 = 0$.

The free-surface boundary layer is *weak* in the sense that the boundary layer vanishes as $\mu \to 0$. From (3.33) it follows that

$$\Omega_j = O(1)\,, \qquad \text{as } \mu \to 0\,. \tag{3.56}$$

The definition (3.28b) then implies

$$\sigma_j = O(1/\sqrt{\mu})\,, \qquad \text{as } \mu \to 0\,. \tag{3.57}$$

Hence, by (3.39), the viscous contribution to the horizontal velocity is $O(\sqrt{\mu})$ and the viscous contribution to the vertical velocity is only $O(\mu)$. This result is consistent with the statement in [5] that the velocity deviation through the free-surface

boundary layer is $O(1/\sqrt{\mathrm{Re}})$. The above implies that the free-surface boundary layer indeed vanishes as $\mu \to 0$. In contrast, the deviation of the horizontal and vertical velocities through the boundary layer near a rigid no-slip boundary is $O(1)$ and $O(\sqrt{\mu})$, respectively; see, e.g., Ref. [35]. Hence, the boundary layer near a rigid no-slip boundary persists as $\mu \to 0$.

Chapter 4

Efficient Numerical Solution of Steady Free-Surface Navier–Stokes Flows

4.1 Introduction

The numerical solution of flows that are partially bounded by a freely moving boundary is of great importance in ship hydrodynamics [3, 12, 17, 45], hydraulics, and many other practical applications, such as coating technology [54, 55]. In ship hydrodynamics, an important area of application is the prediction of the wave pattern that is generated by the ship at forward speed in still water. This wave generation is responsible for a substantial part of the ship's resistance and, therefore, it should be minimized by a proper hull form design. Computational methods play an important role in this design process. Most computational tools that are currently in use for solving gravity subjected free-surface flows around a surface-piercing body rely on a potential flow approximation. Present developments primarily concern the solution of the free-surface Navier–Stokes (or RANS) flow problem.

For time-dependent free-surface flows, generally there is no essential difference in the treatment of the free surface between numerical methods for potential flow or Navier–Stokes flow. Typically, the solution of the flow equations and the adaptation of the free boundary are separated. Each time step begins with computing the flow field with the dynamic conditions imposed at the free surface. Next, the free surface is adjusted through the kinematic condition, using the newly computed velocity field.

For *steady* free-surface flows, however, such a conformity of approaches for viscous and inviscid flow cannot be observed. For instance in ship hydrodynamics, whereas dedicated techniques have been developed for solving the free-surface potential flow problems (see, e.g., Ref. [51]), methods for Navier–Stokes flow usually continue the aforementioned transient process until a steady state is reached (see, e.g., Refs. [3, 12]). However, this time-integration method is often computation-

ally inefficient. In general, the convergence to steady state is retarded by slowly attenuating transient surface gravity waves. Moreover, the separate treatment of the flow equations and the kinematic condition yields a restriction on the allowable time-step. Due to the specific transient behavior of free-surface flows and the time-step restriction, the performance of the time-integration method deteriorates rapidly with decreasing mesh width. In practical computations, tens of thousands of time steps are often required, rendering the time-integration approach prohibitively expensive in actual design processes.

Several approaches have been suggested to improve the efficiency of time-integration methods, e.g., pseudo-time integration and quasi-steady methods; see Refs. [17, 75]. It appears that these approaches indeed improve the efficiency, but do not essentially improve the asymptotic convergence behavior of the time-integration method.

Alternative solution methods for steady free-surface Navier–Stokes flow exist, but they have not been widely applied in the field of ship hydrodynamics. In the field of coating technology successive approximation techniques are often employed, in particular, kinematic iteration and dynamic iteration [55]. Kinematic iteration imposes the dynamic conditions at the free surface and uses the kinematic condition to displace the boundary. Dynamic iteration imposes the kinematic and the tangential dynamic conditions at the free surface and uses the normal dynamic condition to adjust the boundary position. However, the convergence behavior of both iteration schemes depends sensitively on parameters in the problem; see, e.g., Refs. [11, 58]. A method that avoids the deficiencies of the aforementioned iterative methods, is Newton iteration of the full equation set [55]. The positions of the (free-surface) grid nodes are then added as additional unknowns and all equations, including the free-surface conditions, are solved simultaneously. An objection to this method is that simultaneous treatment of all equations is infeasible for problems with many unknowns, such as three-dimensional problems and problems requiring sharp resolution of boundary layers. Finally, the free-surface flow problem can be reformulated into an optimal shape design problem, which can then in principle be solved efficiently by the adjoint optimization method. A problem with this approach is its complexity: although much progress has been made in the formulation of adjoint equations for problems from fluid dynamics, including the Navier–Stokes equations [21], setting up the adjoint method remains involved. Moreover, efficiency is only obtained if proper preconditioning is applied [66, 68], and constructing the preconditioner for the free-surface Navier–Stokes flow problem is intricate.

The current work presents an iterative method for efficiently solving steady free-surface Navier–Stokes flow problems. Although our interest is the previously outlined ship hydrodynamics application, it is anticipated that the method is also applicable to other gravity dominated steady viscous free-surface flows at high Reynolds numbers, such as occur, for instance, in hydraulics. The proposed method is analogous to the method for solving steady free-surface potential flow problems presented in [51]. The method alternatingly solves the steady Navier–

Stokes equations with a so-called quasi free-surface condition imposed at the free surface, and adjusts the free surface using the computed solution. The quasi free-surface condition ensures that the disturbance induced by the subsequent displacement of the boundary is negligible. Each surface adjustment then yields an improved approximation to the actual free-boundary position.

The contents of this chapter are organized as follows: In Section 4.2 the equations governing incompressible, viscous free-surface flow are stated and the quasi free-surface condition is derived. Section 4.3 proves that the usual time-integration approach is generally unsuitable for solving steady free-surface flows. Section 4.4 outlines the iterative solution method and examines its convergence behavior. Numerical experiments and results for a two-dimensional test case are presented in Section 4.5. The application to actual ship wave computations is in progress and will be reported in a sequel. Section 4.6 contains concluding remarks.

4.2 Governing Equations

4.2.1 Incompressible Viscous Flow

An incompressible, viscous fluid flow, subject to a constant gravitational force is considered. Although only steady solutions are of interest, for the purpose of analysis the equations are considered in time-dependent form.

The fluid occupies an open, time-dependent domain $\mathcal{V}_\eta \subset \mathbb{R}^d$ $(d = 2, 3)$, which is enclosed by the free boundary, $\mathcal{S}_\eta$, and a fixed boundary, $\partial\mathcal{V}_\eta \setminus \mathcal{S}_\eta$. Positions in $\mathbb{R}^d$ are identified by their horizontal coordinates $(x_1, \ldots, x_{d-1})$ and a vertical coordinate y, with respect to the Cartesian base vectors $\mathbf{e}_1, \ldots, \mathbf{e}_{d-1}$ and $\mathbf{j}$, respectively. The origin is located in the undisturbed free surface $\mathcal{S}_0$, and the gravitational acceleration, $\mathbf{g}$, acts in the negative vertical direction. We consider free surfaces that can be represented by a so-called *height function*, i.e., $\mathcal{S}_\eta = \{(\mathbf{x}, \eta(\mathbf{x}, t))\}$. The height function η is assumed to be a smooth function of the horizontal coordinates and time. See Figure 4.1 on the following page for an illustration.

The distinguishing parameters of the viscous free-surface flow problem are the Froude number, $\mathrm{Fr} := U/\sqrt{g\ell}$, and the Reynolds number, $\mathrm{Re} := \rho U\ell/\mu$, with U an appropriate reference velocity, g the gravitational acceleration, ℓ a reference length and μ the dynamic viscosity of the fluid. The fluid density ρ is assumed to be constant. The state of the flow is then characterized by the (non-dimensionalized) fluid velocity $\mathbf{v}(\mathbf{x}, y, t)$ and pressure $p(\mathbf{x}, y, t)$. Incompressibility of the fluid implies that the velocity field is solenoidal:

$$\operatorname{div} \mathbf{v} = 0, \qquad (\mathbf{x}, y) \in \mathcal{V}_\eta, t > 0. \tag{4.1a}$$

Conservation of momentum in the fluid is described by the Navier–Stokes equations. The pressure is separated into a hydrodynamic component φ and a hydrostatic contribution as $p(\mathbf{x}, y, t) = \varphi(\mathbf{x}, y, t) - \mathrm{Fr}^{-2} y$. Because the gradient of the

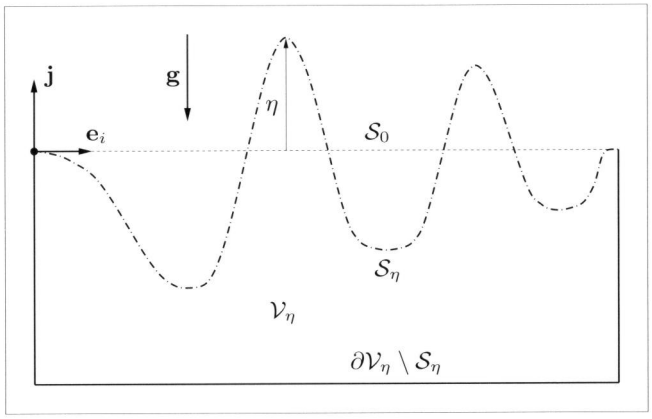

Figure 4.1: Schematic illustration of the free-surface flow problem.

hydrostatic pressure and the gravitational force cancel, the Navier–Stokes equations for a gravity subjected incompressible fluid read:

$$\frac{\partial \mathbf{v}}{\partial t} + \operatorname{div} \mathbf{v}\mathbf{v} + \boldsymbol{\nabla}\varphi - \operatorname{div} \boldsymbol{\tau}(\mathbf{v}) = 0, \qquad (\mathbf{x}, y) \in \mathcal{V}_\eta, t > 0, \tag{4.1b}$$

where $\boldsymbol{\tau}(\mathbf{v})$ is the viscous stress tensor for an incompressible Newtonian fluid:

$$\boldsymbol{\tau}(\mathbf{v}) := \mathrm{Re}^{-1}\big((\boldsymbol{\nabla}\mathbf{v}) + (\boldsymbol{\nabla}\mathbf{v})^T\big). \tag{4.1c}$$

Our primary interest is in turbulent flows. We consider the Reynolds Averaged Navier–Stokes (RANS) equations, supplemented with a turbulence model that is based on eddy viscosity. For our purpose, the RANS equations are essentially the same as the Navier–Stokes equations, with the important difference that the RANS equations have steady solutions even at the envisaged high Reynolds numbers.

4.2.2 Free-Surface Conditions

Free-surface flows are essentially two-fluid flows, of which the properties of the contiguous bulk fluids are such that their mutual interaction at the interface can be ignored. For an elaborate discussion of two-fluid flows, see, e.g., Refs. [4, 57]. The free-surface conditions follow from the general interface conditions and the assumptions that both density and viscosity of the adjacent fluid vanish at the interface and, furthermore, that the interface is impermeable. Here it will moreover be assumed that interfacial stresses can be ignored, which is a valid assumption in the practical applications envisaged.

On the free surface, the fluid satisfies a kinematic condition and d dynamic conditions. Impermeability of the free surface is expressed by the kinematic condition

$$\frac{\partial \eta}{\partial t} + \mathbf{v} \cdot \boldsymbol{\nabla}(\eta - y) = 0, \qquad (\mathbf{x}, y) \in \mathcal{S}_\eta, t > 0. \tag{4.2a}$$

Supposed that the viscous contribution to the normal stress at the free surface is negligible, continuity of stresses at the interface requires that the pressure vanishes at the free surface. This results in the normal dynamic condition

$$\varphi - \mathrm{Fr}^{-2}\eta = 0, \qquad (\mathbf{x}, y) \in \mathcal{S}_\eta, t > 0. \tag{4.2b}$$

The requirement that the tangential stress components vanish at the free surface is expressed by the $d-1$ tangential dynamic conditions

$$\mathbf{t}^i \cdot \boldsymbol{\tau}(\mathbf{v}) \cdot \mathbf{n} = 0, \qquad (\mathbf{x}, y) \in \mathcal{S}_\eta, t > 0. \tag{4.2c}$$

Here, $\mathbf{t}^i$ $(i = 1, \ldots, d-1)$ are orthogonal unit tangent vectors to $\mathcal{S}_\eta$ and $\mathbf{n}$ denotes the unit normal vector to $\mathcal{S}_\eta$.

One may note that the number of free-surface conditions for the viscous free-surface flow problem is $d+1$. The incompressible Navier–Stokes equations in $\mathbb{R}^d$ require d boundary conditions. Hence, the number of free-surface conditions is indeed one more than the number of required boundary conditions.

4.2.3 Quasi Free-Surface Condition

A fundamental problem in analyzing and computing free-surface flow problems, is the interdependence of the state variables $\mathbf{v}, p$ and their spatial domain of definition through the free-surface conditions. This problem can be avoided by deriving a condition that holds to good approximation on a fixed boundary in the neighborhood of the actual free boundary. We refer to such a condition as a *quasi free-surface condition*, because the qualitative solution behavior of the initial boundary value problem with this condition imposed is similar to that of the free-boundary problem, but the boundary does not actually move. A suitable quasi free-surface condition for the free-surface Navier–Stokes flow problem is derived below.

Let $\mathcal{S}_\eta$ denote the actual free surface, as defined before. In a similar manner, a nearby fixed boundary $\mathcal{S}_\theta := \{(\mathbf{x}, \theta(\mathbf{x}))\}$ is introduced, with $\theta(\mathbf{x})$ a smooth function on $\mathcal{S}_0$. We require that $\mathcal{S}_\theta$ is close to the actual free surface in such a manner that

$$\delta(\mathbf{x}, t) := \eta(\mathbf{x}, t) - \theta(\mathbf{x})\,, \tag{4.3}$$

is small and sufficiently smooth. In particular, for all $t > 0$, δ must satisfy $\|\delta\|_{\mathcal{S}_\theta} + \|\boldsymbol{\nabla}\delta\|_{\mathcal{S}_\theta} + \|\delta_t\|_{\mathcal{S}_\theta} \leq \epsilon$, for some $\epsilon \ll 1$. Here $\|\cdot\|_{\mathcal{S}_\theta}$ is a suitable norm on the approximate boundary. Assuming that p and $\mathbf{v}$ can be extended smoothly beyond the boundary $\mathcal{S}_\theta$, Taylor expansion in the neighborhood of $\mathcal{S}_\theta$ yields for p and $\mathbf{v}$

at the actual free surface,

$$p(\mathbf{x}, \eta(\mathbf{x},t), t) = p(\mathbf{x}, \theta(\mathbf{x}), t) + \delta(\mathbf{x},t)\, \mathbf{j}\cdot\boldsymbol{\nabla} p(\mathbf{x}, \theta(\mathbf{x}), t) + O(\epsilon^2), \tag{4.4a}$$

$$\mathbf{v}(\mathbf{x}, \eta(\mathbf{x},t), t) = \mathbf{v}(\mathbf{x}, \theta(\mathbf{x}), t) + \delta(\mathbf{x},t)\, \mathbf{j}\cdot\boldsymbol{\nabla} \mathbf{v}(\mathbf{x}, \theta(\mathbf{x}), t) + O(\epsilon^2), \tag{4.4b}$$

The normal dynamic condition (4.2b) demands that the left-hand side of (4.4a) vanishes. Hence, the elevation of the free surface can be expressed in terms of the pressure and its gradient at the approximate surface:

$$\eta(\mathbf{x},t) = \theta(\mathbf{x}) - \frac{p(\mathbf{x}, \theta(\mathbf{x}), t)}{\mathbf{j}\cdot\boldsymbol{\nabla} p(\mathbf{x}, \theta(\mathbf{x}), t)} + O(\epsilon^2)\,. \tag{4.5}$$

To obtain an $O(\epsilon^2)$ accurate quasi free-surface condition, i.e., an $O(\epsilon^2)$ approximation of the conditions at $\mathcal{S}_\theta$, $\mathbf{v}$ and η in the kinematic condition (4.2a) can be replaced by (4.4b) and (4.5), respectively. The resulting condition is, however, intractable. Instead, two additional assumptions concerning $\mathbf{v}$ and p are introduced to obtain a convenient quasi free-surface condition. The first assumption is that the vertical derivative of the pressure is dominated by the hydrostatic component, $-\mathrm{Fr}^{-2}$. Generally, this assumption is valid for waves of moderate steepness. Specifically, we suppose that a constant $\sigma_p \ll 1$ exists such that for all $t > 0$,

$$\|1 + \mathrm{Fr}^2\, \mathbf{j}\cdot\boldsymbol{\nabla} p\|_{\mathcal{S}_\theta} \leq \sigma_p\,. \tag{4.6}$$

The second assumption is that the vertical derivative of $\mathbf{v}$ is small, in such a manner that a constant $\sigma_{\mathbf{v}} \ll 1$ exists with the property that for all $t > 0$,

$$\|\mathbf{j}\cdot\boldsymbol{\nabla}\mathbf{v}\|_{\mathcal{S}_\theta} \leq \sigma_{\mathbf{v}}\,. \tag{4.7}$$

Under this assumption, the velocity at the actual free boundary, $\mathbf{v}(\mathbf{x}, \eta(\mathbf{x},t), t)$, can be accurately approximated by the velocity at the fixed boundary, $\mathbf{v}(\mathbf{x}, \theta(\mathbf{x}), t)$. By (4.4b), the error in the approximation is only $O(\epsilon\sigma_{\mathbf{v}})$. In [5] it is shown that the velocity-deviation through the free-surface boundary layer is proportional to the surface curvature and $1/\sqrt{\mathrm{Re}}$. Moreover, $\sigma_{\mathbf{v}}$ in (4.7) increases with the wave steepness. Therefore, the assumption $\sigma_{\mathbf{v}} \ll 1$ is valid if the steepness and curvature of the free-surface waves are moderate and if Re is sufficiently large.

Under the above assumptions a convenient quasi free-surface condition can be derived. Substitution of the hydrostatic approximation of the pressure gradient in (4.5) yields

$$\eta(\mathbf{x},t) = \theta(\mathbf{x}) - \frac{p(\mathbf{x}, \theta(\mathbf{x}), t)}{-\mathrm{Fr}^{-2}(1 + O(\sigma_p))} = \theta(\mathbf{x}) + \mathrm{Fr}^2 p(\mathbf{x}, \theta(\mathbf{x}), t)(1 + O(\sigma_p))\,. \tag{4.8}$$

The dynamic condition (4.2b) and (4.4a) imply that $p = O(\epsilon)$ on $\mathcal{S}_\theta$. Hence, ignoring terms $O(\epsilon^2, \epsilon\sigma_p)$, the free-surface elevation is related to the hydrodynamic pressure at the approximate boundary by

$$\eta(\mathbf{x},t) = \theta(\mathbf{x}) + \mathrm{Fr}^2 p(\mathbf{x}, \theta(\mathbf{x}), t) = \mathrm{Fr}^2 \varphi(\mathbf{x}, \theta(\mathbf{x}), t)\,. \tag{4.9}$$

To transfer the kinematic condition (4.2a) to the approximate surface $\mathcal{S}_\theta$, η is replaced by (4.9) and $\mathbf{v}$ on $\mathcal{S}_\eta$ is replaced by $\mathbf{v}$ on $\mathcal{S}_\theta$. The error thus introduced is only $O(\epsilon^2, \epsilon\sigma_p, \epsilon\sigma_\mathbf{v})$. Special care is required in expressing the gradient of η, because (4.9) relates η to φ on the curvilinear surface $\mathcal{S}_\theta$:

$$\boldsymbol{\nabla}\eta = \mathrm{Fr}^2 \frac{d\varphi}{d\mathbf{x}} = \mathrm{Fr}^2 \Big(\frac{\partial \varphi}{\partial \mathbf{x}} + \frac{\partial \varphi}{\partial y} \frac{\partial \theta}{\partial \mathbf{x}} \Big) = \mathrm{Fr}^2 \Big(\boldsymbol{\nabla}\varphi + \frac{\partial \varphi}{\partial y} \Big(\frac{\partial \theta}{\partial \mathbf{x}} - \mathbf{j} \Big) \Big) \,. \tag{4.10}$$

It then follows that

$$\frac{\partial \eta}{\partial t} + \mathbf{v} \cdot \boldsymbol{\nabla}(\eta - y) = \mathrm{Fr}^2 \Big(\frac{\partial \varphi}{\partial t} + \mathbf{v} \cdot \boldsymbol{\nabla}(\varphi - \mathrm{Fr}^{-2} y) \Big) + \mathrm{Fr}^2 \frac{\partial \varphi}{\partial y} \mathbf{v} \cdot \Big(\frac{\partial \theta}{\partial \mathbf{x}} - \mathbf{j} \Big) + O(\epsilon^2, \epsilon\sigma_p, \epsilon\sigma_\mathbf{v}) = 0 \,. \tag{4.11}$$

Using the kinematic condition (4.2a) and definition (4.3), the second term on the right-hand side of (4.11) can be recast into

$$\mathrm{Fr}^2 \frac{\partial \varphi}{\partial y} \mathbf{v} \cdot \boldsymbol{\nabla}(\theta - y) = \mathrm{Fr}^2 \frac{\partial \varphi}{\partial y} \mathbf{v} \cdot \boldsymbol{\nabla}(\eta - \delta - y) = -\mathrm{Fr}^2 \frac{\partial \varphi}{\partial y} (\mathbf{v} \cdot \boldsymbol{\nabla}\delta + \delta_t) \tag{4.12}$$

By virtue of the smoothness of δ, the term in parenthesis is just $O(\epsilon)$ and (4.12) is only $O(\epsilon\sigma_p)$. The second term on the right-hand side of (4.11) can therefore be ignored. Hence, it follows that

$$\frac{\partial \varphi}{\partial t} + \mathbf{v} \cdot \boldsymbol{\nabla}(\varphi - \mathrm{Fr}^{-2} y) = 0 \,, \tag{4.13}$$

approximates the conditions at the boundary $\mathcal{S}_\theta$ to $O(\epsilon^2, \epsilon\sigma_p, \epsilon\sigma_\mathbf{v})$. This implies that (4.13) is a quasi free-surface condition on any fixed boundary that is sufficiently close to the actual free surface, provided that (4.6) and (4.7) are fulfilled.

One may note that (4.13) is exactly satisfied at the actual free surface. Therefore, the quasi free-surface condition can replace either the kinematic condition (4.2a) or the normal dynamic condition (4.2b) in the formulation of the free-surface conditions in §4.2.2.

The importance of the quasi free-surface condition is that the quasi free-surface flow solution, i.e., the solution of the Navier–Stokes equations with (4.13) and (4.2c) imposed at a fixed boundary in the neighborhood of the actual free surface, is an accurate approximation to the actual free-surface flow solution. Because the tangential dynamic conditions are largely irrelevant to the shape of the free surface (see Ref. [5]), it is anticipated that the change in the solution due to imposing (4.2c) at $\mathcal{S}_\theta$ instead of $\mathcal{S}_\eta$ is negligible. In that case, if (4.13) holds at $\mathcal{S}_\theta$, then the free surface conditions (4.2b) and (4.2a) are satisfied to $O(\epsilon^2, \epsilon\sigma_p, \epsilon\sigma_\mathbf{v})$ at the boundary

$$\{(\mathbf{x}, \mathrm{Fr}^2 \varphi(\mathbf{x}, \theta(\mathbf{x}, t)))\} \,. \tag{4.14}$$

Therefore, the solution of the quasi free-surface flow problem is an $O(\epsilon^2, \epsilon\sigma_p, \epsilon\sigma_\mathbf{v})$ approximation to the solution of the free-surface flow problem. Moreover, (4.14)

is an equally accurate approximation of the actual free-surface position. One may note that (4.14) just uses the normal dynamic condition to determine the position of the free surface.

4.3 Time Integration Methods

The most widely applied iterative method for solving gravity dominated steady free-surface Navier–Stokes flow is alternating time integration of the kinematic condition, and the Navier–Stokes equations subject to the dynamic conditions, until steady state is reached. This section examines the computational complexity of this time-integration method, i.e., the number of operations per grid point expended in the solution process.

The computational complexity of the time-integration method depends on the physical time that is required to reduce transient wave components in the initial estimate to the level of other errors in the numerical solution. The transient behavior of surface gravity waves therefore plays an essential part in the complexity analysis. This transient behavior is discussed in detail in Chapter 3. Sections 4.3.1 and 4.3.2 below summarize the main results. The implications on the computational complexity is examined in Section 4.3.3.

4.3.1 Surface Gravity Waves

We consider the specific case of a small amplitude disturbance of a uniform horizontal flow on a domain $\mathcal{V} \subset \mathbb{R}^d$ of infinite horizontal extent and unit vertical extent. The domain is bounded by the undisturbed free surface $\mathcal{S}_0 := \{(\mathbf{x}, 0)\}$ and a rigid impermeable free-slip bottom $\mathcal{B} := \{(\mathbf{x}, -1)\}$. The uniform flow velocity is $\mathbf{v}^{(0)} := (v_1^{(0)}, \ldots, v_{d-1}^{(0)}, 0)$, with $|v^{(0)}| = 1$. The above implies that the undisturbed fluid-depth and flow velocity are designated as reference length and velocity, respectively.

Suppose that a disturbance is generated in the flow, such that for all $t > 0$ the resulting surface elevation satisfies $\|\eta\|_{\mathcal{S}_0} + \|\boldsymbol{\nabla}\eta\|_{\mathcal{S}_0} + \|\eta_t\|_{\mathcal{S}_0} \leq \epsilon$, for some positive ϵ. We assume that the corresponding perturbed free-surface flow solution can be written as

$$\begin{pmatrix} \mathbf{v} \\ \varphi \end{pmatrix} (\mathbf{x}, y, t; \epsilon) = \begin{pmatrix} \mathbf{v}^{(0)} \\ 0 \end{pmatrix} + \epsilon \begin{pmatrix} \mathbf{v}^{(1)} \\ \varphi^{(1)} \end{pmatrix} (\mathbf{x}, y, t) + O(\epsilon^2), \qquad \text{as } \epsilon \to 0\,. \tag{4.15}$$

From §4.2.3 it follows that the solution of the quasi free-surface flow problem on $\mathcal{V}$ is an $O(\epsilon^2, \epsilon\sigma_p, \epsilon\sigma_{\mathbf{v}})$ approximation of the actual free-surface flow, with σ_p and $\sigma_{\mathbf{v}}$ defined by (4.6) and (4.7), respectively. However, (4.15) implies that σ_p and $\sigma_{\mathbf{v}}$ are of $O(\epsilon)$. Hence, the quasi free-surface flow solution on $\mathcal{V}$ is an $O(\epsilon^2)$ approximation to the actual free-surface flow solution. Consequently, for sufficiently small and smooth perturbations the results on the behavior of the quasi free-surface flow solution apply immediately to the behavior of the actual free-surface flow solution.

Suppose that the disturbance can be written as a linear combination of horizontal Fourier modes $\exp\bigl(\mathrm{i}\mathbf{k}\cdot\mathbf{x}+\mathrm{i}\omega t\bigr)$, with $\mathbf{k}\in\mathbb{R}^{d-1}$ the wave number of the Fourier mode and ω its radian frequency. Because the perturbed quasi free-surface flow problem is linear to $O(\epsilon^2)$, it suffices to consider a single mode. If the following Fourier mode is inserted for the perturbations in (4.15),

$$\begin{pmatrix} v_1^{(1)} \\ \vdots \\ v_{d-1}^{(1)} \\ v_d^{(1)} \\ \varphi^{(1)} \end{pmatrix}(\mathbf{x},y,t) = \begin{pmatrix} \mathrm{i}k_1\cosh(|\mathbf{k}|\,(1+y)) \\ \vdots \\ \mathrm{i}k_{d-1}\cosh(|\mathbf{k}|\,(1+y)) \\ |\mathbf{k}|\sinh(|\mathbf{k}|\,(1+y)) \\ (-1)^j\,\mathrm{i}\Phi(\mathbf{k})\cosh(|\mathbf{k}|\,(1+y)) \end{pmatrix}\exp\bigl(\mathrm{i}\mathbf{k}\cdot\mathbf{x}+\mathrm{i}\omega_j(\mathbf{k})\,t\bigr)\,, \tag{4.16a}$$

where $\omega_j(\mathbf{k})$ is either of the two roots of the dispersion relation:

$$\omega_j(\mathbf{k}) := -\mathbf{v}^{(0)}\cdot\mathbf{k}-(-1)^j\Phi(\mathbf{k}), \qquad j=1,2, \tag{4.16b}$$

and

$$\Phi(\mathbf{k}) := \sqrt{\mathrm{Fr}^{-2}|\mathbf{k}|\tanh(|\mathbf{k}|)}\,, \tag{4.16c}$$

then the corresponding $\mathbf{v}$ and φ comply to $O(\epsilon^2)$ with the quasi free-surface flow problem, except the tangential dynamic conditions (4.2c), which yield

$$\mathbf{t}^i\cdot\boldsymbol{\tau}(\mathbf{v})\cdot\mathbf{n} = \mathrm{Re}^{-1}\,\epsilon\,2\,\mathrm{i}\,k_j\,|\mathbf{k}|\sinh(|\mathbf{k}|)\exp\bigl(\mathrm{i}\mathbf{k}\cdot\mathbf{x}+\mathrm{i}\omega_j(\mathbf{k})\,t\bigr)\,. \tag{4.17}$$

Because (4.17) is only $O(\epsilon|\mathbf{k}|^3/\mathrm{Re})$ as $|\mathbf{k}|\to 0$, the error is negligible for sufficiently small $\mathbf{k}$ and large Re. Hence, equation (4.16a) accurately describes the behavior of smooth free-surface waves in a uniform horizontal flow at sufficiently high Reynolds numbers. The perturbations (4.16a) are called *surface gravity waves*. For an elaborate discussion of surface gravity waves in potential flow see, e.g., Refs. [37, 44].

4.3.2 Asymptotic Temporal Behavior

The asymptotic temporal behavior of surface gravity waves is determined by the asymptotic properties of the Fourier integral of the modes (4.16a). The behavior of the integral transform for $t\to\infty$ can be determined by means of the asymptotic expansion

$$\int_0^\infty F(k)\exp\bigl(\mathrm{i}t\psi(k)\bigr)\,\mathrm{d}k = F(k_0)\sqrt{\frac{2\pi}{t|\psi''(k_0)|}}\exp\bigl(\mathrm{i}[t\psi(k_0)+\tfrac{1}{4}\pi\,\mathrm{sign}\,\psi''(k_0)]\bigr)+O(e^{-\beta t}), \tag{4.18}$$

with β a positive constant, $F(k)$ an analytic function and k_0 a stationary point of $\psi(k)$, i.e., $\psi'(k_0) = 0$. The expansion (4.18) requires that $\psi(k)$ is smooth in the neighborhood of stationary points in the sense that the ratio $\psi'''(k_0)/|\psi''(k_0)|^{3/2}$ is small; see Ref. [37]. The method of stationary phase (sometimes called method of steepest descent) can be used to prove (4.18); see, e.g., Refs. [44, 79].

The Fourier integral of (4.16a) can be evaluated for $t \to \infty$ by introducing a suitable coordinate transformation for $\mathbf{k}$ and applying (4.18) recursively with respect to the transformed coordinates. Denoting by $\sigma(\mathbf{x}, y, t)$ a component in (4.16a) and by $\hat{\sigma}(\mathbf{k}, y)$ its Fourier transform, one obtains

$$\sigma(\mathbf{x}, y, t) = \hat{\sigma}(\mathbf{k}_0, y)\,(2\pi/t)^{(d-1)/2}\big(\det \mathbf{H}(\mathbf{k}_0)\big)^{-1/2} \exp\big(\mathrm{i}t\psi(\mathbf{k}_0) + \mathrm{i}\zeta\big) + O(e^{-\beta t}), \tag{4.19a}$$

as $t \to \infty$, where

$$\psi(\mathbf{k}) := \mathbf{k}\cdot\mathbf{x}/t + \omega_\alpha(\mathbf{k})\,, \tag{4.19b}$$

$\mathbf{H}(\mathbf{k})$ denotes its Hessian and ζ is a multiple of $\pi/4$ depending on the properties of the Hessian; see also [78]. By (4.16b) and (4.16c), for fixed $\mathbf{x}$ and $t \to \infty$, a stationary point $\mathbf{k}_0$ of $\psi(\mathbf{k})$ occurs when

$$\frac{\partial\Phi(\mathbf{k})}{\partial k_j} = \mathrm{Fr}^{-1}\frac{\tanh|\mathbf{k}| + |\mathbf{k}|(1-\tanh^2|\mathbf{k}|)}{2\sqrt{|\mathbf{k}|\tanh|\mathbf{k}|}}\frac{k_j}{|\mathbf{k}|} = v_j^{(0)}, \qquad j = 1, \ldots, d-1. \tag{4.20}$$

Assuming that $\mathbf{v}^{(0)}$ is scaled such that $|\mathbf{v}^{(0)}| = 1$, a sufficient and necessary condition for a stationary point to exist is $\mathrm{Fr}^{-2}\Lambda(|\mathbf{k}|) = 1$, with

$$\Lambda(|\mathbf{k}|) := \frac{(\tanh|\mathbf{k}| + |\mathbf{k}|(1-\tanh^2|\mathbf{k}|))^2}{4\,|\mathbf{k}|\tanh|\mathbf{k}|}. \tag{4.21}$$

One can show that $\Lambda(|\mathbf{k}|)$ is a bijection from $\mathbb{R}_+$ to $(0, 1]$. Therefore, a single stationary point exists iff $\mathrm{Fr} \le 1$, i.e., for subcritical flows. This stationary point corresponds to a wave of which the *group velocity* (see, e.g., Refs. [44, 78]) equals the flow-velocity. Consequently, the energy associated with this wave remains at a fixed position and decays only due to dispersion.

By (4.19a), at subcritical Froude numbers the asymptotic temporal behavior of the surface gravity waves (4.16) in $\mathbb{R}^d$ is $O(t^{(1-d)/2})$ as $t \to \infty$. In particular, surface gravity waves attenuate as $1/\sqrt{t}$ in $\mathbb{R}^2$ and as $1/t$ in $\mathbb{R}^3$. At supercritical Froude numbers, a stationary point of $\psi(\mathbf{k})$ does not exist and the first term in (4.19a) disappears. The surface gravity waves then vanish exponentially as $t \to \infty$.

4.3.3 Computational Complexity

Suppose the objective is to solve a steady free-surface flow problem by the time-integration method. The asymptotic temporal behavior of surface gravity waves can then be used to estimate the asymptotic computational complexity of the method.

Spatial discretization of the incompressible Navier–Stokes equations with appropriate boundary conditions on fixed boundaries and the free-surface conditions on the free boundary yields a discrete operator $\mathbf{L}_h : \mathcal{A}_h \mapsto \mathcal{B}_h$, with $\mathcal{A}_h$ denoting the space of grid functions on a grid with characteristic mesh width h. The operator $\mathbf{L}_h$ is assumed to be stable and pth order consistent, i.e., the *discretization error*, ϵ_h, is $O(h^p)$ as $h \to 0$.

Numerical time integration of the spatially discretized free-surface flow problem yields a sequence $\mathbf{q}_h^n \in \mathcal{A}_h$, $n = 0, 1, 2, \ldots$. The grid-function $\mathbf{q}_h^0$ is a restriction of initial conditions to the grid. Assuming the time step in the time-integration method, τ, to be constant, $\mathbf{q}_h^n$ approximates the solution of the free-surface flow problem at time $t = n\tau$. Suppose that the discretized free-surface flow problem has a unique solution $\mathbf{q}_h^* \in \mathcal{A}_h$, and that the sequence $\mathbf{q}_h^n$ indeed approaches $\mathbf{q}_h^*$ as $n\tau \to \infty$. The evaluation error is defined by

$$\gamma^n := \|q_h^n - q_h^*\|. \tag{4.22}$$

If the aim is to approximate the solution of the steady free-surface flow problem, it is sufficient to reduce the evaluation error to the level of the discretization error. Further reduction does not yield an essential improvement in the approximation of the *continuum* solution anyway. By (4.19a), the asymptotic behavior of the evaluation error at subcritical Froude numbers is

$$\gamma^n = O((n\tau)^{(1-d)/2}) , \qquad \text{as } n\tau \to \infty . \tag{4.23}$$

For an example of this convergence behavior in actual computations, see the numerical experiments on fine grids in [75]. From (4.23) it follows that $\gamma^n \leq \epsilon_h$ requires

$$n = O(h^{2p/(1-d)}\tau^{-1}), \qquad \text{as } h \to 0 . \tag{4.24}$$

Equation (4.24) implies an increase of the number of time-steps to reach steady state within the required tolerance. This is particularly manifest for high-order discretizations (large p) and low spatial dimension ($d = 2$).

An additional complication is that usually the allowable time-step decreases with h. Time integration of free-surface flow problems typically proceeds in two alternating steps:

(T1) Integrate the incompressible Navier–Stokes equations, subject to the dynamic conditions at the free surface and appropriate boundary conditions at fixed boundaries.

(T2) Integrate the kinematic condition to adjust the free-surface position, using the solution from (T1).

Due to this separate treatment and the hyperbolic character of the kinematic condition, stability of the numerical time-integration method requires that the time step complies with a CFL-condition, $\tau \propto h$.

Summarizing, equation (4.24) and the CFL-condition imply that the number of time steps required to reach $\gamma^n \leq \epsilon_h$ is $O(h^{-(1+2p/(d-1))})$. Assuming that the computational complexity of the time-integration method is proportional to the number of time steps, at subcritical Froude numbers the computational complexity is

$$W = O\big(h^{-(1+2p/(d-1))}\big), \qquad \text{as } h \to 0. \tag{4.25}$$

Equation (4.25) implies a severe increase in the computational expenses as h decreases. For example, in the typical case of a 2-nd order discretization of the three-dimensional problem, if the mesh-width is halved, the required computational work *per grid point* increases by a factor of 8.

4.4 Efficient Solution of Steady Free-Surface Flows

From Section 4.3 it is evident that the usual time-integration approach is inappropriate for solving steady free-surface flows at subcritical Froude numbers. In this section we present an efficient iterative solution method for gravity subjected steady free-surface flows. The method is outlined in Sect. 4.4.1. The convergence properties of the method and its computational complexity are examined in Sects. 4.4.2 and 4.4.3.

4.4.1 Iterative Solution Method

From the results in §4.2.3, it follows that an accurate approximation to the free-surface flow and to the free-surface position can be obtained by the following operations:

(I1) For a given initial boundary $\mathcal{S}$, solve $(\mathbf{v}, \varphi)$ from

$$\left.\begin{aligned} \operatorname{div} \mathbf{v}\mathbf{v} + \boldsymbol{\nabla}\varphi - \operatorname{div} \boldsymbol{\tau}(\mathbf{v}) &= 0 \\ \operatorname{div} \mathbf{v} &= 0 \end{aligned}\right\}, \qquad (\mathbf{x}, y) \in \mathcal{V}, \tag{4.26a}$$

$$\mathbf{B}(\mathbf{v}, p) = \mathbf{b}(\mathbf{x}, y), \qquad (\mathbf{x}, y) \in \partial\mathcal{V} \setminus \mathcal{S}, \tag{4.26b}$$

$$\left.\begin{aligned} \mathbf{t}^i \cdot \boldsymbol{\tau}(\mathbf{v}) \cdot \mathbf{n} &= 0 \\ \mathbf{v} \cdot \boldsymbol{\nabla}\varphi - \mathrm{Fr}^{-2}\, \mathbf{j} \cdot \mathbf{v} &= 0 \end{aligned}\right\}, \qquad (\mathbf{x}, y) \in \mathcal{S}\,, \tag{4.26c}$$

where (4.26b) represents boundary conditions on the fixed boundary.

(I2) Use the solution of (I1) to adjust the boundary $\mathcal{S}$ to

$$\big\{(\mathbf{x}, y + \mathrm{Fr}^2 \varphi(\mathbf{x}, y)) : (\mathbf{x}, y) \in \mathcal{S}\big\}\,. \tag{4.27}$$

Note the appearance of the quasi free-surface condition in its steady form in (4.26c). The modified boundary approximates the actual free surface more accurately than

the initial boundary, provided that the conditions discussed in §4.2.3 are fulfilled. Hence, it is anticipated that the solution to the free-surface flow problem can be obtained by iterating the operations (I1) and (I2).

If $\mathcal{S}$ is the actual free surface, then the normal dynamic condition is satisfied, i.e., p vanishes on $\mathcal{S}$. In that case, $\mathbf{n} \parallel \boldsymbol{\nabla} p$, and (4.26c) implies that the solution of (4.26) complies with the kinematic condition and the tangential dynamic conditions. Hence, operation (I1) then yields the free-surface flow. Moreover, the normal dynamic condition ensures that the surface adjustment in (I2) vanishes, so that the solution of the free-surface flow problem is indeed a fixed point of the iteration.

It is important to notice the absence of time-dependent terms in (I1) and (I2). Therefore, the slow decay of transient waves described in Section 4.3 is irrelevant to the convergence of the iterative process. The actual convergence properties of (I1)-(I2) are examined below.

4.4.2 Convergence

The convergence behavior of the iterative method (I1)-(I2) can be conveniently examined by rephrasing the free-surface flow problem as an optimal shape design problem. A general characteristic of free-boundary problems is that the number of free-boundary conditions is one more than the number of boundary conditions required by the governing boundary-value problem. A free-boundary problem can therefore be reformulated into the equivalent optimal shape design problem of finding the boundary that minimizes a norm of the residual of one of the free-surface conditions, subject to the boundary-value problem with the remaining free-surface conditions imposed.

To obtain an optimal shape design formulation of the steady free-surface flow problem, the *cost functional* E is defined by

$$E\big(\mathcal{S}, (\mathbf{v}, p)\big) := \int_{\mathcal{S}} |p(\mathbf{x}, y)| \, \mathrm{d}\mathcal{S} \,. \tag{4.28}$$

Assuming that (4.26) is well posed for all surfaces $\mathcal{S}$ in a space of admissible boundaries $\mathcal{O}$, and that $\mathcal{O}$ contains the actual free-surface, the free-surface flow problem is equivalent with the optimal shape design problem

$$\min_{\mathcal{S} \in \mathcal{O}} \big\{ E\big(\mathcal{S}, (\mathbf{v}, p)\big) : (\mathbf{v}, p) \text{ satisfies (4.26)} \big\} \,. \tag{4.29}$$

Notice that (4.29) is in fact a constrained optimization problem, with the boundary value problem (4.26) acting as a *constraint* on $(\mathbf{v}, p)$.

The optimal shape design formulation of the free surface flow problem allows convenient assessment of the convergence properties of the iterative method (I1)-(I2). Each iteration adjusts the approximation to the free-surface position. Convergence of the iterative method is ensured if each surface adjustment yields a

reduction of the cost functional (4.28). Moreover, the reduction of the cost functional between successive iterations is a measure of the efficiency of the method.

To determine the effect of a surface adjustment, consider the boundary $\mathcal{S}$ and the modified boundary

$$\mathcal{S}_{\epsilon\alpha} := \{(\mathbf{x}, y) + \epsilon\alpha(\mathbf{x}, y)\,\mathbf{j} : (\mathbf{x}, y) \in \mathcal{S}\}\,, \tag{4.30}$$

for a suitably smooth function α independent of ϵ on $\mathcal{S}$. The modified boundary is the boundary of a domain $\mathcal{V}_{\epsilon\alpha}$, which approaches $\mathcal{V}$ as $\epsilon \to 0$. Following [50], $\mathcal{V}$ and $\mathcal{V}_{\epsilon\alpha}$ are embedded in a bounded set $\mathcal{E}$ and it is assumed that for all $\mathcal{V} \subset \mathcal{E}$ with $\mathcal{S} \in \mathcal{O}$, a solution of (4.26) can be extended smoothly beyond the boundary, so that $(\mathbf{v}, p)$ is well defined everywhere in $\mathcal{E}$.

The displacement of the boundary from $\mathcal{S}$ to $\mathcal{S}_{\epsilon\alpha}$ induces a disturbance in the solution of (4.26). Denoting by $(\mathbf{v}, p)_{\epsilon\alpha}$ the solution of (4.26) on $\mathcal{V}_{\epsilon\alpha}$, the *induced disturbance* is defined by

$$(\mathbf{v}, p)'_\alpha := \lim_{\epsilon \to 0} \tfrac{1}{\epsilon}\big((\mathbf{v}, p)_{\epsilon\alpha} - (\mathbf{v}, p)\big)\,. \tag{4.31}$$

Taylor expansion of the cost functional then yields

$$E\big(\mathcal{S}_{\epsilon\alpha}, (\mathbf{v}, p)_{\epsilon\alpha}\big) = \int_{\mathcal{S}} |p + \epsilon(\alpha\,\mathbf{j}\cdot\boldsymbol{\nabla} p + p'_\alpha)|\,(1 + \epsilon\mu_\alpha)\,\mathrm{d}\mathcal{S} + O(\epsilon^2), \qquad \text{as } \epsilon \to 0. \tag{4.32}$$

In (4.32), the function $\mu_\alpha : \mathcal{S} \mapsto \mathbb{R}$ accounts for the change in the surface area from $\mathrm{d}\mathcal{S}$ to $\mathrm{d}\mathcal{S}_{\epsilon\alpha}$. Ignoring terms $O(\epsilon^2)$, the modified boundary $\mathcal{S}_{\epsilon\alpha}$ improves on $\mathcal{S}$ if a positive constant $\zeta < 1$ exists such that

$$\int_{\mathcal{S}} |p + \epsilon(\alpha\,\mathbf{j}\cdot\boldsymbol{\nabla} p + p'_\alpha)|\,(1 + \epsilon\mu_\alpha)\,\mathrm{d}\mathcal{S} \le \zeta \int_{\mathcal{S}} |p|\,\mathrm{d}\mathcal{S}\,. \tag{4.33}$$

If (4.33) holds for some $\zeta < 1$, then the modification of the boundary from $\mathcal{S}$ to $\mathcal{S}_{\epsilon\alpha}$ yields a reduction of the cost functional. The smallest positive constant that satisfies (4.33) is called the *contraction number*. Clearly, a small contraction number implies a successful surface modification.

Operation (I2) in the iterative procedure gives a correction of the boundary position $\epsilon\alpha = \mathrm{Fr}^2 p$. In that case, the value of the cost functional corresponding to the modified surface is bounded by

$$E\big(\mathcal{S}_{\epsilon\alpha}, (\mathbf{v}, p)_{\epsilon\alpha}\big) \le \int_{\mathcal{S}} |p|\,|1 + \mathrm{Fr}^2\mathbf{j}\cdot\boldsymbol{\nabla} p|\,(1 + \epsilon\mu_\alpha)\,\mathrm{d}\mathcal{S} + \int_{\mathcal{S}} |\epsilon p'_\alpha|\,\mathrm{d}\mathcal{S}\,. \tag{4.34}$$

Hence, the contraction number ζ of the iterative process (I1)-(I2) is bounded by

$$\zeta \le \sigma_p + \frac{\int_{\mathcal{S}} |\epsilon p'_\alpha|\,\mathrm{d}\mathcal{S}}{\int_{\mathcal{S}} |p|\,\mathrm{d}\mathcal{S}} + O(\epsilon)\,, \tag{4.35}$$

with σ_p defined by (4.6). From (4.35) it follows that if ϵ and σ_p are indeed small, then the induced disturbance determines the convergence behavior of the iterative method.

To establish convergence of (I1)-(I2), it remains to show that the induced disturbance p'_α is indeed small. Sec. 4.2.3 shows that the quasi free-surface condition (4.13) approximates the conditions at a fixed boundary in the neighborhood of the free surface to $O(\epsilon^2, \epsilon\sigma_p, \epsilon\sigma_{\mathbf{v}})$. Hence, displacing this condition from $\mathcal{S}$ to $\mathcal{S}_{\epsilon\alpha}$ yields no greater disturbance than that. In [5] it is shown that the tangential dynamic conditions are largely irrelevant to the shape of the free surface. Conversely, the induced disturbance due to enforcing the tangential dynamic conditions at $\mathcal{S}$ instead of $\mathcal{S}_{\epsilon\alpha}$ can be neglected. Therefore, the contraction number of the method (I1)-(I2) is estimated

$$\zeta = O(\epsilon, \sigma_p, \sigma_{\mathbf{v}}) \,. \tag{4.36}$$

4.4.3 Computational Complexity

Eq. (4.36) provides an upper bound for the contraction number of the method (I1)-(I2). One may note that if the approximate boundary is sufficiently close to the actual free surface (ϵ small), then (4.36) depends on properties of the continuum solution only. Therefore, if the free-surface flow problem is solved numerically, the behavior of the iterative method is asymptotically independent of the mesh width.

The iteration must be continued until the pressure defect at the free surface (4.28) has been reduced to the level of the spatial discretization error. Further reduction does not essentially improve the approximation of the *continuum* solution anyway. Each iteration reduces the pressure defect at the free-surface by a factor ζ. Therefore, the number of iterations n must satisfy

$$\zeta^n = O(h^p), \tag{4.37}$$

where p denotes the order of consistency of the spatial discretization. This implies that $n = O(p \log h / \log \zeta)$. Assuming that the computational complexity of the iterative method is proportional to the number of iterations, the following estimate of the computational complexity is obtained:

$$W = O(\log h) \,. \tag{4.38}$$

Hence, the efficiency of the method (I1)-(I2) decays only moderately as h decreases.

To eliminate the remaining weak h-dependence of the computational complexity, *nested iteration* can be used. Generally, an iterative solution method is used to solve the boundary value problem (4.26) in step (I1) of the algorithm. The nesting involves the use of the solution from the previous iteration as an initial estimate for the solution process. Because this initial estimate becomes increasingly accurate, the cost of performing (I1) reduces as the iteration progresses. In particular, assuming that the cost of solving (4.26) is proportional to the pressure defect at the free surface, the amount of work that is required to achieve (4.37) is

$$W = w + \zeta\, w + \zeta^2 w + \cdots + \zeta^n w \leq \frac{1}{1-\zeta} w \,, \tag{4.39}$$

with w the cost of solving (4.26) initially. Observe that the computational complexity (4.39) is indeed entirely independent of the mesh width.

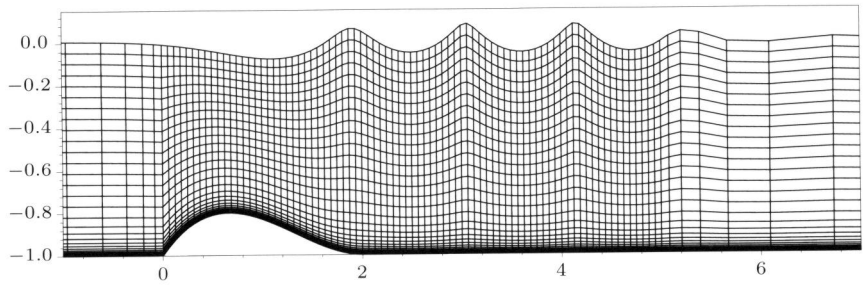

Figure 4.2: Example of a grid used in the numerical experiments. The grid is coarsened for illustration purposes.

4.5 Numerical Experiments and Results

The method is tested for subcritical flow over an obstacle in a channel of unit depth, at $\mathrm{Fr} = 0.43$ and $\mathrm{Re} = 1.5 \times 10^5$, with the undisturbed fluid depth and the undisturbed flow velocity at the free surface assigned as the reference length and velocity, respectively. The geometry of the obstacle is

$$y(x) = -1 + \frac{27}{4}\frac{H}{L^3}\, x\,(x-L)^2\,, \qquad 0 \le x \le L\,, \tag{4.40}$$

with H and L the (non-dimensionalized) height and length of the obstacle, respectively. Choosing $H = 0.2$ and $L = 2$, the setup is in agreement with [11]. At the bottom boundary no-slip boundary conditions are imposed. A boundary-layer velocity profile in accordance with the experiments from [11] is imposed at the inflow boundary.

The test case with $H = 0.2$ displays large amplitude waves that exhibit typical nonlinear effects, such as sharp wave crests and wave-length reduction. In addition, $H = 0.15$ is considered. This test case displays waves more in accordance with linear wave-theory, see, e.g., Refs. [37, 44].

The experiments are performed on grids with horizontal mesh widths $h = 2^{-5}, 2^{-6}$. The number of grid cells in the vertical direction is 70 and exponential grid stretching is applied to resolve the boundary layer at the bottom. Furthermore, the grid is coarsened towards the inflow and outflow boundaries to reduce reflections. A typical example of a grid used in the numerical experiments is presented in Figure 4.2. The RANS equations, closed with an eddy viscosity model due to Cebeci and Smith [13], and the boundary conditions are discretized and solved by the method described in [29]. After each evaluation, the grid is adapted using vertical stretching. An initial estimate of the solution on the adapted grid is subsequently generated by linear interpolation from the solution on the previous grid. Details of the discretization method and the setup of the numerical experiments can be found in [9].

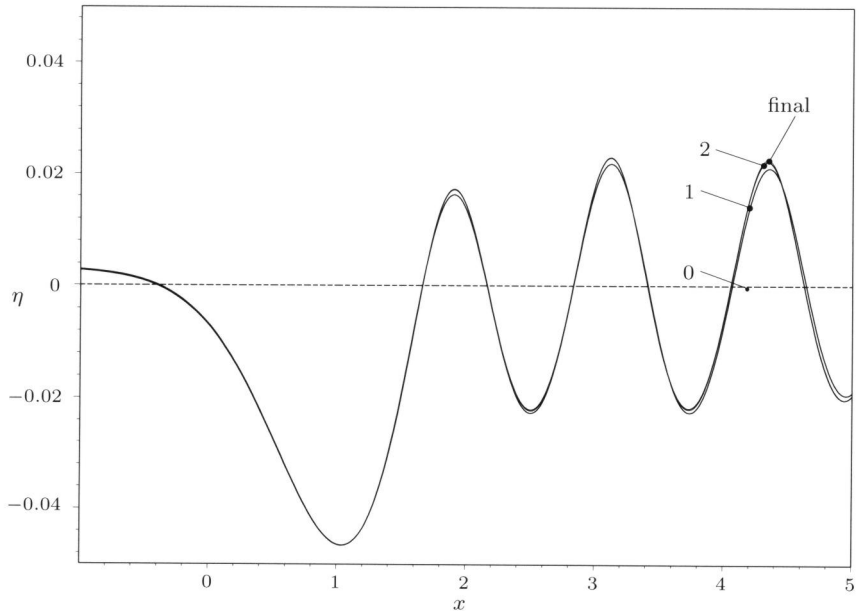

Figure 4.3: Wave profile obtained after successive iterations ($H = 0.15$).

Figure 4.3 and Figure 4.4 show the wave profiles obtained in successive iterations for $H = 0.15$ and $H = 0.2$, respectively. The initial estimate (0th iterate) is just the undisturbed free surface. One may note that the first iterate already displays a qualitatively correct wave profile. This confirms that the quasi free-surface flow solution is an accurate approximation to the actual free-surface flow solution. A converged solution is obtained in approximately 2 iterations for $H = 0.15$ and in approximately 10 iterations for $H = 0.2$. Due to the decreasing computational cost of each iteration (refer to §4.4.3), even for $H = 0.2$ the entire computation is just 2 to 3 times as expensive as the corresponding fixed domain problem with symmetry boundary conditions at the undisturbed surface.

Figure 4.5 on page 53 displays the pressure defect at the free surface after consecutive iterations. The results confirm convergence of the method. For $H = 0.15$, the average contraction number is $\zeta \approx 0.15$ and the convergence behavior is indeed independent of h. After several iterations the contraction number increases. However, this is entirely due to the fact that the quasi free-surface flow problem (4.26) is solved only by approximation. If the tolerance on the residual of (4.26) is reduced, i.e., if (4.26) is solved more accurately, then the original contraction number is recovered. For $H = 0.20$, the average contraction number is

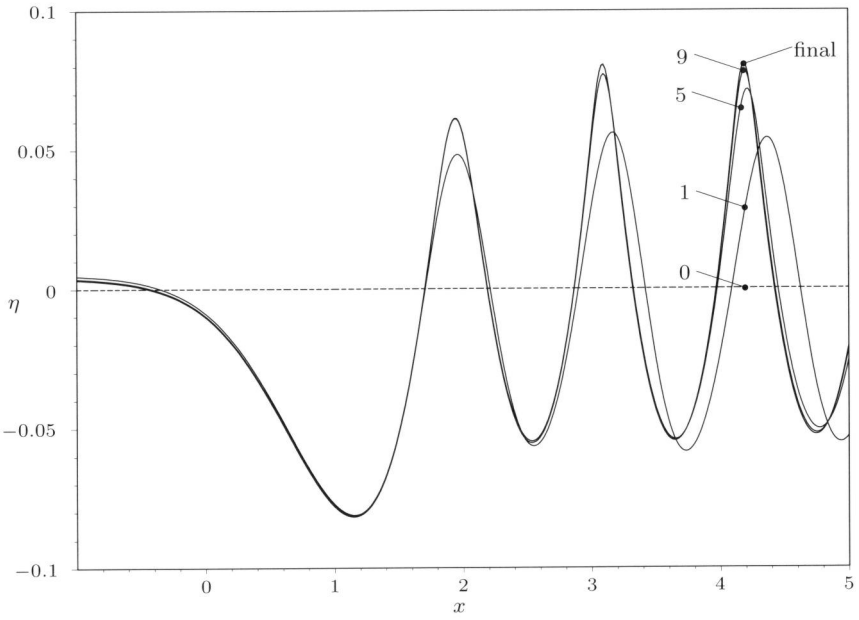

Figure 4.4: Wave profile obtained after successive iterations ($H = 0.2$).

$\zeta \approx 0.45$ for $h = 2^{-5}$ and $\zeta \approx 0.52$ for $h = 2^{-6}$. As a result of strong nonlinearity, the asymptotic mesh width independence of the convergence behavior is in this case not yet apparent.

A detailed investigation of the convergence behavior of time-integration methods for the test case with $H = 0.20$ is presented in [75]. Typically, the time-integration method requires approximately 10^4 surface adjustments to reduce the initial error by a factor of 10. The presented method achieves this in approximately 4 iterations, for a similar setting of the numerical experiment.

Figure 4.6 on page 54 compares the computed wave elevation with measurements from [11]. In [11], a non-dimensionalized amplitude $a = 4.5 \times 10^{-2} \pm 15\%$ and wave length $\lambda = 1.10 \pm 10\%$ are reported for the trailing wave. The trailing wave of the computed wave elevation on the grid with $h = 2^{-6}$ displays amplitude $a = 6.5 \times 10^{-2}$ and wave length $\lambda = 1.11$. Hence, the computed wave length agrees well with the measurements. The amplitude appears to be overestimated. However, the difference between the amplitude of the numerical results and of the experimental data is not unusual, see, e.g., Refs. [75, 76]. Observe also that the difference in the amplitude of the first wave and the second wave is correctly predicted.

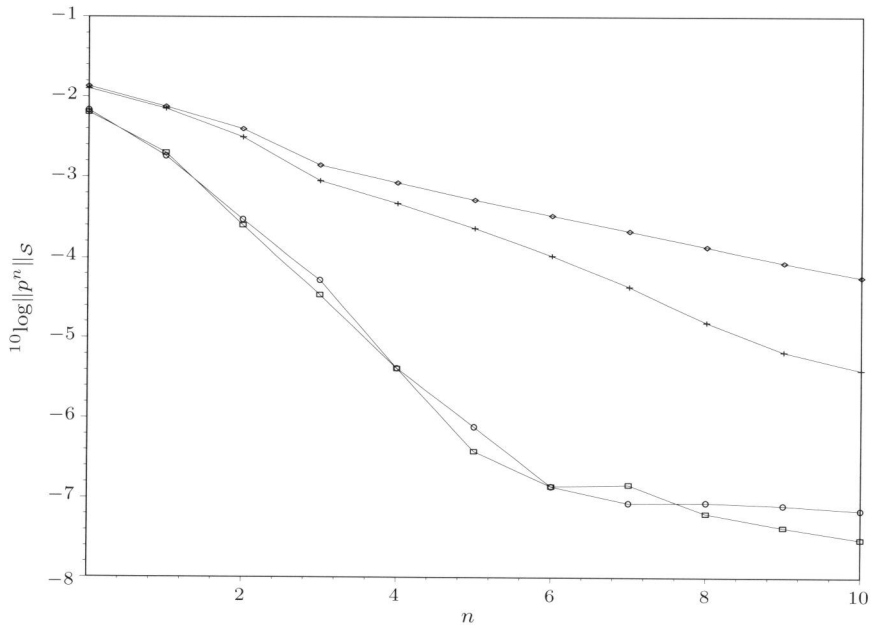

Figure 4.5: Pressure defect at the free surface versus the iteration number for $H = 0.15$, $h = 2^{-5}$ (□), $h = 2^{-6}$ (○) and $H = 0.20$, $h = 2^{-5}$ (+), $h = 2^{-6}$ (◇).

4.6 Conclusion

The usual time-integration method for solving steady free-surface Navier–Stokes flow problems was shown to be inefficient due to the specific transient behavior of surface gravity waves and a CFL-condition on the allowable time step.

Motivated by the demand for efficient computational methods in practical applications, we proposed a new iterative solution method. The method alternatingly solves the steady Navier–Stokes equations with a quasi free-surface condition imposed at the free surface, and adjusts the free surface using the computed solution and the

Examination of the convergence properties of the iterative method revealed that the method uses the quasi free-surface condition to ensure that the disturbance induced by the displacement of the boundary is small. It was shown that the behavior of the method is asymptotically independent of the mesh width. The asymptotic computational complexity of the iterative method deteriorates only moderately with decreasing mesh width. Mesh width independence of the computational complexity can be achieved by means of nested iteration.

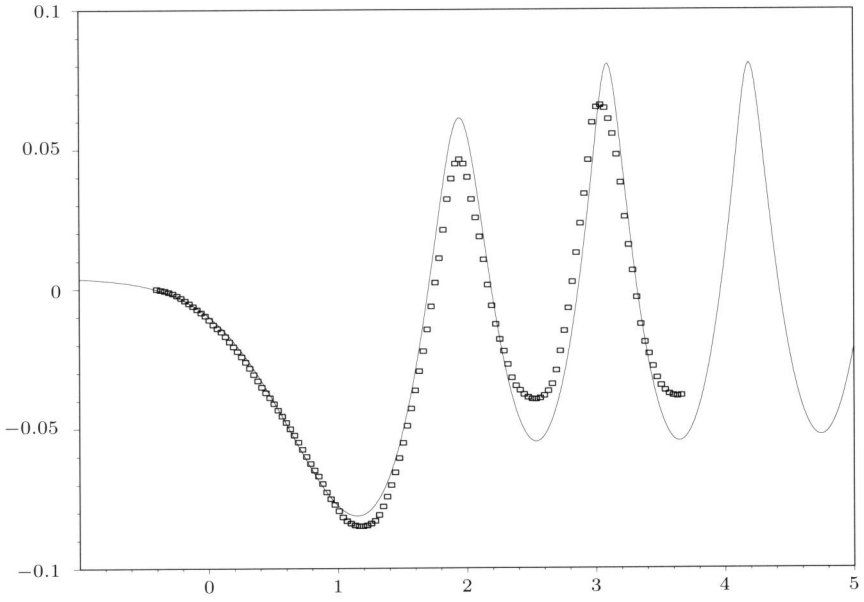

Figure 4.6: Computed wave elevation for $h = 2^{-6}$ (*solid line*) and measurements from [11] (*markers only*), for $H = 0.20$. The obstacle is located in the interval $x \in [0, 2]$.

Numerical results were presented for two-dimensional flow over an obstacle in a channel. For the presented test cases, a converged solution was obtained in at most 10 iterations. The numerical results agree well with measurements. The numerical experiments confirmed that the behavior of the method is asymptotically independent of the mesh width.

We believe that the proposed method will be useful in ship hydrodynamics, hydraulics and other fields of application in which the efficient computation of steady free-surface flows at high Reynolds number is required.

Chapter 5

Adjoint Shape Optimization for Steady Free-Surface Flows

5.1 Introduction

The numerical solution of flows that are partly bounded by a free boundary is of great importance in engineering applications, e.g., ship hydrodynamics [3, 12, 17], hydraulics and coating technology [54, 55]. A relevant class of free-surface flow problems are *steady* free-surface flows. An example of a steady free-surface flow is the wave pattern carried by a ship at forward speed in still water. The numerical techniques for free-surface potential flow are well developed; for an overview, see [74]. In particular, dedicated techniques have been developed for solving the steady free-surface potential-flow equations, e.g., Ref. [51]. In contrast, methods for the steady free-surface Navier–Stokes equations typically continue a transient process until a steady state is reached. This time-integration method is often computationally inefficient, due to the specific transient behavior of free-surface flows; see [10, 80]. Alternative solution methods for the steady free-surface Navier–Stokes equations exist. However, the performance of these methods usually depends sensitively on the parameters in the problem, or their applicability is too restricted; see, for instance, Refs. [55, 58]. In [10], an efficient iterative algorithm was presented. However, the implementation of the quasi free-surface condition that underlies the efficiency of this method can be involved. Hence, the investigation of numerical methods for the steady free-surface Navier–Stokes equations is warranted.

A general characteristic of free-boundary problems is that the number of free-boundary conditions is one more than the number of boundary conditions required by the governing boundary value problem. A free-boundary problem can therefore be reformulated into the equivalent shape optimization problem of finding the boundary that minimizes a norm of the residual of one free-boundary condition, subject to the boundary value problem with the other free-boundary conditions imposed.

Optimal shape design problems can in principle be solved efficiently by means of the adjoint method. In recent years, much progress has been made in the development of adjoint techniques for problems from fluid dynamics. Applications to the Navier–Stokes equations include flow control (see [20] and the references therein), a posteriori error estimation and adaptivity (for instance, [6, 7]) optimal design (e.g., Refs. [21, 23]) and domain decomposition (cf. Ref. [24]). The techniques that are required to solve the optimal shape design problem associated with steady free-surface flow are readily available.

The present work investigates the suitability of the adjoint shape optimization method for solving steady free-surface flow problems. Our primary interest is in the steady free-surface Navier–Stokes equations. However, because inviscid, irrotational flow adequately describes the prominent features of free-surface flow and to avoid the excessive complexity of the Navier–Stokes equations, we base our investigation on the free-surface potential-flow equations. It is anticipated that the adjoint shape optimization method is equally applicable to the free-surface Navier–Stokes equations, although the specifics of the method are much more involved in that case. Our investigation serves as an indication of the properties of the adjoint shape optimization method for steady free-surface flow problems.

The contents of this chapter are organized as follows: In Section 5.2 the equations governing steady free-surface potential flow and the associated design problem are stated. Section 5.3 formulates the adjoint equations and sets up the adjoint optimization method. Section 5.4 presents an analysis of the properties of the optimization problem and the behavior of the adjoint method, using Fourier techniques from [68]. Motivated by the results of the Fourier analysis, we describe a preconditioning for the optimization problem in Section 5.5. Numerical experiments and results are presented in Section 5.6. Section 5.7 contains concluding remarks.

5.2 Problem Statement

We consider an incompressible, inviscid fluid flow, subject to a constant gravitational force, acting in the negative vertical direction. The fluid occupies a domain $\mathcal{V} \subset \mathbb{R}^d$ $(d = 2, 3)$ which is bounded by a free boundary, $\mathcal{S}$, and a fixed boundary $\partial\mathcal{V} \setminus \mathcal{S}$. The fixed boundary can be subdivided in an inflow boundary, an outflow boundary and a rigid, impermeable boundary.

5.2.1 Governing Equations

The (non-dimensionalized) fluid velocity and pressure are identified by $\mathbf{v}(\mathbf{x})$ and $p(\mathbf{x})$, respectively. Assuming that the velocity-field is irrotational, a velocity potential $\phi(\mathbf{x})$ exists such that $\mathbf{v} = \boldsymbol{\nabla}\phi$. Enforcing incompressibility then yields that the velocity potential is governed by Laplace's equation,

$$\Delta\phi = 0\,, \qquad \mathbf{x} \in \mathcal{V}\,. \tag{5.1}$$

Assuming that $|\nabla\phi| = 1$ at the inflow boundary, Bernoulli's equation relates the pressure to the velocity potential by

$$p(\mathbf{x}) := \tfrac{1}{2} - (\tfrac{1}{2}|\nabla\phi|^2 + \mathrm{Fr}^{-2}x_d)\,, \tag{5.2}$$

with x_d the vertical coordinate and Fr the Froude number, defined by $\mathrm{Fr} := V/\sqrt{gL}$ with V an appropriate reference velocity, g the gravitational acceleration and L a reference length.

The free-surface conditions prescribe that the free surface is impermeable and that the pressure vanishes at the free surface:

$$\mathbf{n}\cdot\nabla\phi = 0, \qquad \mathbf{x}\in\mathcal{S}, \tag{5.3a}$$

$$p = 0, \qquad \mathbf{x}\in\mathcal{S}, \tag{5.3b}$$

with $\mathbf{n}(\mathbf{x})$ the unit normal vector to $\mathcal{S}$. Conditions (5.3a) and (5.3b) are referred to as the kinematic condition and the dynamic condition, respectively. A single appropriate boundary condition must be specified at the fixed boundary. We assume that this condition is of the form

$$a\,\mathbf{n}\cdot\nabla\phi + b\,\phi = c\,, \qquad \mathbf{x}\in\partial\mathcal{V}\setminus\mathcal{S}, \tag{5.4}$$

for certain functions $a, b, c : \partial\mathcal{V}\setminus\mathcal{S} \mapsto \mathbb{R}$.

The steady free-surface flow problem under consideration is the problem of finding $\mathcal{S}$ and ϕ such that ϕ satisfies (5.1)–(5.4). However, this problem is not necessarily well posed. Firstly, solutions can be non-unique due to the occurrence of arbitrary non-physical upstream waves. To remove these waves, a radiation condition must be imposed; cf., for instance, [37, 44, 63]. In numerical computations, this radiation condition can be conveniently enforced by introducing artificial damping (see Section 5.6) or by selecting a suitable discretization (see, e.g., Ref. [51]). Secondly, a steady solution can be nonexistent, in the sense that the transient problem underlying (5.1)–(5.4) does not approach a steady state as time progresses ad infinitum; see, for instance, Ref. [80].

5.2.2 Optimal Shape Design Formulation

One may note that the number of free-surface conditions (5.3) is one more than the number of boundary conditions required by (5.1). The free-boundary problem can therefore be reformulated into the equivalent optimal shape design problem of finding the boundary that minimizes a norm of the residual of one of the free-surface conditions, subject to the boundary value problem with the remaining free-surface conditions imposed.

To obtain an optimal shape design formulation of the steady free-surface flow problem, the *cost functional* E is defined by

$$E(\mathcal{S},\phi) := \int_{\mathcal{S}} \tfrac{1}{2}p(\mathbf{x})^2\,\mathrm{d}\mathbf{x}\,, \tag{5.5}$$

and the *constraint* C is defined by the boundary value problem (5.1), (5.3a) and (5.4):

$$C(\mathcal{S},\phi) := \begin{cases} \Delta\phi = 0\,, & \mathbf{x} \in \mathcal{V}\,, \\ \mathbf{n}\cdot\boldsymbol{\nabla}\phi = 0\,, & \mathbf{x} \in \mathcal{S}\,, \\ a\,\mathbf{n}\cdot\boldsymbol{\nabla}\phi + b\,\phi = c\,, & \mathbf{x} \in \partial\mathcal{V}\setminus\mathcal{S}\,. \end{cases} \tag{5.6}$$

Note that the cost functional is a norm of the residual of the dynamic condition (5.3b) and that the kinematic condition (5.3a) appears in the constraint. The free-surface flow problem is equivalent to the optimal shape design problem

$$\min_{\mathcal{S}}\{E(\mathcal{S},\phi) : C(\mathcal{S},\phi)\}\,, \tag{5.7}$$

i.e., minimize (5.5) over all $\mathcal{S}$, subject to the constraint that ϕ satisfies (5.6). Because the boundary value problem (5.6) associates a unique ϕ with each free boundary $\mathcal{S}$, it is often convenient to use the notation $E(\mathcal{S})$ for $E(\mathcal{S},\phi)$ with ϕ from (5.6).

5.3 Adjoint Optimization Method

Shape-optimization problems can in principle be solved efficiently by means of the adjoint optimization method. The essential problem in treating shape optimization problems is that a displacement of the free boundary induces a disturbance in the solution of the boundary value problem and, consequently, it is attended with an induced change in the cost functional. Efficient solution of a shape optimization problem requires control over the induced change in the cost functional. The adjoint optimization method eliminates the induced change by means of the solution of a dual problem. Upon elimination of the induced change, the gradient of the cost functional with respect to the free-boundary position is obtained. Improvement of the free-boundary position is then straightforward. This section outlines the adjoint optimization method for solving (5.7).

5.3.1 Induced Disturbance

To formulate the adjoint optimization method for (5.7), the induced disturbance in the solution of the constraint and the corresponding change in the cost functional must first be identified. To this end, we consider a domain $\mathcal{V}$ with free boundary $\mathcal{S}$ and a modified domain $\mathcal{V}_{\epsilon\alpha}$ with free boundary

$$\mathcal{S}_{\epsilon\alpha} := \{\mathbf{x} + \epsilon\alpha(\mathbf{x})\,\mathbf{n}(\mathbf{x}) : \mathbf{x} \in \mathcal{S}\}, \tag{5.8}$$

where α is a smooth function on $\mathcal{S}$, independent of ϵ. Following [50], $\mathcal{V}$ and $\mathcal{V}_{\epsilon\alpha}$ are embedded in a bounded set $\mathcal{E}$ and it is assumed that a solution of the constraint can be extended smoothly beyond the boundary, so that it is well defined in $\mathcal{E}$.

Denoting by ϕ the solution of $C(\mathcal{S},\phi)$ and by $\phi_{\epsilon\alpha}$ the solution of $C(\mathcal{S}_{\epsilon\alpha},\phi_{\epsilon\alpha})$, we define the *induced disturbance* by the function $\phi'_\alpha : \mathcal{E} \mapsto \mathbb{R}$ with the property

$$\phi_{\epsilon\alpha} = \phi + \epsilon\phi'_\alpha + O(\epsilon^2)\,, \qquad \text{as } \epsilon \to 0\,, \tag{5.9}$$

i.e., $\epsilon\phi'_\alpha$ approximates to $O(\epsilon^2)$ the change in the solution of the constraint (5.6) due to the displacement of the free boundary from $\mathcal{S}$ to $\mathcal{S}_{\epsilon\alpha}$. The kinematic condition corresponding to the modified boundary yields:

$$\begin{aligned}&\big[\mathbf{n}_{\epsilon\alpha}\cdot\boldsymbol{\nabla}\phi_{\epsilon\alpha}\big]\big(\mathbf{x}+\epsilon\alpha(\mathbf{x})\mathbf{n}(\mathbf{x})\big) = \\ &\left[\left(\mathbf{n}-\epsilon\sum_{j=1}^{d-1}(\mathbf{t}_j\cdot\boldsymbol{\nabla}\alpha)\,\mathbf{t}_j+O(\epsilon^2)\right)\cdot\left(\boldsymbol{\nabla}\phi+\epsilon\boldsymbol{\nabla}\phi'_\alpha+\epsilon\alpha\mathbf{n}\cdot\boldsymbol{\nabla}\boldsymbol{\nabla}\phi+O(\epsilon^2)\right)\right](\mathbf{x}) = 0\,,\end{aligned} \tag{5.10}$$

for $\mathbf{x}\in\mathcal{S}$, with $\mathbf{n}_{\epsilon\alpha}$ the unit normal vector to $\mathcal{S}_{\epsilon\alpha}$ and $\mathbf{t}_j$ orthogonal tangent vectors to $\mathcal{S}$. Hence, inserting (5.9) in $C(\mathcal{S}_{\epsilon\alpha},\phi_{\epsilon\alpha})$ and collecting terms $O(\epsilon)$, it follows that the induced disturbance satisfies the boundary value problem:

$$\Delta\phi'_\alpha = 0\,, \qquad \mathbf{x}\in\mathcal{V}\,, \tag{5.11a}$$

$$\mathbf{n}\cdot\boldsymbol{\nabla}\phi'_\alpha = -\alpha\mathbf{n}\mathbf{n} : \boldsymbol{\nabla}\boldsymbol{\nabla}\phi + \sum_{j=1}^{d-1}(\mathbf{t}_j\cdot\boldsymbol{\nabla}\alpha)\,(\mathbf{t}_j\cdot\boldsymbol{\nabla}\phi)\,, \qquad \mathbf{x}\in\mathcal{S}\,, \tag{5.11b}$$

$$a\,\mathbf{n}\cdot\boldsymbol{\nabla}\phi'_\alpha + b\,\phi'_\alpha = 0\,, \qquad \mathbf{x}\in\partial\mathcal{V}\setminus\mathcal{S}\,. \tag{5.11c}$$

The operator $\mathbf{nn} : \boldsymbol{\nabla}\boldsymbol{\nabla}$ in (5.11b) represents the second order derivative in the normal direction.

To identify the induced change in the cost functional, the functional value corresponding to the modified boundary, $E(\mathcal{S}_{\epsilon\alpha})$, is expanded as

$$E(\mathcal{S}_{\epsilon\alpha}) := E(\mathcal{S}_{\epsilon\alpha},\phi_{\epsilon\alpha}) = E(\mathcal{S})+\epsilon\left(I'_\alpha(\mathcal{S})+J'_\alpha(\mathcal{S})\right)+O(\epsilon^2), \qquad \text{as } \epsilon\to 0, \tag{5.12a}$$

with

$$I'_\alpha(\mathcal{S}) := -\int_{\mathcal{S}} p\,\boldsymbol{\nabla}\phi\cdot\boldsymbol{\nabla}\phi'_\alpha \mathrm{d}\mathbf{x}\,, \tag{5.12b}$$

$$J'_\alpha(\mathcal{S}) := -\int_{\mathcal{S}} \alpha\left(\frac{p^2}{2R}+p\,\mathbf{n}\cdot\boldsymbol{\nabla}\tfrac{1}{2}|\boldsymbol{\nabla}\phi|^2+p\,\mathrm{Fr}^{-2}\mathbf{n}\cdot\mathbf{e}_d\right)\mathrm{d}\mathbf{x}\,, \tag{5.12c}$$

where $R(\mathbf{x})$ is the radius of curvature ($d=2$) or mean radius of curvature ($d=3$) and $\mathbf{e}_d$ is the vertical unit vector. The curvature-term in (5.12c) results from the change in the surface area from $\mathcal{S}$ to $\mathcal{S}_{\epsilon\alpha}$; see, e.g., Ref. [50]. Noting that only (5.12b) depends on ϕ'_α, the induced change in the cost functional is readily

identified as (5.12b). Integration by parts recasts (5.12b) into the convenient form:

$$I'_\alpha(\mathcal{S}) = \int_{\mathcal{S}} \phi'_\alpha \sum_{j=1}^{d-1} \mathbf{t}_j \cdot \boldsymbol{\nabla}(p\,\mathbf{t}_j \cdot \boldsymbol{\nabla}\phi)\,\mathrm{d}\mathbf{x}\,. \tag{5.13a}$$

Moreover, the second term in (5.12c) vanishes due to the kinematic condition (5.3a):

$$J'_\alpha(\mathcal{S}) = -\int_{\mathcal{S}} \alpha \left(\frac{p^2}{2R} + p\,\mathrm{Fr}^{-2}\mathbf{n}\cdot\mathbf{e}_d\right)\mathrm{d}\mathbf{x}\,. \tag{5.13b}$$

If $\alpha(\mathbf{x})$ is chosen such that $I'_\alpha + J'_\alpha < 0$, an adjustment of the free boundary from $\mathcal{S}$ to $\mathcal{S}_{\gamma\alpha}$, with γ a small positive number, results in a reduction of the cost functional and thus improves the approximation to the actual free-boundary position. Such a choice of α is called a *descent direction*.

5.3.2 Adjoint Operators and Duality

The inherent problem in determining a descent direction from (5.13), is the dependence of (5.13a) on ϕ'_α, which is connected to α through the boundary value problem (5.11). Equations (5.11) and (5.13) are useful to verify if a particular α is a descent direction. However, they are unsuitable to determine a descent direction.

The adjoint optimization method uses the equivalence of (5.11), (5.13a) to its dual problem to eliminate the induced change in the functional. To define the duality property, adjoint operators must be introduced. Let $(\cdot,\cdot)_{\mathcal{V}}$ and $(\cdot,\cdot)_{\partial\mathcal{V}}$ denote the L_2 integral inner products over the domain $\mathcal{V}$ and its boundary $\partial\mathcal{V}$, respectively. Consider the linear boundary value problem:

$$L_i(\phi) = l_i\,, \qquad \mathbf{x} \in \mathcal{V}\,, \tag{5.14a}$$

$$L_b(\phi) = l_b\,, \qquad \mathbf{x} \in \partial\mathcal{V}\,, \tag{5.14b}$$

and the functional

$$I = \big(f_i, F_i(\phi)\big)_{\mathcal{V}} + \big(f_b, F_b(\phi)\big)_{\partial\mathcal{V}}\,, \tag{5.15}$$

for certain interior operators L_i, F_i and boundary operators L_b, F_b. The adjoint operators L_i^*, F_i^* and adjoint boundary operators L_b^*, F_b^* are defined by the identity

$$\big(L_i^*(\lambda), F_i(\phi)\big)_{\mathcal{V}} + \big(L_b^*(\lambda), F_b(\phi)\big)_{\partial\mathcal{V}} = \big(F_i^*(\lambda), L_i(\phi)\big)_{\mathcal{V}} + \big(F_b^*(\lambda), L_b(\phi)\big)_{\partial\mathcal{V}}, \tag{5.16}$$

for all appropriate functions ϕ and λ. For example, if

$$L_i(\phi) = \Delta\phi\,, \quad L_b(\phi) = a\mathbf{n}\cdot\boldsymbol{\nabla}\phi + b\phi\,, \quad F_i(\phi) = \phi\,, \quad F_b(\phi) = \underline{a}\mathbf{n}\cdot\boldsymbol{\nabla}\phi + \underline{b}\phi\,, \tag{5.17a}$$

for certain functions $a, b, \underline{a}, \underline{b} : \partial\mathcal{V} \mapsto \mathbb{R}$ such that $b\underline{a} - a\underline{b} \neq 0$, then

$$L_i^*(\lambda) = L_i(\lambda)\,, \quad L_b^*(\lambda) = \frac{L_b(\lambda)}{b\underline{a} - a\underline{b}}\,, \quad F_i^*(\lambda) = F_i(\lambda)\,, \quad F_b^*(\lambda) = \frac{F_b(\lambda)}{b\underline{a} - a\underline{b}}\,. \tag{5.17b}$$

To prove that (5.17a) and (5.17b) indeed satisfy the identity (5.16):

$$\begin{aligned}
&\big(L_i^*(\lambda), F_i(\phi)\big)_{\mathcal{V}} + \big(L_b^*(\lambda), F_b(\phi)\big)_{\partial\mathcal{V}} \\
&\quad = \int_{\mathcal{V}} \phi\,\Delta\lambda\,\mathrm{d}\mathbf{x} + \oint_{\partial\mathcal{V}} \left(\frac{a\mathbf{n}\cdot\boldsymbol{\nabla}\lambda + b\lambda}{b\underline{a} - a\underline{b}}\right)\left(\underline{a}\mathbf{n}\cdot\boldsymbol{\nabla}\phi + \underline{b}\phi\right)\mathrm{d}\mathbf{x} \\
&\quad = \int_{\mathcal{V}} \lambda\,\Delta\phi\,\mathrm{d}\mathbf{x} + \oint_{\partial\mathcal{V}} (\phi\,\mathbf{n}\cdot\boldsymbol{\nabla}\lambda - \lambda\,\mathbf{n}\cdot\boldsymbol{\nabla}\phi)\,\mathrm{d}\mathbf{x} \\
&\qquad + \oint_{\partial\mathcal{V}} \left(\frac{a\mathbf{n}\cdot\boldsymbol{\nabla}\lambda + b\lambda}{b\underline{a} - a\underline{b}}\right)\left(\underline{a}\mathbf{n}\cdot\boldsymbol{\nabla}\phi + \underline{b}\phi\right)\mathrm{d}\mathbf{x} \\
&\quad = \int_{\mathcal{V}} \lambda\,\Delta\phi\,\mathrm{d}\mathbf{x} + \oint_{\partial\mathcal{V}} \left(\frac{\underline{a}\mathbf{n}\cdot\boldsymbol{\nabla}\lambda + \underline{b}\lambda}{b\underline{a} - a\underline{b}}\right)\left(a\mathbf{n}\cdot\boldsymbol{\nabla}\phi + b\phi\right)\mathrm{d}\mathbf{x} \\
&\quad = \big(F_i^*(\lambda), L_i(\phi)\big)_{\mathcal{V}} + \big(F_b^*(\lambda), L_b(\phi)\big)_{\partial\mathcal{V}}\,.
\end{aligned} \tag{5.18}$$

The identity (5.16) implies that (5.15) subject to (5.14) is equivalent to

$$I = \big(l_i, F_i^*(\lambda)\big)_{\mathcal{V}} + \big(l_b, F_b^*(\lambda)\big)_{\partial\mathcal{V}} \tag{5.19}$$

subject to

$$L_i^*(\lambda) = f_i\,, \qquad \mathbf{x} \in \mathcal{V}\,, \tag{5.20a}$$

$$L_b^*(\lambda) = f_b\,, \qquad \mathbf{x} \in \partial\mathcal{V}\,. \tag{5.20b}$$

To prove the equivalence:

$$\begin{aligned}
I &= \big(f_i, F_i(\phi)\big)_{\mathcal{V}} + \big(f_b, F_b(\phi)\big)_{\partial\mathcal{V}} = \big(L_i^*(\lambda), F_i(\phi)\big)_{\mathcal{V}} + \big(L_b^*(\lambda), F_b(\phi)\big)_{\partial\mathcal{V}} \\
&= \big(F_i^*(\lambda), L_i(\phi)\big)_{\mathcal{V}} + \big(F_b^*(\lambda), L_b(\phi)\big)_{\partial\mathcal{V}} = \big(F_i^*(\lambda), l_i\big)_{\mathcal{V}} + \big(F_b^*(\lambda), l_b\big)_{\partial\mathcal{V}}\,.
\end{aligned} \tag{5.21}$$

In this context, (5.14)–(5.15) is called the *primal* problem and (5.19)–(5.20) is called the *dual* problem. *Duality* is the equivalence of the primal and dual problem.

The adjoint optimization method uses duality to eliminate the induced change in the cost functional (5.13a). Observe that for given ϕ, the functional (5.13a) is the L_2 inner product of ϕ'_α with a given function and (5.11) acts as a constraint on ϕ'_α. Hence, (5.13a) subject to (5.11) is of the form (5.14)–(5.15). To obtain the dual problem for (5.11)–(5.13a), we note that (5.11) implies

$$\begin{aligned}
\int_{\mathcal{V}} \lambda\Delta\phi'_\alpha\mathrm{d}\mathbf{x} + \int_{\mathcal{S}} \psi\,\mathbf{n}\cdot\boldsymbol{\nabla}\phi'_\alpha\,\mathrm{d}\mathbf{x} + \int_{\mathcal{S}} \psi\left(\alpha\,\mathbf{nn} : \boldsymbol{\nabla}\boldsymbol{\nabla}\phi - \sum_{j=1}^{d-1}(\mathbf{t}_j\cdot\boldsymbol{\nabla}\alpha)\,(\mathbf{t}_j\cdot\boldsymbol{\nabla}\phi)\right)\mathrm{d}\mathbf{x} \\
+ \int_{\partial\mathcal{V}\setminus\mathcal{S}} \psi\left(a\,\mathbf{n}\cdot\boldsymbol{\nabla}\phi'_\alpha + b\,\phi'_\alpha\right)\mathrm{d}\mathbf{x} = 0\,,
\end{aligned} \tag{5.22}$$

for all admissible functions $\lambda : \mathcal{V} \mapsto \mathbb{R}$ and $\psi : \partial\mathcal{V} \mapsto \mathbb{R}$. Integrating by parts, (5.22) can be recast into

$$\int_{\mathcal{V}} \phi'_\alpha \Delta\lambda \,\mathrm{d}\mathbf{x} - \int_{\mathcal{S}} \phi'_\alpha \mathbf{n}\cdot\boldsymbol{\nabla}\lambda \,\mathrm{d}\mathbf{x} + \int_{\mathcal{S}} \alpha \left(\psi\, \mathbf{nn} : \boldsymbol{\nabla}\boldsymbol{\nabla}\phi + \sum_{j=1}^{d-1} \mathbf{t}_j \cdot \boldsymbol{\nabla}(\psi\, \mathbf{t}_j \cdot \boldsymbol{\nabla}\phi) \right) \mathrm{d}\mathbf{x}$$
$$+ \int_{\mathcal{S}} (\lambda + \psi)\, \mathbf{n}\cdot\boldsymbol{\nabla}\phi'_\alpha \,\mathrm{d}\mathbf{x} + \int_{\partial\mathcal{V}\setminus\mathcal{S}} (b\,\psi - \mathbf{n}\cdot\boldsymbol{\nabla}\lambda)\, \phi'_\alpha + (a\,\psi + \lambda)\, \mathbf{n}\cdot\boldsymbol{\nabla}\phi'_\alpha \,\mathrm{d}\mathbf{x} = 0. \tag{5.23}$$

Hence, if ψ in (5.23) is set to

$$\psi(\mathbf{x}) = \begin{cases} -\lambda(\mathbf{x}), & \mathbf{x} \in \mathcal{S}, \\ -\lambda(\mathbf{x})/a(\mathbf{x}), & \mathbf{x} \in \partial\mathcal{V} \setminus \mathcal{S},\ a(\mathbf{x}) \neq 0\,, \\ \mathbf{n}\cdot\boldsymbol{\nabla}\lambda(\mathbf{x})/b(\mathbf{x}), & \mathbf{x} \in \partial\mathcal{V} \setminus \mathcal{S},\ \text{otherwise}, \end{cases}$$

and if λ satisfies the dual problem

$$\Delta\lambda = 0\,, \qquad \mathbf{x} \in \mathcal{V}\,, \tag{5.24a}$$

$$\mathbf{n}\cdot\boldsymbol{\nabla}\lambda = \sum_{j=1}^{d-1} \mathbf{t}_j \cdot \boldsymbol{\nabla}(p\, \mathbf{t}_j \cdot \boldsymbol{\nabla}\phi)\,, \qquad \mathbf{x} \in \mathcal{S}\,, \tag{5.24b}$$

$$a\,\mathbf{n}\cdot\boldsymbol{\nabla}\lambda + b\,\lambda = 0\,, \qquad \mathbf{x} \in \partial\mathcal{V} \setminus \mathcal{S}\,, \tag{5.24c}$$

then

$$I'_\alpha(\mathcal{S}) = -\int_{\mathcal{S}} \alpha \left(\lambda\, \mathbf{nn} : \boldsymbol{\nabla}\boldsymbol{\nabla}\phi + \sum_{j=1}^{d-1} \mathbf{t}_j \cdot \boldsymbol{\nabla}(\lambda\, \mathbf{t}_j \cdot \boldsymbol{\nabla}\phi) \right) \mathrm{d}\mathbf{x}\,. \tag{5.25}$$

One may note that (5.25) expresses the induced change in the functional independent of the induced disturbance in the solution.

5.3.3 Optimization Method

Due to the absence of the induced disturbance in (5.25), a descent direction for α can be determined from (5.13b) and (5.25) in a straightforward manner. For this purpose, we define the gradient of E with respect to $\mathcal{S}$ by the function $grad\, E(\mathcal{S}) : \mathcal{S} \mapsto \mathbb{R}$ with the property:

$$\int_{\mathcal{S}} \alpha(\mathbf{x})\, grad\, E(\mathcal{S})(\mathbf{x}) \,\mathrm{d}\mathbf{x} = \lim_{\epsilon\to 0} \tfrac{1}{\epsilon}[E(\mathcal{S}_{\epsilon\alpha}) - E(\mathcal{S})]\,, \tag{5.26}$$

for all suitable α. By (5.12), (5.13) and (5.25), the gradient is readily identified as:

$$grad\, E(\mathcal{S}) = -\lambda\, \mathbf{nn} : \boldsymbol{\nabla}\boldsymbol{\nabla}\phi - \sum_{j=1}^{d-1} \mathbf{t}_j \cdot \boldsymbol{\nabla}(\lambda\, \mathbf{t}_j \cdot \boldsymbol{\nabla}\phi) - \frac{p^2}{2R} - p\,\mathrm{Fr}^{-2}\mathbf{n}\cdot\mathbf{e}_d\,. \tag{5.27}$$

From (5.26) it follows that if $\alpha = -grad\, E(\mathcal{S})$ and γ is set to a small positive number, then

$$E(\mathcal{S}_{\gamma\alpha}) - E(\mathcal{S}) = -\gamma \int_{\mathcal{S}} \left(grad\, E(\mathcal{S})\right)^2 \mathrm{d}\mathbf{x} + O(\gamma^2) \leq 0 + O(\gamma^2)\,. \tag{5.28}$$

Therefore, $\alpha = -grad\, E(\mathcal{S})$ is a descent direction and $\mathcal{S}_{\gamma\alpha}$ improves on $\mathcal{S}$. The free-surface flow problem can thus be solved by repeating the following operations:

(A1) For given $\mathcal{S}$, solve the primal problem (5.6) for ϕ.

(A2) Solve the dual problem (5.24) for λ.

(A3) Determine $\alpha = -grad\, E(\mathcal{S})$ from (5.27).

(A4) Choose the step size $\gamma > 0$ and adjust $\mathcal{S}$ to $\mathcal{S}_{\gamma\alpha}$.

The iterative process (A1)–(A4) is called the *adjoint optimization method*. The actual free boundary $\mathcal{S}^*$ is obtained if $grad\, E(\mathcal{S}^*) = 0$.

The condition $grad\, E(\mathcal{S}^*) = 0$ only ensures that a *local* minimum is attained. If the cost functional is non-convex, then multiple local minima can occur. The actual solution to the steady free-surface flow problem is then determined by the *global* minimum. The dynamic condition (5.3b) implies that the cost functional vanishes for the actual solution. Hence, the correct minimum is identifiable. If the cost functional is indeed non-convex, then it is important that the adjoint optimization method is provided with an initial approximation that is sufficiently close to the actual solution. For instance, a prolongated coarse-grid approximation to the solution can serve for this purpose.

5.4 Fourier Analysis of the Optimization Problem

The behavior of the cost functional in the neighborhood of a minimum is characterized by the *Hessian*, i.e., the second derivative of the cost functional with respect to the free boundary. As a result, the properties of the optimization problem and the convergence behavior of the adjoint optimization method depend on the characteristics of the Hessian. In this section we use Fourier analysis to examine the properties of the Hessian and we consider the implications for the solution behavior and the posedness of the optimal shape design problem and the convergence behavior of the adjoint method.

5.4.1 Hessian of the Functional

The behavior of the cost functional in the neighborhood of a minimum is characterized by its *Hessian*, which is defined by the function $grad^2 E(\mathcal{S}) : S \times \mathcal{S} \mapsto \mathbb{R}$ with the property:

$$\int_{\mathcal{S}} \alpha(\mathbf{y})\, grad^2 E(\mathcal{S})(\mathbf{x},\mathbf{y})\, \mathrm{d}\mathbf{y} = \lim_{\epsilon \to 0} \tfrac{1}{\epsilon}[grad\, E(\mathcal{S}_{\epsilon\alpha})(\mathbf{x}) - grad\, E(\mathcal{S})(\mathbf{x})]\,, \tag{5.29}$$

for all suitable α. To show that the properties of the optimization problem are essentially contained in the Hessian, we consider the following expansion of the cost functional:

$$E(\mathcal{S}_{\epsilon\alpha}) = E(\mathcal{S}) + \epsilon \int_{\mathcal{S}} \alpha(\mathbf{x})\, grad\, E(\mathcal{S})(\mathbf{x})\, \mathrm{d}\mathbf{x} + \frac{\epsilon^2}{2} \int_{\mathcal{S}} \int_{\mathcal{S}} \alpha(\mathbf{x})\, \alpha(\mathbf{y})\, grad^2 E(\mathcal{S})(\mathbf{x}, \mathbf{y})\, \mathrm{d}\mathbf{y}\, \mathrm{d}\mathbf{x} + O(\epsilon^3)\,, \qquad \text{as } \epsilon \to 0. \quad (5.30)$$

Clearly, in order to have a minimum, the gradient must vanish, so that indeed the Hessian determines the behavior of the cost functional in the neighborhood of a minimum.

To demonstrate that the Hessian determines the convergence behavior of the adjoint optimization method, we consider a perturbation $\mathcal{S}^*_{\epsilon\alpha}$ of the optimal boundary $\mathcal{S}^*$. Because $grad\, E(\mathcal{S}^*) = 0$, it follows from (5.29) that for sufficiently small ϵ,

$$grad\, E(\mathcal{S}^*_{\epsilon\alpha})(\mathbf{x}) = \epsilon \int_{\mathcal{S}} \alpha(\mathbf{y})\, grad^2 E(\mathcal{S}^*)(\mathbf{x}, \mathbf{y})\, \mathrm{d}\mathbf{y} + O(\epsilon^2)\,. \quad (5.31)$$

This implies that in the neighborhood of the optimum, the Hessian relates the gradient to the disturbance in the free-boundary position. Because the adjoint method uses the gradient to adjust the free boundary, the Hessian determines the change in the error in the boundary position. Hence, the Hessian indeed determines the convergence behavior of the adjoint optimization method.

5.4.2 Fourier Analysis of the Hessian

The properties of the Hessian can be conveniently examined by means of the Fourier analysis for optimization problems presented in [68]. We perform the analysis for the generic case of a domain $\mathcal{V}^* := \{\mathbf{x} \in \mathbb{R}^d : -1 < x_d < 0\}$ with free boundary $\mathcal{S}^* := \{\mathbf{x} \in \mathbb{R}^d : x_d = 0\}$ and fixed boundary $\partial\mathcal{V}^* \setminus \mathcal{S}^* = \{\mathbf{x} \in \mathbb{R}^d : x_d = -1\}$. Recall that x_d is the vertical coordinate. Assuming that the fixed boundary is impermeable, a in (5.6) is set to 1 and b and c are set to 0. The uniform horizontal flow potential $\phi^* = \mathbf{U}\cdot\mathbf{x}$, with $\mathbf{U}$ a constant vector in $\{\mathbf{U} \in \mathbb{R}^d : \|\mathbf{U}\| = 1, U_d = 0\}$, then satisfies the boundary value problem (5.6). The corresponding solution of the dual problem (5.24) is $\lambda^* = 0$ and the gradient (5.27) vanishes, so that $\mathcal{S}^*$ is the optimal boundary. Indeed, the uniform horizontal flow is a solution of the steady free-surface flow problem.

Next, consider the perturbed boundary $\mathcal{S}^*_{\epsilon\alpha}$. The solutions of the perturbed primal and dual problem are expanded as

$$\phi^*_{\epsilon\alpha} = \mathbf{U}\cdot\mathbf{x} + \epsilon\phi'_\alpha(\mathbf{x}) + O(\epsilon^2)\,, \quad (5.32a)$$

$$\lambda^*_{\epsilon\alpha} = 0 + \epsilon\lambda'_\alpha(\mathbf{x}) + O(\epsilon^2)\,. \quad (5.32b)$$

If (5.32a) and (5.32b) are inserted in (5.6) and (5.24), respectively, and the normal vector to $\mathcal{S}^*_{\epsilon\alpha}$ is expanded in the same manner as in (5.10), then collection of terms of $O(\epsilon)$ reveals that the induced disturbances are governed by:

$$\Delta\phi'_\alpha = 0\,, \qquad \mathbf{x} \in \mathcal{V}^*\,, \tag{5.33a}$$
$$\mathbf{e}_d \cdot \boldsymbol{\nabla}\phi'_\alpha = 0\,, \qquad \mathbf{x} \in \partial\mathcal{V}^* \setminus \mathcal{S}^*\,, \tag{5.33b}$$
$$\mathbf{e}_d \cdot \boldsymbol{\nabla}\phi'_\alpha = \mathbf{U} \cdot \boldsymbol{\nabla}\alpha\,, \qquad \mathbf{x} \in \mathcal{S}^*, \tag{5.33c}$$

and

$$\Delta\lambda'_\alpha = 0\,, \qquad \mathbf{x} \in \mathcal{V}^*\,, \tag{5.34a}$$
$$\mathbf{e}_d \cdot \boldsymbol{\nabla}\lambda'_\alpha = 0\,, \qquad \mathbf{x} \in \partial\mathcal{V}^* \setminus \mathcal{S}^*\,, \tag{5.34b}$$
$$\mathbf{e}_d \cdot \boldsymbol{\nabla}\lambda'_\alpha = -\mathbf{U} \cdot \boldsymbol{\nabla}(\mathbf{U} \cdot \boldsymbol{\nabla}\phi'_\alpha + \mathrm{Fr}^{-2}\alpha)\,, \qquad \mathbf{x} \in \mathcal{S}^*\,. \tag{5.34c}$$

Moreover, upon inserting (5.32) in (5.27), one obtains that the gradient corresponding to the perturbed boundary $\mathcal{S}^*_{\epsilon\alpha}$ reads

$$grad\, E(\mathcal{S}^*_{\epsilon\alpha}) = \epsilon\left(\mathrm{Fr}^{-2}(\mathbf{U} \cdot \boldsymbol{\nabla}\phi'_\alpha + \mathrm{Fr}^{-2}\alpha) - \mathbf{U} \cdot \boldsymbol{\nabla}\lambda'_\alpha\right) + O(\epsilon^2)\,. \tag{5.35}$$

Note that for any perturbation α, the induced disturbances follow from (5.33) and (5.34). The gradient corresponding to the perturbed boundary can then be obtained from (5.35). Because $grad\, E(\mathcal{S}^*) = 0$, important information about the Hessian can subsequently be extracted from (5.29).

The analysis proceeds by assuming α, ϕ'_α and λ'_α to be a linear combination of horizontal Fourier modes. Because (5.33) through (5.35) are linear in α, ϕ'_α and λ'_α, it suffices to consider a single mode. Denoting by $\mathbf{k} = k_1\mathbf{e}_1 + \cdots + k_{d-1}\mathbf{e}_{d-1}$ the horizontal wave number, α is set to

$$\alpha(\mathbf{x}) := \hat{\alpha}(\mathbf{k}) \exp(\mathrm{i}\mathbf{k} \cdot \mathbf{x})\,, \tag{5.36}$$

with $\mathrm{i} = \sqrt{-1}$. The induced disturbances ϕ'_α and λ'_α comply with (5.33) and (5.34), respectively, if

$$\phi'_\alpha = \hat{\phi}(\mathbf{k}) \exp(\mathrm{i}\mathbf{k} \cdot \mathbf{x}) \cosh\left(|\mathbf{k}|\,(x_d + 1)\right)\,, \tag{5.37a}$$
$$\lambda'_\alpha = \hat{\lambda}(\mathbf{k}) \exp(\mathrm{i}\mathbf{k} \cdot \mathbf{x}) \cosh\left(|\mathbf{k}|\,(x_d + 1)\right)\,, \tag{5.37b}$$

and

$$|\mathbf{k}| \sinh|\mathbf{k}|\, \hat{\phi}(\mathbf{k}) = \mathrm{i}\mathbf{k} \cdot \mathbf{U}\, \hat{\alpha}(\mathbf{k})\,, \tag{5.38a}$$
$$|\mathbf{k}| \sinh|\mathbf{k}|\, \hat{\lambda}(\mathbf{k}) = -\mathrm{i}\mathbf{k} \cdot \mathbf{U}\left(\mathrm{i}\mathbf{k} \cdot \mathbf{U} \cosh|\mathbf{k}|\, \hat{\phi}(\mathbf{k}) + \mathrm{Fr}^{-2}\, \hat{\alpha}(\mathbf{k})\right)\,. \tag{5.38b}$$

Recalling that $grad\, E(\mathcal{S}^*) = 0$, by (5.35) through (5.38), the change in the gradient satisfies

$$\lim_{\epsilon \to 0} \tfrac{1}{\epsilon}[grad\, E(\mathcal{S}^*_{\epsilon\alpha}) - grad\, E(\mathcal{S}^*)] = \hat{H}(\mathbf{k})\, \hat{\alpha}(\mathbf{k}) \exp(\mathrm{i}\mathbf{k} \cdot \mathbf{x})\,, \tag{5.39}$$

with

$$\hat{H}(\mathbf{k}) := \left(\mathrm{Fr}^{-2} - \frac{(\mathbf{k}\cdot\mathbf{U})^2}{|\mathbf{k}|\tanh|\mathbf{k}|} \right)^2 . \tag{5.40}$$

The object $\hat{H}(\mathbf{k})$ is referred to as the *Fourier symbol* of the Hessian.

5.4.3 Properties of the Optimization Problem

The Fourier symbol of the Hessian contains important information about the posedness and the solution behavior of the optimization problem. To illustrate this, we consider the Fourier transform of the perturbation $\alpha(\mathbf{x})$ and its inverse

$$\hat{\alpha}(\mathbf{k}) := (2\pi)^{1-d} \int_{\mathcal{S}^*} \alpha(\mathbf{x}) \exp(-\mathrm{i}\mathbf{k}\cdot\mathbf{x}) \,\mathrm{d}\mathbf{x} , \qquad \alpha(\mathbf{x}) = \int_{-\infty}^{\infty} \hat{\alpha}(\mathbf{k}) \exp(\mathrm{i}\mathbf{k}\cdot\mathbf{x}) \,\mathrm{d}\mathbf{k} . \tag{5.41}$$

From (5.29) and (5.39) it then follows that

$$\int_{\mathcal{S}^*} \alpha(\mathbf{y})\, grad^2 E(\mathcal{S}^*)(\mathbf{x},\mathbf{y}) \,\mathrm{d}\mathbf{y} = \int_{-\infty}^{\infty} \hat{H}(\mathbf{k})\, \hat{\alpha}(\mathbf{k}) \exp(\mathrm{i}\mathbf{k}\cdot\mathbf{x}) \,\mathrm{d}\mathbf{k} . \tag{5.42}$$

Hence, by (5.30), if terms of $O(\epsilon^3)$ are ignored, the change in the cost functional due to the perturbation of the free boundary reads:

$$\begin{aligned}
E(\mathcal{S}^*_{\epsilon\alpha}) - E(\mathcal{S}^*) &= \frac{\epsilon^2}{2} \int_{\mathcal{S}} \alpha(\mathbf{x}) \int_{\mathcal{S}} \alpha(\mathbf{y})\, grad^2 E(\mathcal{S}^*)(\mathbf{x},\mathbf{y}) \,\mathrm{d}\mathbf{y} \,\mathrm{d}\mathbf{x} \\
&= \frac{\epsilon^2}{2} \int_{\mathcal{S}} \alpha(\mathbf{x}) \int_{-\infty}^{\infty} \hat{H}(\mathbf{k})\, \hat{\alpha}(\mathbf{k}) \exp(\mathrm{i}\mathbf{k}\cdot\mathbf{x}) \,\mathrm{d}\mathbf{k} \,\mathrm{d}\mathbf{x} \\
&= \frac{\epsilon^2}{2} \int_{-\infty}^{\infty} \hat{H}(\mathbf{k})\, \hat{\alpha}(\mathbf{k}) \int_{\mathcal{S}} \alpha(\mathbf{x}) \exp(\mathrm{i}\mathbf{k}\cdot\mathbf{x}) \,\mathrm{d}\mathbf{x} \,\mathrm{d}\mathbf{k} \\
&= \frac{\epsilon^2}{2} (2\pi)^{d-1} \int_{-\infty}^{\infty} \hat{H}(\mathbf{k})\, \hat{\alpha}(\mathbf{k})\, \overline{\hat{\alpha}(\mathbf{k})} \,\mathrm{d}\mathbf{k} \\
&= \frac{\epsilon^2}{2} (2\pi)^{d-1} \int_{-\infty}^{\infty} \hat{H}(\mathbf{k})\, |\hat{\alpha}(\mathbf{k})|^2 \,\mathrm{d}\mathbf{k} ,
\end{aligned} \tag{5.43}$$

with $\overline{\hat{\alpha}(\mathbf{k})}$ the complex conjugate of $\hat{\alpha}(\mathbf{k})$. Equation (5.43) implies that $\hat{H}(\mathbf{k})$ expresses the ability of the optimization problem to distinguish a boundary $\mathcal{S}^*$ from a perturbed boundary $\mathcal{S}^*_{\epsilon\alpha}$, with $\alpha(\mathbf{x})$ a Fourier mode with wave number $\mathbf{k}$.

To illustrate the behavior of the Fourier symbol $\hat{H}(\mathbf{k})$, we consider (5.40) for $\mathbf{k} \in \mathbb{R}^2$ (i.e., $d = 3$). Without loss of generality, we assume that $\mathbf{U} = \mathbf{e}_1$, so that $\mathbf{k}\cdot\mathbf{U} = k_1$. Figure 5.1 on the next page then displays contours of $\mathrm{Fr}^{-2} \pm \sqrt{\hat{H}(\mathbf{k})}$, e.g., if $\mathrm{Fr} = 1/2$, then $\mathrm{Fr}^{-2} \pm \sqrt{\hat{H}(\mathbf{k})} = 4$ is the contour for which $\hat{H}(\mathbf{k}) = 0$ and $\mathrm{Fr}^{-2} \pm \sqrt{\hat{H}(\mathbf{k})} \in \{0, 8\}$ are the contours for which $\hat{H}(\mathbf{k}) = 16$.

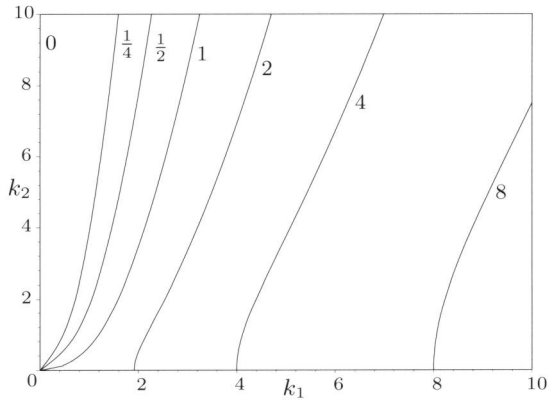

Figure 5.1: Contours of $\mathrm{Fr}^{-2} \pm \sqrt{\hat{H}(\mathbf{k})}$.

The solution behavior of the shape optimization problem is determined by the *critical modes*, i.e., the wave numbers for which $\hat{H}(\mathbf{k})$ vanishes. These critical modes yield a change in the cost functional of just $O(\epsilon^3)$, instead of $O(\epsilon^2)$. Hence, a small perturbation of the uniform free-surface flow is composed of a linear combination of the critical modes. It is important to observe that to each Froude number corresponds a curve of critical wave numbers. The critical modes are associated with steady surface gravity waves; see, e.g., Refs. [37, 44]. Note that for $d = 2$ ($k_2 = 0$) and $\mathrm{Fr} < 1$, the condition $\hat{H}(k) = 0$ yields a unique relation between the wave number of the surface gravity wave and the Froude number. For $d = 2$ and $\mathrm{Fr} \geq 1$, critical modes are absent and steady surface gravity waves do not occur.

The Fourier symbol of the Hessian also gives information about the posedness of the optimization problem. The optimization problem is said to be well posed if it has a unique solution that is stable to perturbations in the auxiliary data. Uniqueness is ensured if $\hat{H}(\mathbf{k}) > 0$ for all $\mathbf{k}$. From the above considerations, it is clear that uniqueness cannot be ensured. However, this does not necessarily imply that the optimization problem is ill posed. It merely implies that the behavior of critical modes is not described by the above theory. Linear stability of the optimization problem generally demands that

$$\hat{H}(\mathbf{k}) = O\big(|\mathbf{k}|^{\theta}\big), \qquad \text{as } |\mathbf{k}| \to \infty, \tag{5.44}$$

for some $\theta \geq 0$; see [68]. This requirement expresses that the optimization problem clearly notices high wave number perturbations of the free boundary. Unfortunately, if $\mathbf{k} \in \mathbb{R}^2$, the contours on which $\hat{H}(\mathbf{k}) = 0$ contain waves with $|\mathbf{k}| \to \infty$. Hence, the linear theory is insufficient to establish the stability of the 3 dimensional free-surface flow problem. However, such waves do not occur for $d = 2$ and, therefore, linear stability of the two-dimensional optimization problem is ensured.

5.4.4 Stability of the Adjoint Method

To examine the stability of the adjoint method, we consider a perturbation $\mathcal{S}^*_{\epsilon\alpha}$ of the optimal free boundary $\mathcal{S}^*$. One iteration of the adjoint optimization method yields a new approximation $\mathcal{S}^*_{\epsilon\underline{\alpha}}$, with

$$\epsilon\underline{\alpha}(\mathbf{x}) = \epsilon\alpha(\mathbf{x}) - \gamma\, grad\, E(\mathcal{S}^*_{\epsilon\alpha})(\mathbf{x})\,, \tag{5.45}$$

for some step-size $\gamma > 0$. Hence, by (5.31), $\underline{\alpha}$ and α are related in the following manner:

$$\underline{\alpha}(\mathbf{x}) = \alpha(\mathbf{x}) - \gamma \int_{\mathcal{S}} \alpha(\mathbf{y})\, grad^2 E(\mathcal{S}^*)(\mathbf{x},\mathbf{y})\, \mathrm{d}\mathbf{y}\,. \tag{5.46}$$

The *contraction number* ζ of the adjoint method is defined by the reduction of the error in the free-boundary position between successive iterations, i.e.,

$$\zeta := \sup_{\alpha} \frac{\left\| \alpha(\mathbf{x}) - \gamma \int_{\mathcal{S}^*} \alpha(\mathbf{y})\, grad^2 E(\mathcal{S}^*)(\mathbf{x},\mathbf{y})\, \mathrm{d}\mathbf{y} \right\|}{\|\alpha(\mathbf{x})\|}\,, \tag{5.47}$$

where the supremum is taken over all admissible functions $\alpha(\mathbf{x})$. Because $\|\underline{\alpha}\| \leq \zeta\|\alpha\|$, stability of the adjoint method is ensured if $\zeta \leq 1$.

If the L_2 norm is implied in (5.47), we can use (5.42) and Parseval's identity to recast (5.47) into:

$$\zeta = \sup_{\hat{\alpha}} \left(\frac{\int_{-\infty}^{\infty} \left(1 - \gamma \hat{H}(\mathbf{k})\right)^2 |\hat{\alpha}(\mathbf{k})|^2\, \mathrm{d}\mathbf{k}}{\int_{-\infty}^{\infty} |\hat{\alpha}(\mathbf{k})|^2\, \mathrm{d}\mathbf{k}} \right)^{1/2}\,. \tag{5.48}$$

If the problem (5.7) is solved numerically, then the infinite domain is usually truncated and $\alpha(\mathbf{x})$ is represented on a grid. In that case, if $\boldsymbol{\ell} = (\ell_1, \ldots, \ell_{d-1})$ is the horizontal length of the truncated domain and $\mathbf{h} = (h_1, \ldots, h_{d-1})$ is the horizontal mesh width of the applied grid, then we only have to consider isolated wave numbers in the set

$$\mathcal{W}_{\mathbf{h}} := \{\mathbf{k} : k_j = n\pi/\ell_j, n = \pm 1, \pm 2, \ldots, |k_j| \leq \pi/h_j\}\,; \tag{5.49}$$

see Figure 5.2 on the facing page for an illustration. It follows from (5.48) that ζ is then given by

$$\zeta = \sup_{\mathbf{k}\in\mathcal{W}_{\mathbf{h}}} |1 - \gamma \hat{H}(\mathbf{k})|\,. \tag{5.50}$$

Stability of the adjoint optimization method is ensured if the right hand side of (5.50) is at most 1. This can be accomplished by choosing the step size γ according to

$$\gamma = c \left(\sup_{\mathbf{k}\in\mathcal{W}_{\mathbf{h}}} \hat{H}(\mathbf{k}) \right)^{-1}\,, \tag{5.51}$$

for some constant $c \in]0, 2[$.

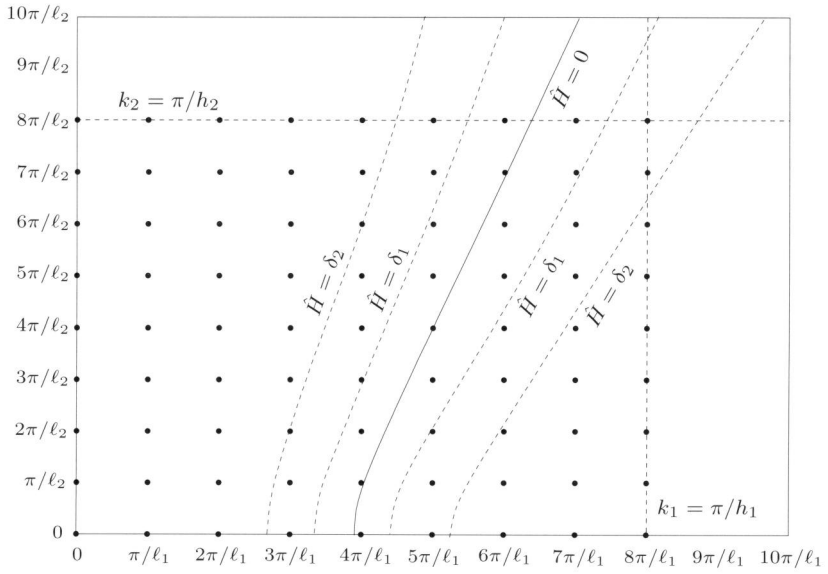

Figure 5.2: The set of wave numbers $\mathcal{W}_\mathbf{h}$ (dots) and $\hat{H}(\mathbf{k}) = 0$, $\hat{H}(\mathbf{k}) = \delta_{1,2}$.

The supremum of $\hat{H}$ in $\mathcal{W}_\mathbf{h}$ is for well posed problems determined by the highest wave number components in $\mathcal{W}_\mathbf{h}$; refer to (5.44). From (5.49) it follows that the highest wave number in $\mathcal{W}_\mathbf{h}$ is $O(1/|\mathbf{h}|)$. Hence, in general, the step size diminishes as $\gamma = O(|\mathbf{h}|^\theta)$ as $|\mathbf{h}| \to 0$. In particular, for the Fourier symbol (5.40), if the grid is refined in such a manner that $\mathbf{h} = |\mathbf{h}|\mathbf{c}$ as $|\mathbf{h}| \to 0$, with $\mathbf{c}$ a constant vector, then the supremum of $\hat{H}(\mathbf{k})$ in $\mathcal{W}_\mathbf{h}$ is $O(|\mathbf{h}|^{-2})$. The step size must then comply with

$$\gamma = O(|\mathbf{h}|^2)\,, \qquad \text{as } |\mathbf{h}| \to 0\,, \tag{5.52}$$

to maintain stability of the oscillatory modes, i.e., the modes with large $|\mathbf{k}|$. This implies that the step size in the adjoint optimization method must be reduced as the spatial grid is refined to maintain stability of the high wave number modes.

5.4.5 Convergence of the Adjoint Method

The convergence behavior of an iterative method is usually characterized by its contraction number. However, this characterization is inappropriate for problems with critical modes ($\hat{H}(\mathbf{k}) = 0$) and dispersive behavior, such as the considered free-surface flow problem. The contraction number is based on the behavior of isolated waves, whereas for dispersive problems the behavior of *wave groups* is relevant; see, e.g., Refs. [44, 78]. This distinction is essential if critical modes occur. As a result of the critical modes, the contraction number indicates that convergence lacks. However, due to the dispersive properties of the problem, this indication is too pessimistic.

To determine the convergence behavior of the adjoint optimization method (A1)–(A4), we reconsider the perturbation $\mathcal{S}^*_{\epsilon\alpha}$ of the optimal free boundary $\mathcal{S}^*$. The Fourier components of the perturbation can be separated into a contribution $\hat{\rho}(\mathbf{k})$ of the modes in the neighborhood of the critical modes and a remainder:

$$\hat{\alpha}(\mathbf{k}) = \hat{\rho}(\mathbf{k}) + \big(\hat{\alpha}(\mathbf{k}) - \hat{\rho}(\mathbf{k})\big)\,, \tag{5.53a}$$

where $\hat{\rho}(\mathbf{k}) := \hat{w}(\mathbf{k})\,\hat{\alpha}(\mathbf{k})$,

$$\hat{w}(\mathbf{k}) := \begin{cases} 1 & \text{if } \hat{H}(\mathbf{k}) \le \delta_1, \\ 0 & \text{if } \hat{H}(\mathbf{k}) \ge \delta_2, \end{cases} \tag{5.53b}$$

and $\delta_{1,2}$ are constants such that $\delta_2 > \delta_1 > 0$; see the illustration in Figure 5.2 on the page before. The transition of $\hat{w}(\mathbf{k})$ from 1 to 0 can be constructed in any suitable manner and is largely arbitrary. However, below, $\hat{\rho}(\mathbf{k})$ is required to be an analytic function.

Denoting by $\epsilon\alpha_n(\mathbf{x})$ the disturbance in the free-boundary position after n iterations of the adjoint method, we obtain from (5.42) and (5.46):

$$\hat{\alpha}_n(\mathbf{k}) = \Big(1 - \gamma\hat{H}(\mathbf{k})\Big)^n\,\hat{\alpha}(\mathbf{k})\,. \tag{5.54}$$

Hence, it follows from (5.53) that

$$\alpha_n(\mathbf{x}) = \int_{-\infty}^{\infty} \Big(1 - \gamma\hat{H}(\mathbf{k})\Big)^n\,\hat{\rho}(\mathbf{k})\exp\left(\mathrm{i}\mathbf{k}\cdot\mathbf{x}\right)\mathrm{d}\mathbf{k} + O\big(|1-\gamma\delta_1|^n\big)\,. \tag{5.55}$$

Because $|1 - \gamma\delta_1| < 1$, the remainder vanishes exponentially as $n \to \infty$. This implies that the asymptotic behavior of $\alpha_n(\mathbf{x})$ for large n is determined by the Fourier components in the neighborhood of the critical modes.

From (5.55) it follows that if $\hat{\rho}_n(\mathbf{k})$ is defined recursively by

$$\hat{\rho}_0(\mathbf{k}) = \hat{\rho}(\mathbf{k})\,, \tag{5.56a}$$

$$\hat{\rho}_n(\mathbf{k}) = \Big(1 - \gamma\hat{H}(\mathbf{k})\Big)\,\hat{\rho}_{n-1}(\mathbf{k}), \qquad n = 1, 2, \ldots, \tag{5.56b}$$

then $\alpha_n(\mathbf{x}) \sim \rho_n(\mathbf{x})$ as $n \to \infty$. Equation (5.56b) can be recast into:

$$\frac{\hat{\rho}_{n+1}(\mathbf{k}) - \hat{\rho}_n(\mathbf{k})}{\gamma} + \hat{H}(\mathbf{k})\,\hat{\rho}_n(\mathbf{k}) = 0\,. \tag{5.57}$$

Note that for sufficiently small γ, the first term can be conceived as a difference approximation to the derivative of $\hat{\rho}_n(\mathbf{k})$ with respect to *pseudo time* $n\gamma$. We assume that $\hat{\rho}_n(\mathbf{k}) \sim \exp(\tau n\gamma)\,\hat{\rho}_0(\mathbf{k})$ as $n \to \infty$. Equation (5.57) then implies

$$(\exp(\tau\gamma) - 1)/\gamma + \hat{H}(\mathbf{k}) = 0\,. \tag{5.58}$$

Taylor expansion of $\exp(\tau\gamma)$ yields

$$\tau = -\hat{H}(\mathbf{k})\,, \tag{5.59}$$

provided that $O(\tau^2)$ terms are negligible. By (5.53b), $\hat{H}(\mathbf{k}) \leq \delta_2$. Hence, if δ_2 is chosen sufficiently small, the $O(\tau^2)$ terms in the Taylor expansion can indeed be ignored. Equation (5.59) relates the pseudo time behavior of a disturbance in the free-boundary position to its spatial behavior. Therefore, it appears appropriate to refer to (5.59) as the *pseudo dispersion relation* of the adjoint method.

From (5.55) to (5.59) it follows that as $n\gamma \to \infty$,

$$\alpha_n(\mathbf{x}) \sim \int_{-\infty}^{\infty} \hat{\rho}(\mathbf{k}) \exp\left(\mathrm{i}\Omega(\mathbf{k})\, n\gamma\right) \mathrm{d}\mathbf{k}\,, \tag{5.60}$$

with

$$\Omega(\mathbf{k}) := \mathrm{i}\hat{H}(\mathbf{k}) + \frac{\mathbf{k}\cdot\mathbf{x}}{n\gamma}\,. \tag{5.61}$$

The integral in (5.60) vanishes exponentially as $n\gamma \to \infty$, except near critical stationary points of $\hat{H}(\mathbf{k})$, i.e., the wave numbers $\mathbf{k}_0$ such that

$$\hat{H}(\mathbf{k}_0) = 0\,, \qquad \frac{\partial \hat{H}}{\partial k_j}(\mathbf{k}_0) = 0\,. \tag{5.62}$$

Each critical stationary point yields a contribution

$$\hat{\rho}(\mathbf{k}_0)\left(\frac{2\pi}{n\gamma}\right)^{(d-1)/2}\left(\det\left|\frac{\partial^2 \hat{H}}{\partial k_i \partial k_j}(\mathbf{k}_0)\right|\right)^{-1/2} \exp\left(\mathrm{i}\mathbf{k}_0\cdot\mathbf{x} + \mathrm{i}\xi\right), \tag{5.63}$$

with ξ a multiple of $\pi/4$, depending on the properties of $\partial^2\hat{H}/\partial k_i \partial k_j$. The above can be proved by the method of stationary phase; see, e.g., Refs. [78, 79].

Due to the quadratic form of (5.40), any critical point is a stationary point as well. Hence, if we define the *evaluation error* e_n by the L_2 norm of the error in the boundary position, i.e., $\mathsf{e}_n := \|\epsilon\alpha_n\|$, then we anticipate that the adjoint method yields the following asymptotic convergence behavior:

$$\mathsf{e}_n = O\left(\zeta^{n\gamma}\right) \qquad \text{if } \forall\mathbf{k} : \hat{H}(\mathbf{k}) > 0\,, \tag{5.64a}$$

$$\mathsf{e}_n = O\left((n\gamma)^{(1-d)/2}\right) \qquad \text{if } \exists\mathbf{k} : \hat{H}(\mathbf{k}) = 0\,, \tag{5.64b}$$

as $n \to \infty$, for some constant ζ in $]0, 1[$. The implications of (5.64) for the convergence behavior of the adjoint method are summarized in Table 5.1 on the following page.

5.5 Preconditioning

The asymptotic error behavior (5.64) and the stability condition (5.52) imply that the performance of the adjoint optimization method deteriorates with decreasing mesh width. This deficiency of the method can be repaired by means of preconditioning. This section outlines the preconditioning operation.

Table 5.1: Convergence behavior of the adjoint method: asymptotic behavior of the evaluation error e_n for sub- and supercritical flow in 2D and 3D, with n the iteration counter, γ the step size and ζ a constant in $]0,1[$.

	$d=2$	$d=3$
subcritical	$O(1/\sqrt{n\gamma})$	$O(1/(n\gamma))$
supercritical	$O(\zeta^{n\gamma})$	$O(1/(n\gamma))$

5.5.1 Reconsideration of Objectives

To introduce the preconditioning operation, we consider the gradient of the cost functional at a perturbation $\mathcal{S}^*_{\epsilon\alpha}$ of the optimal boundary $\mathcal{S}^*$. By (5.39), the Fourier components of the gradient read:

$$\widehat{grad\, E(\mathcal{S}^*_{\epsilon\alpha})}(\mathbf{k}) = \epsilon\, \hat{H}(\mathbf{k})\, \hat{\alpha}(\mathbf{k})\,. \tag{5.65}$$

Equation (5.65) implies that for problems that are stable according to (5.44) with θ strictly positive, the gradient primarily contains highly oscillatory modes (large $|\mathbf{k}|$). Consequently, the adjoint optimization method effectively reduces the cost functional by removing the highly oscillatory disturbances in the boundary position. However, smooth error components are inadequately resolved.

In general, one is interested in obtaining the free-boundary position rather than minimizing the cost functional. If the objective is indeed to obtain the free boundary, then the gradient is unsuitable for adjusting the boundary position.

5.5.2 General Outline

The aim of preconditioning is to restore the relation between the boundary adjustment and the error in the boundary position. An accurate approximation to the error in the free-boundary position can be recovered from the gradient by solving

$$P\,\beta = grad\, E(\mathcal{S}^*_{\epsilon\alpha})\,, \tag{5.66}$$

where P is any convenient operator of which the Fourier symbol satisfies

$$\hat{H}(\mathbf{k}) \le \hat{P}(\mathbf{k})\,, \qquad \text{for all } \mathbf{k}\,, \tag{5.67a}$$

$$\lim_{|\mathbf{k}|\to\infty} \hat{H}(\mathbf{k})/\hat{P}(\mathbf{k}) = C\,, \qquad \text{for some } C \in]\,0,1\,]\,. \tag{5.67b}$$

The operator P simulates the relation between the gradient and the disturbance in the boundary position. The Fourier components $\hat{\beta}(\mathbf{k})$ are related to the components of the disturbance by:

$$\hat{\beta}(\mathbf{k}) = \big(\hat{H}(\mathbf{k})/\hat{P}(\mathbf{k})\big)\, \hat{\alpha}(\mathbf{k})\,. \tag{5.68}$$

Therefore, $\beta(\mathbf{x})$ is an accurate approximation to $\alpha(\mathbf{x})$ if $\hat{H}(\mathbf{k})/\hat{P}(\mathbf{k}) \approx 1$.

If the adjoint method uses $\beta(\mathbf{x})$ instead of the gradient to displace the free boundary, then the corresponding stability condition reads:

$$|1 - \gamma\, \hat{H}(\mathbf{k})/\hat{P}(\mathbf{k})| \leq 1\,. \tag{5.69}$$

Requirement (5.67a) ensures that $\hat{H}/\hat{P} \leq 1$ for all $\mathbf{k}$, so that the step size γ in the preconditioned method can be set to 1. Consequently, if the problem is solved numerically, the convergence behavior of the preconditioned method is independent of the mesh width of the applied grid. Condition (5.67b) makes certain that all Fourier components that are present in the boundary disturbance are also present in the correction, so that the error indeed vanishes as the iteration progresses.

It is important that the numerical methods for solving (5.66) do not reintroduce the mesh-width dependence. In general, preconditioners P can be constructed for which efficient solution methods, e.g., multigrid methods [8, 67], are available.

5.5.3 A Preconditioner for 2D Free-Surface Flows

The construction of the preconditioner from its symbol relies on the theory of pseudo-differential operators; see also [66]. In this section we set up a preconditioner for the 2D steady free-surface flow problem. It is anticipated that a preconditioner for 3D free-surface flows can be constructed similarly.

In two dimensions, the free-boundary is one dimensional and the considered wave number is $k \in \mathbb{R}$. Without loss of generality, we assume that the velocity is scaled such that $U = 1$ in (5.40). To derive the preconditioner, we first consider the asymptotic behavior of (5.40) for large k:

$$\hat{H}(k) \sim k^2\,, \qquad \text{as } k \to \infty\,. \tag{5.70}$$

The Fourier symbol $-k^2$ corresponds to a Laplace operator. An operator which has the desired behavior for high wave-number components is:

$$P_H\, \beta := (\mathrm{Fr}^{-2} - 1)^2 \beta - \frac{\partial^2 \beta}{\partial t^2}\,, \tag{5.71}$$

where $\partial/\partial t$ denotes the tangential derivative along the free boundary. The Fourier symbol of (5.71) is

$$\hat{P}_H(k) = (\mathrm{Fr}^{-2} - 1)^2 + k^2\,. \tag{5.72}$$

Indeed, $\hat{P}_H(k) \sim k^2$ as $k \to \infty$. Figure 5.3 on the next page compares the Fourier symbols $\hat{P}_H$ and $\hat{H}$. The behavior of $\hat{P}_H$ closely resembles that of $\hat{H}$ at high wave-numbers. Hence, P_H accurately recovers highly oscillatory errors in the boundary position. Moreover, P_H eliminates the mesh-width dependence of the step size.

The Fourier symbols $\hat{P}_H$ and $\hat{H}$ differ markedly at low wave numbers if $\mathrm{Fr} < 1$. For $\mathrm{Fr} < 1$, the low wave-number behavior of $\hat{H}$ is accurately approximated by:

$$\hat{P}_L(k) = \left(1 - (2 - 2\mu)(k/k_0)^2 + (1 - \mu)(k/k_0)^4\right)\left(\mathrm{Fr}^{-2} - 1\right)^2\,, \tag{5.73}$$

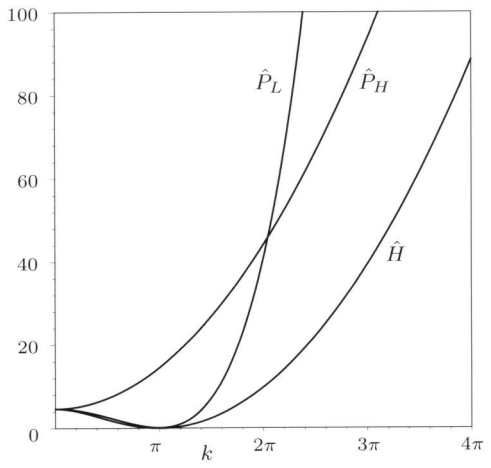

Figure 5.3: Fourier symbols $\hat{P}_L(k)$, $\hat{P}_H(k)$ and $\hat{H}(k)$ for $\mathrm{Fr} = \sqrt{\tanh(\pi)/\pi}$

with k_0 the critical wave number critical mode of (5.40) and μ a small positive constant; see Figure 5.3. The symbol $\hat{P}_L(k)$ corresponds to the differential operator

$$P_L\,\beta := \left(\mathrm{Fr}^{-2} - 1\right)^2 \left(\beta + \frac{2-2\mu}{k_0^2}\,\frac{\partial^2\beta}{\partial t^2} + \frac{1-\mu}{k_0^4}\,\frac{\partial^4\beta}{\partial t^4}\right). \tag{5.74}$$

The constant μ ensures that the polynomial $\hat{P}_L(k)$ has no real roots. This is a prerequisite for stability of the preconditioner. Unfortunately, it also implies that the preconditioner leaves the root of $\hat{H}$ undisturbed, i.e., $\hat{H}(k)/\hat{P}_L(k) = 0$ for critical modes. Hence, the asymptotic convergence behavior (5.64b) is not essentially improved.

Summarizing, for supercritical flows an effective correction of the free boundary can be obtained from (5.66) and (5.71). The mesh-width dependence of the convergence behavior is then eliminated. For subcritical flows, the correction is a combination of a high wave number correction β_H from (5.66), (5.71) and a low wave number correction β_L from (5.66), (5.74), e.g., $(\beta_L + \beta_H)/2$. The mesh-width dependence of the convergence behavior is then removed. However, the asymptotic convergence behavior is not improved, because the preconditioning does not remove the critical modes.

5.6 Numerical Experiments

The preconditioned adjoint optimization method is tested for 2 dimensional sub- and supercritical flow over an obstacle in a channel of unit depth at $\mathrm{Fr} = 0.43$ and $\mathrm{Fr} = 2.05$. The geometry of the obstacle is

$$y(x) = -1 + \frac{27}{4}\frac{H}{L^3}x(x-L)^2\,, \qquad 0 \le x \le L\,, \tag{5.75}$$

with H and L the (non-dimensionalized) height and length of the obstacle, respectively. We choose $H = 0.2$, $L = 2$ for the subcritical test case and $H = 0.44$ and $L = 4.4$ for the supercritical test case, in accordance with the experimental setup from [11]. In addition, we consider the subcritical test case with $H = 0.1$, $L = 2$ and the supercritical test case with $H = 0.22$ and $L = 4.4$.

The boundary value problems (5.7) and (5.24) are discretized with bilinear finite elements. The differential operators in the gradient (5.27) are discretized with central differences. The resulting discrete optimization problem is unstable and displays odd/even oscillations. These are simply removed by smoothing the gradient with the biharmonic operator. For subcritical flows (Fr < 1), a radiation condition must be imposed to avoid nonphysical upstream waves; cf. §5.2.1. The upstream waves are eliminated by smoothing the gradient upstream of the obstacle with the Laplace operator, and by applying the low wave number preconditioner P_L only downstream.

The numerical experiments are performed on grids with horizontal mesh width $h \in \{L/36, L/72\}$ and vertical mesh width $1/24$. For the supercritical test case, the correction is computed using (5.66) and (5.71). For the subcritical test case, the upstream correction is determined in the same manner and the downstream correction is taken as $(\beta_L + \beta_H)/2$, with β_H from (5.66), (5.71) and β_L from (5.66), (5.74). The constant μ in (5.74) is set to 0.025. In all cases the step size $\gamma = 1$ is employed.

For the supercritical test case, Fig. 5.4 on the following page plots the L_2 norm of the correction after n iterations, $\|\beta_n\|$, versus the iteration counter. The correction behaves as $\|\beta_n\| = O(\zeta^n)$, for some constant $\zeta \in]0, 1[$. The norm of the evaluation error after n iterations can be bounded by

$$\mathsf{e}_n \leq \sum_{j=n}^{\infty} \|\beta_j\| \,. \tag{5.76}$$

It follows from (5.76) that the evaluation error converges as $O(\zeta^n)$ as well. This is in accordance with the entry in Table 5.1 on page 72. From Fig. 5.4 we obtain $\zeta \approx 0.35$ for $H = 0.22$ and $\zeta \approx 0.5$ for $H = 0.44$. One may note that the convergence behavior is indeed independent of the mesh width. Fig. 5.5 on page 77 compares the computed surface elevation with measurements from [11] for the supercritical test case. The computed result agrees well with the measurements.

For the subcritical test case, $\|\beta_n\|$ is plotted versus n in Fig. 5.6 on page 77. Note that Fig. 5.6 is a log-log plot. In this case, $\|\beta_n\|$ behaves as $O(n^{-\sigma})$, with $\sigma \approx 1.5$ for $H = 0.1$ and $\sigma \approx 1.2$ for $H = 0.2$. It follows from (5.76) that the convergence behavior of the evaluation error is approximately $O(n^{-0.5})$ for $H = 0.1$ and $O(n^{-0.2})$ for $H = 0.2$. Hence, the test case with $H = 0.1$ confirms the entry in Table 5.1 on page 72. The deteriorated converge behavior for $H = 0.2$ can be attributed to apparent nonlinear behavior. One may note that the convergence behavior is virtually independent of the mesh width. Fig. 5.7 on page 78 compares the computed surface elevation with measurements from [11] for the subcritical

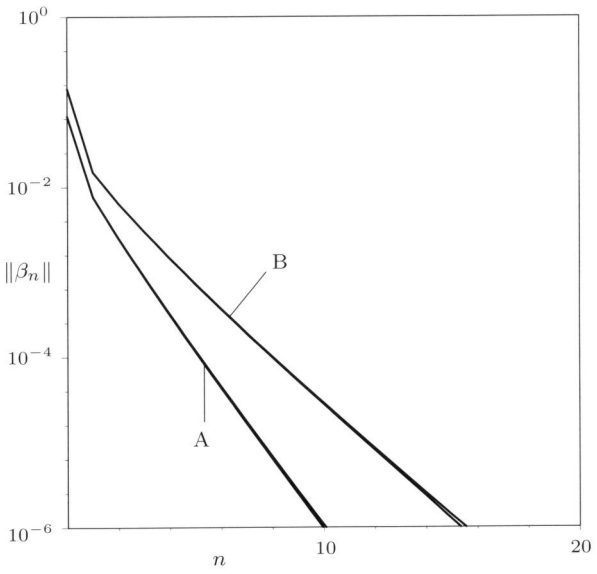

Figure 5.4: Supercritical test case: norm of the correction versus the iteration counter for $H = 0.22$ (A) and $H = 0.44$ (B) ($h = L/36$ and $h = L/72$ coincide).

test case. The surface elevation displays typical nonlinear effects, such as sharp wave crests and wave length reduction. The amplitude of the computed result is overestimated. However, the overestimation of the amplitude of the trailing wave is not unusual; see, for instance, [10, 75, 76]. The wave length of the computed result is in good agreement with the measurements.

5.7 Conclusions and Discussion

We investigated the suitability of the adjoint optimal shape design method for solving steady free-surface flows. To this end, the free-surface potential flow problem was reformulated into an equivalent optimal shape design problem. We then presented the adjoint optimization method for solving the design problem. We determined the asymptotic convergence behavior of the adjoint method for sub- and supercritical flows in 2D and 3D. Moreover, we showed that preconditioning is imperative to avoid mesh-width dependence of the convergence behavior and we presented a suitable preconditioner for the free-surface flow problem.

Numerical results were presented for two-dimensional flow over an obstacle in a channel. The observed convergence behavior is in agreement with the asymptotic estimates, i.e., the evaluation error behaves as $O(\zeta^n)$ for the supercritical test case and as $O(n^{-1/2})$ for the subcritical test case. Moreover, the numerical results confirm that the convergence behavior of the preconditioned adjoint method is

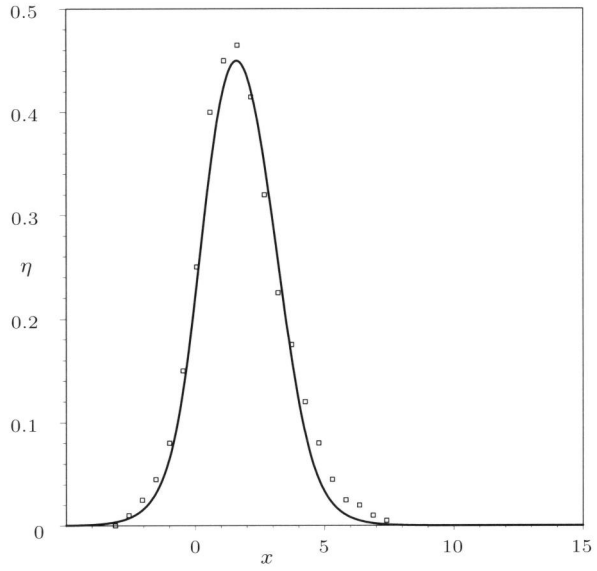

Figure 5.5: Supercritical test case: computed surface elevation with $H = 0.44$ and $h = L/72$ (*solid line*) and measurements from [11] (*markers only*)

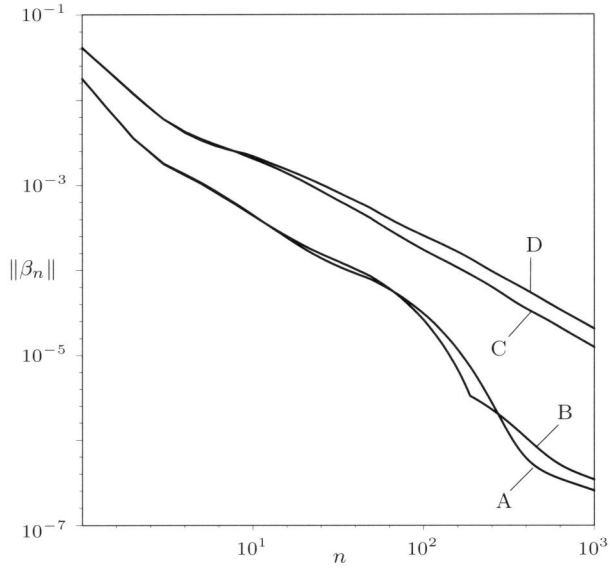

Figure 5.6: Subcritical test case: norm of the correction versus the iteration counter for $H = 0.1$, $h = L/36$ (A), $h = L/72$ (B) and $H = 0.2$, $h = L/36$ (C), $h = L/72$ (D)

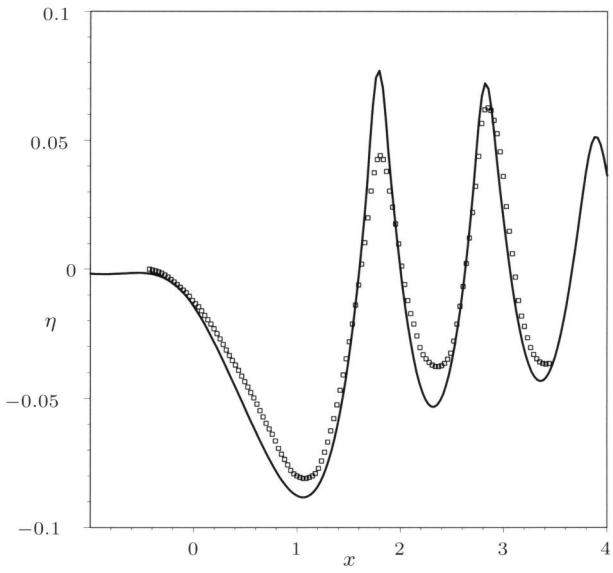

Figure 5.7: Subcritical test case: computed surface elevation with $H = 0.2$ and $h = L/72$ (*solid line*) and measurements from [11] (*markers only*)

independent of the mesh width. For both test cases the computed results agree well with measurements.

The convergence behavior of the adjoint shape optimization method for steady free surface flows is for two-dimensional problems similar to that of time-integration methods (see also [10]): the error converges as $O(\zeta^n)$ for supercritical flows and as $O(n^{-1/2})$ for subcritical flows. For three-dimensional problems, the anticipated convergence behavior of the adjoint method is $O(n^{-1})$ for sub- and supercritical flows. The convergence behavior of time-integration methods is $O(n^{-1})$ for subcritical flows and $O(\zeta^n)$ for supercritical flows. The convergence behavior of the preconditioned adjoint method is independent of the mesh width, whereas the convergence behavior of the usual time-integration method deteriorates with decreasing mesh width, due to a CFL-restriction on the admissible time step. Therefore, the preconditioned adjoint method is expected to be more efficient than time-integration methods, except in the case of 3D supercritical flow. However, for 3D flows and 2D subcritical flows, the convergence behavior of the adjoint method is less efficient than the mesh-width independent $O(\zeta^n)$ behavior of the method presented in [10].

The $O(n^{-1/2})$ (2D, subcritical) and $O(n^{-1})$ (3D) convergence behavior of the adjoint method is caused by the critical modes. It is therefore anticipated that a combination of the adjoint method and a solution method that effectively eliminates these critical modes yields $O(\zeta^n)$ convergence behavior.

Chapter 6
Interface Capturing

6.1 Introduction

Free-surface flows can be construed as a particular instance of *two-fluid flow*, in which the stresses exerted on the interface by one fluid are negligible on a reference scale that is appropriate for the other. If the objective is the numerical solution of a free-surface flow problem, then it can be attractive to adhere to the two-fluid-flow formulation. The interface behaves as a contact discontinuity and can be treated as such. This treatment of the interface is referred to as *interface capturing*. For examples of interface capturing see, for instance, Refs. [14, 34, 46].

The interface capturing approach requires that the employed numerical techniques remain robust and accurate in the presence of discontinuities. Godunov-type schemes [22] can be particularly useful in these circumstances. These schemes apply the (approximate) solution of an associated Riemann problem to determine the fluxes that are required in the numerical computation. This approach ensures robustness and accuracy at discontinuities. Godunov-type schemes can be suitably combined with finite volume methods and with discontinuous Galerkin finite element methods. For finite volume methods, the schemes can be implemented with higher-order limited interpolation methods, to achieve accuracy and secure monotonicity preservation in regions where large gradients occur (see, e.g., Refs. [61, 65]). For discontinuous Galerkin methods, accuracy and monotonicity preservation is obtained by appropriate *hp*-adaptivity; see, e.g., Refs. [27, 64].

A disadvantage of the method originally proposed by Godunov is that it requires the solution of an associated Riemann problem with each flux evaluation. In practice, many such evaluations are performed during an actual computation. Consequently, the method is notorious for its high computational costs. To avoid this problem, several approaches have been suggested to reduce the computational costs of the flux evaluations, by approximating the Riemann solution. Examples

of such approximate Riemann solvers are the flux vector splitting schemes (such as those by Van Leer [40] and Steger & Warming [62]) and the flux-difference splitting schemes (such as Roe's [53] and Osher's [49]).

A common objection to interface capturing is the occurrence of so-called *pressure oscillations*. These pressure oscillations expose the loss of certain invariance properties of the continuum problem under discretization. Several correctives have been proposed to avoid pressure oscillations, e.g., (locally) nonconservative discretization methods [1, 32, 33, 56], correction methods [31] and the ghostfluid method [18]. For an overview of these correctives, and of their merits and deficiencies, see [2]. However, it is not evident that the loss of the aforementioned invariance properties is inevitable. In fact, since the invariance properties are inherent to the continuum equations, it should be possible to devise conservative numerical schemes that inherit these invariance properties.

In the present chapter we consider the interface capturing approach to solving two-fluid flow problems. We investigate an eminent flux-difference splitting scheme for the approximate solution of Riemann problems, viz., Osher's scheme, and we consider its application to two-fluid flows. Moreover, we examine the pressure oscillations that are commonly incurred by discrete approximations to two-fluid flow problems, and we set up a non-oscillatory conservative discretization.

The contents of this chapter are organized as follows: As a preliminary, Section 6.2 presents a general introduction to the Riemann problem. In Section 6.3 we examine Osher's approximate Riemann solver. Motivated by the fact that Osher's scheme suffers loss of accuracy in the presence of slow, strong shock waves, we propose a modified scheme. Section 6.4 presents the specifics for two-fluid flows. In Section 6.5 we examine pressure oscillations and we propose a non-oscillatory conservative discretization.

6.2 Riemann Problem

In this section we investigate the Riemann problem. To define the problem, we represent space and time by $x \in (-\infty, \infty)$ and $t \in [0, \infty)$, respectively, and we consider *state variables* $\mathbf{q} := (q_1, \ldots, q_n)$ with $q_k := q_k(x,t)$ and a continuously differentiable *flux function* $\mathbf{f} : \mathbb{R}^n \mapsto \mathbb{R}^n$. The Riemann problem is defined by

$$\frac{\partial \mathbf{q}}{\partial t} + \frac{\partial \mathbf{f}(\mathbf{q})}{\partial x} = 0, \qquad (x,t) \in (-\infty, \infty) \times (0, \infty) \tag{6.1a}$$

subject to the initial condition

$$\mathbf{q}(x,0) = \begin{cases} \mathbf{q}_L\,, & \text{if} \quad x < 0\,, \\ \mathbf{q}_R\,, & \text{if} \quad x > 0\,, \end{cases} \tag{6.1b}$$

for certain constant left and right states, $\mathbf{q}_L$ and $\mathbf{q}_R$.

6.2.1 Weak Formulation

To allow discontinuous solutions a different setting of the Riemann problem is required. Classical solutions of (6.1) are differentiable. Discontinuous solutions can be taken into consideration if (6.1) is replaced by its *weak formulation*, viz., the variational problem: find $\mathbf{q}(x,t)$ such that

$$\int_0^\infty \int_{-\infty}^{\infty} (\mathbf{q}a_t + \mathbf{f}(\mathbf{q})a_x)\,\mathrm{d}x\,\mathrm{d}t + \int_{-\infty}^{0} \mathbf{q}_L a(0,x)\,\mathrm{d}x + \int_0^\infty \mathbf{q}_R a(0,x)\,\mathrm{d}x = 0\,, \quad (6.2)$$

for all continuously differentiable $a(x,t)$ with compact support in $(-\infty,\infty)\times[0,\infty)$. A discontinuous solution of (6.2) is called a *weak solution*.

The variational formulation (6.2) generally allows multiple solutions, because a classical solution can often be replaced by a weak solution. Therefore, the weak formulation (6.2) must be supplemented with an *entropy condition* to single out the physically correct solution. For entropy conditions we refer to [39, 47, 60].

6.2.2 Preliminaries

To facilitate the presentation, we first introduce some elementary concepts. The Jacobian of $\mathbf{f}(\mathbf{q})$ is denoted by $\mathbf{A}(\mathbf{q}) := \partial_{\mathbf{q}}\mathbf{f}(\mathbf{q})$. Its eigenvalues are $\lambda_k(\mathbf{q})$, with $k = 1, 2, \ldots, n$, and are assumed to be indexed such that $\lambda_1 \le \lambda_2 \le \ldots \le \lambda_n$. The corresponding eigenvectors are $\mathbf{r}_k(\mathbf{q})$.

The differential equation (6.1a) constitutes a *hyperbolic system* if the eigenvalues $\lambda_k(\mathbf{q})$ are real and nonzero. The Jacobian-matrix $\mathbf{A}(\mathbf{q})$ can then be decomposed with respect to a basis of its eigenvectors:

$$\mathbf{A}(\mathbf{q}) = \mathbf{R}(\mathbf{q})\cdot\mathbf{\Lambda}(\mathbf{q})\cdot\mathbf{R}(\mathbf{q})^{-1}\,, \quad (6.3)$$

where $\mathbf{\Lambda}(\mathbf{q}) := \mathrm{diag}(\lambda_1(\mathbf{q}), \ldots, \lambda_n(\mathbf{q}))$ and the matrix $\mathbf{R}(\mathbf{q}) := (\mathbf{r}_1(\mathbf{q}), \ldots, \mathbf{r}_n(\mathbf{q}))$ contains the eigenvectors.

From [38] we adopt the following classification of the eigenpairs: An eigenvalue $\lambda_k(\mathbf{q})$ and an eigenvector $\mathbf{r}_k(\mathbf{q})$ are called *genuinely nonlinear* in $\Omega \subseteq \mathbb{R}^n$ if

$$\partial_{\mathbf{q}}\lambda_k(\mathbf{q})\cdot\mathbf{r}_k(\mathbf{q}) \neq 0, \qquad \text{for all } \mathbf{q} \in \Omega. \quad (6.4)$$

Equation (6.4) implies that the eigenvalue is a strictly convex or concave function of $\mathbf{q}$ in the direction of the corresponding eigenvector. An eigenvalue $\lambda_k(\mathbf{q})$ and an eigenvector $\mathbf{r}_k(\mathbf{q})$ are said to be *linearly degenerate* in Ω if

$$\partial_{\mathbf{q}}\lambda_k(\mathbf{q})\cdot\mathbf{r}_k(\mathbf{q}) = 0\,, \qquad \text{for all } \mathbf{q} \in \Omega\,. \quad (6.5)$$

Equation (6.5) implies that $\lambda_k(\mathbf{q})$ is constant in the direction of the corresponding eigenvector. The eigenvalues that are genuinely nonlinear are related to *rarefaction waves* and *shock waves* in the solution of the Riemann problem. The eigenvalues that are linearly degenerate correspond to *contact discontinuities* in the solution.

More complicated wave types can occur for eigenvalues that are neither genuinely nonlinear nor linearly degenerate. This occurs, for instance, in the case of the Buckley-Leverett equation; see, e.g., Refs. [42, 77].

With each of the eigenpairs $(\lambda_k(\mathbf{q}), \mathbf{r}_k(\mathbf{q}))$ we associate two paths in state space: Firstly, the *k-shock path*, which is defined by the set

$$\mathcal{S}_k(\mathbf{q}_L) := \{\mathbf{q} \in \mathbb{R}^n : s(\mathbf{q};\mathbf{q}_L)(\mathbf{q}-\mathbf{q}_L) = \mathbf{f}(\mathbf{q}) - \mathbf{f}(\mathbf{q}_L)\}\,, \tag{6.6}$$

where $s(\mathbf{q};\mathbf{q}_L)$ is referred to as the *shock speed*. Secondly, the *k-rarefaction path*, defined by the set

$$\mathcal{R}_k(\mathbf{q}_L) := \{\mathbf{q} \in \mathbb{R}^n : \mathbf{q} = \mathbf{h}(\xi), \xi \in \mathbb{R}\}\,, \tag{6.7}$$

with $\mathbf{h}(\xi)$ the solution to the ordinary differential equation

$$\mathbf{h}'(\xi) = \mathbf{r}_k(\mathbf{h}(\xi))\,, \qquad \xi \in \mathbb{R}\,, \tag{6.8a}$$

$$\mathbf{h}(\xi_L) = \mathbf{q}_L\,, \tag{6.8b}$$

for some $\xi_L \in \mathbb{R}$.

To each k-rarefaction path corresponds a set of *Riemann invariants*, i.e., functions which are invariant on $\mathcal{R}_k$. If $\mathbf{r}_k(\mathbf{q})$ denotes the k^{th} eigenvector of the Jacobian, then a k-Riemann invariant is any continuously differentiable function $\psi_k : \mathbb{R}^n \mapsto \mathbb{R}$ with the property

$$\partial_{\mathbf{q}}\psi_k(\mathbf{q}) \cdot \mathbf{r}_k(\mathbf{q}) = 0\,, \tag{6.9}$$

for all considered states. There are at most $n-1$ such k-Riemann invariants with linearly independent derivatives with respect to $\mathbf{q}$ in $\mathbb{R}^n$. Note that for a linearly degenerate eigenpair $(\lambda_k(\mathbf{q}), \mathbf{r}_k(\mathbf{q}))$ the eigenvalue $\lambda_k(\mathbf{q})$ is a k-Riemann invariant.

6.2.3 Waves

The general solution to (6.1) consists of regions in the (x,t)-plane where the solution is constant, separated by waves, in particular, rarefaction waves, contact discontinuities and shock waves. Before constructing the general solution, we first obtain the solution to (6.1) or (6.2) in the case that it contains only one of the aforementioned waves.

Classical and weak solutions of the Riemann problem can generally be written in the similarity form

$$\mathbf{q}(x,t) = \mathbf{h}(x/t)\,; \tag{6.10}$$

see, e.g., Ref. [60]. To prove this, we note that if $\mathbf{q}(x,t)$ solves (6.1), then for all $\zeta \in \mathbb{R}$, $\mathbf{q}_\zeta(x,t) := \mathbf{q}(\zeta x, \zeta t)$ is also a solution. This is evident from

$$\frac{\partial \mathbf{q}(\zeta x,\zeta t)}{\partial t} + \frac{\partial \mathbf{f}(\mathbf{q}(\zeta x,\zeta t))}{\partial x} = \zeta\left[\mathrm{D}_2\mathbf{q}(\zeta x,\zeta t) + \mathbf{A}(\mathbf{q}(\zeta x,\zeta t)) \cdot \mathrm{D}_1\mathbf{q}(\zeta x,\zeta t)\right] = 0\,, \tag{6.11}$$

where D_l denotes differentiation with respect to the l^{th} function argument. If the solution is unique, then $\mathbf{q}(x,t) = \mathbf{q}_\varsigma(x,t)$ and, hence, $\mathbf{q}(x,t)$ can be cast into the similarity form (6.10).

A classical *k-rarefaction wave* (or *k-simple wave*) solution of (6.1) exists if $\lambda_k(\mathbf{q})$ is a genuinely nonlinear eigenvalue, $\lambda_k(\mathbf{q}_L) < \lambda_k(\mathbf{q}_R)$ and $\mathbf{q}_R$ is on the k-rarefaction path through $\mathbf{q}_L$. For later reference, we note that this implies that the k-Riemann invariants are equal for $\mathbf{q}_L$ and $\mathbf{q}_R$, i.e., $\psi_k^m(\mathbf{q}_L) = \psi_k^m(\mathbf{q}_R)$ for $m = 1, \ldots, n$, $m \neq k$. To determine the rarefaction wave solution, we assume that the eigenvector in (6.8) is normalized such that

$$\partial_{\mathbf{q}} \lambda_k(\mathbf{q}) \cdot \mathbf{r}_k(\mathbf{q}) = 1 \,, \qquad \text{for all } \mathbf{q} \in \mathbb{R}^n \,. \tag{6.12}$$

This assumption does not restrict generality. The solution of (6.8) is then the similarity solution in the simple wave region $\lambda_k(\mathbf{q}_L) < x/t < \lambda_k(\mathbf{q}_R)$; see, e.g., Refs. [39, 60]. For verification, we insert $\mathbf{q}(x,t) = \mathbf{h}(x/t)$ in (6.1a):

$$\frac{\partial \mathbf{h}(x/t)}{\partial t} + \frac{\partial \mathbf{f}(\mathbf{h}(x/t))}{\partial x} = \frac{1}{t}\left(-\mathbf{I}\frac{x}{t} + \mathbf{A}(\mathbf{h}(x/t))\right) \cdot \mathrm{D}\mathbf{h}(x/t) = 0 \,, \tag{6.13}$$

where $\mathbf{I}$ denotes the $\mathbb{R}^{n\times n}$ identity matrix and D denotes differentiation with respect to the function argument. Equation (6.13) requires that $x/t = \lambda_k(\mathbf{h}(x/t))$ and that $\mathrm{D}\mathbf{h}(x/t) = \mathbf{r}_k(\mathbf{h}(x/t))$. The latter trivially follows from (6.8), the former from (6.12). Hence, the Riemann solution in the case of a k-rarefaction wave reads

$$\mathbf{q}(x,t) = \begin{cases} \mathbf{q}_L \,, & \text{if} \quad x/t < \lambda(\mathbf{q}_L) \,, \\ \mathbf{h}(x/t) \,, & \text{if} \quad \lambda(\mathbf{q}_L) < x/t < \lambda(\mathbf{q}_R) \,, \\ \mathbf{q}_R \,, & \text{if} \quad x/t > \lambda(\mathbf{q}_R) \,. \end{cases} \tag{6.14}$$

The states $\mathbf{q}_L$ and $\mathbf{q}_R$ are connected by an isolated *k-contact discontinuity* if $(\lambda_k(\mathbf{q}), \mathbf{r}_k(\mathbf{q}))$ is a linearly degenerate eigenpair and $\mathbf{q}_R$ is on the k-rarefaction path through $\mathbf{q}_L$. By (6.5), $\lambda_k(\mathbf{q}_R) = \lambda_k(\mathbf{q}_L)$. The solution to the Riemann problem can be obtained from (6.14):

$$\mathbf{q}(x,t) = \begin{cases} \mathbf{q}_L \,, & \text{if} \quad x/t < \lambda(\mathbf{q}_L) = \lambda(\mathbf{q}_R) \,, \\ \mathbf{q}_R \,, & \text{if} \quad x/t > \lambda(\mathbf{q}_L) = \lambda(\mathbf{q}_R) \,. \end{cases} \tag{6.15}$$

However, because (6.15) is discontinuous at $x/t = \lambda(\mathbf{q}_L) = \lambda(\mathbf{q}_R)$, it must be verified that (6.15) complies with the variational problem (6.2). Inserting (6.15) in (6.2) and using integration by parts and the compact support of a, it follows that (6.15) indeed satisfies (6.2).

A *k-shock wave* occurs if $\lambda_k(\mathbf{q})$ is a genuinely nonlinear eigenvalue, $\lambda_k(\mathbf{q}_L) > \lambda_k(\mathbf{q}_R)$ and $\mathbf{q}_R$ is on the k-shock path through $\mathbf{q}_L$. A solution of the form (6.14) is then necessarily multiple valued and must therefore be discarded. Instead, the weak solution reads

$$\mathbf{q}(x,t) = \begin{cases} \mathbf{q}_L \,, & \text{if} \quad x/t < s(\mathbf{q}_L; \mathbf{q}_R) \,, \\ \mathbf{q}_R \,, & \text{if} \quad x/t > s(\mathbf{q}_L; \mathbf{q}_R) \,, \end{cases} \tag{6.16}$$

where $s(\mathbf{q}_L;\mathbf{q}_R)$ denotes the *shock speed*, determined by the *Rankine–Hugoniot relation*

$$s(\mathbf{q}_L;\mathbf{q}_R)(\mathbf{q}_L - \mathbf{q}_R) = \mathbf{f}(\mathbf{q}_L) - \mathbf{f}(\mathbf{q}_R). \tag{6.17}$$

The shock relation (6.17) is in fact implied by the variational problem (6.2); see, for instance, Refs. [77]. Conversely, (6.17) ensures that (6.16) satisfies (6.2) for all appropriate a with support on the discontinuity. Clearly, (6.16) satisfies (6.2) for all a with support outside the discontinuity. Hence, (6.16) is a valid weak solution of (6.1).

6.2.4 General Solution

If the eigenvalues of the Jacobian are either genuinely nonlinear or linearly degenerate, then the general solution to the Riemann problem consists of $n+1$ (possibly empty) regions Ω_l in the (x,t)-plane where the solution is constant, separated by rarefaction waves, contact discontinuities and shock waves. To construct the general solution, we define $\mathbf{q}_0 := \mathbf{q}_L$, $\mathbf{q}_1 := \mathbf{q}_R$ and $\mathbf{q}_{l/n}$, $l = 0,\dots,n$ is the solution in Ω_l. If $\mathbf{q}_{(l-1)/n}$ is connected to $\mathbf{q}_{l/n}$ by a rarefaction wave, then $\mathbf{h}_l(x/t)$ denotes the similarity solution in the rarefaction wave region. Moreover, if $\mathbf{q}_{(l-1)/n}$ is connected to $\mathbf{q}_{l/n}$ by a shock wave, then s_l is the corresponding shock speed. The Riemann solution reads

$$\mathbf{q}(x,t) = \begin{cases} \mathbf{q}_0\,, & \text{if} \quad x/t < \sigma_0^+\,, & \\ \mathbf{q}_{l/n}\,, & \text{if} \quad \sigma_l^- < x/t < \sigma_l^+\,, & l = 1,\dots,n-1\,, \\ \mathbf{h}_l(x/t)\,, & \text{if} \quad \sigma_{l-1}^+ < x/t < \sigma_l^-\,, & l = 1,\dots,n-1\,, \\ \mathbf{q}_1\,, & \text{if} \quad x/t > \sigma_n^-\,, & \end{cases} \tag{6.18a}$$

with

$$\sigma_l^+ = \begin{cases} \lambda_{l+1}(\mathbf{q}_{l/n})\,, & \text{if} \quad \lambda_{l+1}(\mathbf{q}_{l/n}) \le \lambda_{l+1}(\mathbf{q}_{(l+1)/n})\,, \\ s_{l+1}\,, & \text{otherwise}\,, \end{cases} \tag{6.18b}$$

$$\sigma_l^- = \begin{cases} \lambda_l(\mathbf{q}_{l/n})\,, & \text{if} \quad \lambda_l(\mathbf{q}_{l/n}) \ge \lambda_l(\mathbf{q}_{(l-1)/n})\,, \\ s_l\,, & \text{otherwise}\,. \end{cases} \tag{6.18c}$$

We refer to the velocities $\sigma_l^\pm$ as *contact speeds*. The general solution (6.18) is schematically depicted in Figure 6.1 on the facing page. The figure illustrates the contiguity of regions connected by shock waves and contact discontinuities (e.g., $\Omega_{(l-1)/n}$ and $\Omega_{l/n}$) and the separation of regions connected by rarefaction waves (e.g., $\Omega_{l/n}$ and $\Omega_{(l+1)/n}$).

As an important side note, we mention that existence of a solution to the Riemann problem is not evident. Depending on the properties of $\mathbf{f}$, if $\|\mathbf{q}_L - \mathbf{q}_R\|$ is too large, then it can occur that a solution does not exist; see, for instance, Ref. [60].

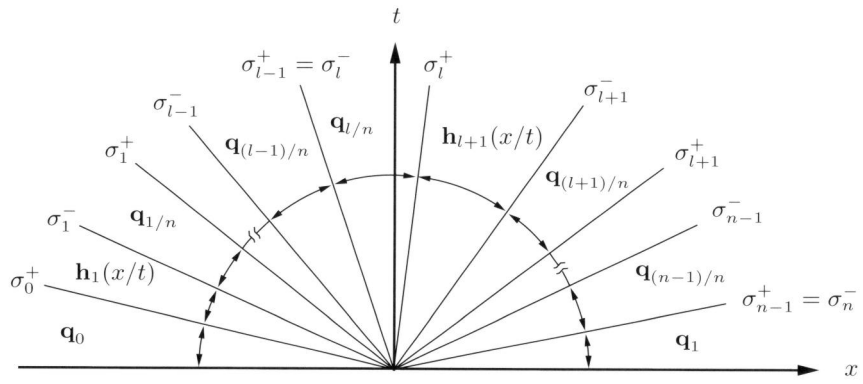

Figure 6.1: The general solution to the Riemann problem.

6.3 Approximate Riemann Solution

The solution to the Riemann problem plays an important role in numerical methods for hyperbolic conservation laws: Following Godunov's approach [22], it can be used to determine the flux across the discontinuities in a piecewise continuous approximation to the solution of a hyperbolic problem.

The benefits of Godunov's method are widely appreciated. However, a disadvantage of the method is the high computational cost of solving the Riemann problem. It is therefore attractive to revert to approximate solution techniques.

In this section we investigate an eminent approximate Riemann solver, viz., Osher's scheme. We examine the approximate Riemann solution underlying Osher's scheme and, based on the results, we propose a modified scheme.

6.3.1 Osher's Scheme

We consider the Riemann solution in similarity form for given left and right states, $\mathbf{h}(x/t; \mathbf{q}_L, \mathbf{q}_R)$. The *Godunov flux* is defined by the flux at $x = 0$:

$$\mathbf{f}(\mathbf{q}_L, \mathbf{q}_R) := \mathbf{f}(\mathbf{h}(0; \mathbf{q}_L, \mathbf{q}_R)) \,, \tag{6.19}$$

The flux (6.19) is referred to as the Godunov flux, in view of its role in the numerical method proposed by Godunov.

In Osher's scheme [48, 49], the Godunov flux is approximated by

$$\tilde{\mathbf{f}}(\mathbf{q}_L, \mathbf{q}_R) := \frac{1}{2}\mathbf{f}(\mathbf{q}_L) + \frac{1}{2}\mathbf{f}(\mathbf{q}_R) - \frac{1}{2}\mathbf{d}(\mathbf{q}_L, \mathbf{q}_R) \,, \tag{6.20a}$$

with

$$\mathbf{d}(\mathbf{q}_L, \mathbf{q}_R) := \int_{\mathbf{q}_L}^{\mathbf{q}_R} |\mathbf{A}(\mathbf{w})| \cdot \mathrm{d}\mathbf{w} \,, \tag{6.20b}$$

and

$$|\mathbf{A}(\mathbf{q})| := \mathbf{R}(\mathbf{q}) \cdot |\mathbf{\Lambda}(\mathbf{q})| \cdot \mathbf{R}(\mathbf{q})^{-1} , \tag{6.20c}$$

$$|\mathbf{\Lambda}(\mathbf{q})| := \mathrm{diag}(|\lambda_1(\mathbf{q})|, \ldots, |\lambda_n(\mathbf{q})|) . \tag{6.20d}$$

The term (6.20b) contributes to the *numerical dissipation*. In general, upwind schemes can be cast into the canonical form (6.20a) (see, for instance, Ref. [73]), with $\mathbf{d}(\mathbf{q}_L, \mathbf{q}_R)$ depending on the specifics of a scheme. The integral (6.20b) characterizes Osher's scheme.

The integral (6.20b) is evaluated along a path in state space. To facilitate the description of the integration path, we represent it by

$$\Gamma := \{\mathbf{q}(s) : 0 \leq s \leq 1 \, , \, \mathbf{q}(0) = \mathbf{q}_L \, , \, \mathbf{q}(1) = \mathbf{q}_R\} . \tag{6.21}$$

Osher proposed to compose the integration path of the k-rarefaction paths: The path (6.21) is separated into subpaths Γ_l, $l = 1, 2, \ldots, n$. Each of these subpaths connects two states $\tilde{\mathbf{q}}_{(l-1)/n}$ and $\tilde{\mathbf{q}}_{l/n}$. The initial and end state are defined by $\tilde{\mathbf{q}}_0 := \mathbf{q}_L$ and $\tilde{\mathbf{q}}_1 := \mathbf{q}_R$, respectively. Moreover, Γ_l is tangential to the eigenvector $\mathbf{r}_{k(l)}$, where $k : \{1, 2, \ldots, n\} \to \{1, 2, \ldots, n\}$ is a bijective mapping. This implies that Γ_l is a section of the $k(l)$-rarefaction path, connecting $\tilde{\mathbf{q}}_{(l-1)/n}$ to $\tilde{\mathbf{q}}_{l/n}$. An illustration of the integration path is presented in Figure 6.2.

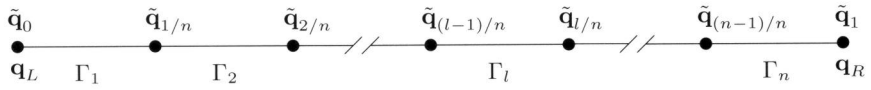

Figure 6.2: Osher's integration path.

Usual choices for the ordering of the subpaths are the O-variant $k(l) = n+1-l$ (cf. Ref. [49]) and the P-variant $k(l) = l$ (cf. Ref. [28]). Note that the O-variant and the P-variant have mutually reversed orderings.

For the O- and P-variant orderings of the subpaths, if a linearly degenerate eigenvalue with algebraic multiplicity $\mu > 1$ occurs, then this eigenvalue appears on successive subpaths. It is then possible to condense the corresponding subpaths. The integral (6.20b) can be rewritten as a sum of the contributions of the integral over each of the subpaths:

$$\mathbf{d}(\mathbf{q}_L, \mathbf{q}_R) = \sum_{l=1}^{n} \mathbf{d}_l \, , \tag{6.22a}$$

with

$$\mathbf{d}_l := \int_{\Gamma_l} \big|\mathbf{A}\big(\mathbf{w}(\xi)\big)\big| \cdot \mathbf{r}_{k(l)}\big(\mathbf{w}(\xi)\big) \, \mathrm{d}\xi \, . \tag{6.22b}$$

From (6.20c)–(6.20d) it follows that

$$\mathbf{d}_l = \int_{\Gamma_l} \mathrm{sign}\big(\lambda_{k(l)}(\mathbf{w}(\xi))\big) \, \mathbf{A}\big(\mathbf{w}(\xi)\big) \cdot \mathbf{r}_{k(l)}\big(\mathbf{w}(\xi)\big) \, \mathrm{d}\xi \, . \tag{6.23}$$

If $\lambda_{k(l)}$ does not change sign along Γ_l, then the sub-integral (6.23) evaluates to

$$\mathbf{d}_l = \operatorname{sign}\bigl(\lambda_{k(l)}\bigr)\left(\mathbf{f}(\tilde{\mathbf{q}}_{l/n}) - \mathbf{f}(\tilde{\mathbf{q}}_{(l-1)/n})\right). \tag{6.24}$$

This implies that if successive eigenvalues have equal signs on their subpaths, then the sum of their contributions concatenates. In particular, if $\lambda_{k(l_0)}(\mathbf{q}) = \lambda_{k(l_0+1)}(\mathbf{q}) = \ldots = \lambda_{k(l_0+\mu-1)}(\mathbf{q})$ is a linearly degenerate eigenvalue with sign S and algebraic multiplicity μ, then

$$\sum_{j=0}^{\mu-1} \mathbf{d}_{l_0+j} = S\left(\mathbf{f}(\tilde{\mathbf{q}}_{(l_0+\mu-1)/n}) - \mathbf{f}(\tilde{\mathbf{q}}_{(l_0-1)/n})\right). \tag{6.25}$$

The intermediate states $\tilde{\mathbf{q}}_{(l_0+j)/n}$, $j = 0, 1, \ldots, \mu-2$ are of no consequence and can be eliminated from the composite integration path *a priori*.

Due to the choice of the subpaths, the intermediate states can be conveniently determined by means of the Riemann invariants. Because the subpath Γ_l is the $k(l)$-rarefaction path between $\tilde{\mathbf{q}}_{(l-1)/n}$ and $\tilde{\mathbf{q}}_{l/n}$,

$$\psi^m_{k(l)}(\tilde{\mathbf{q}}_{(l-1)/n}) = \psi^m_{k(l)}(\tilde{\mathbf{q}}_{l/n}), \quad l, m = 1, 2, \ldots, n, \quad m \neq k(l); \tag{6.26}$$

cf. Section 6.2.3. If the k-Riemann invariants have linearly independent derivatives with respect to $\mathbf{q}$, then, by the implicit function theorem, (6.26) is a solvable system of equations from which the intermediate states can be extracted. In many practical cases the intermediate states can then be solved explicitly from (6.26). Otherwise, it is necessary to determine the intermediate states by numerical approximation. Once the intermediate states have been obtained, the flux approximation follows by straightforward operations.

6.3.2 Accuracy

The flux obtained by means of the Osher scheme is based on an approximation to the solution of the Riemann problem. Because the approximate Riemann solution can again be written in similarity form, it is useful to introduce the notation

$$\tilde{\mathbf{f}}(\mathbf{q}_L, \mathbf{q}_R) = \mathbf{f}(\tilde{\mathbf{h}}(0; \mathbf{q}_L, \mathbf{q}_R)), \tag{6.27}$$

where $\tilde{\mathbf{h}}(x/t; \mathbf{q}_L, \mathbf{q}_R)$ represents the approximate Riemann solution in similarity form.

To assess the accuracy of the approximate Riemann solution underlying Osher's scheme, we examine its representation of rarefaction waves, contact discontinuities and shock waves. We consider only the P-variant ordering of the subpaths. However, by virtue of the fact that the O-variant and P-variant have mutually reversed orderings, it follows that

$$\tilde{\mathbf{h}}_O(x/t; \mathbf{q}_L, \mathbf{q}_R) = \tilde{\mathbf{h}}_P(-x/t; \mathbf{q}_R, \mathbf{q}_L), \tag{6.28}$$

where the subscript distinguishes the variants. By (6.28), the results for the P-variant can be extended mutatis mutandis to the O-variant.

In section 6.3.1 it was emphasized that the subpaths in Osher's scheme are subsets of the $k(l)$-rarefaction paths. Referring to Section 6.2.4, it follows that the intermediate states in the approximate Riemann solution are connected by simple waves only. Clearly, this representation is correct for simple waves and contact discontinuities. However, shock waves in the actual solution are then replaced by so-called *overturned simple waves*; see Ref. [41].

To examine the appropriateness of the overturned-simple-wave representation of shocks. We consider a left state $\mathbf{q}_L$ and a right state $\mathbf{q}_R$, connected by a weak k-shock. The *k-shock strength* is defined by:

$$\epsilon := \lambda_k(\mathbf{q}_L) - \lambda_k(\mathbf{q}_R)\,. \tag{6.29}$$

In [60] it is proved that the change in the k-Riemann invariants across a k-shock with strength ϵ is $O(\epsilon^3)$ as $\epsilon \to 0$. This implies that a $\tilde{\mathbf{q}}_R \in \mathcal{R}_k(\mathbf{q}_L)$ exists such that $\lambda_k(\tilde{\mathbf{q}}_R) = \lambda_k(\mathbf{q}_R)$ and $\|\tilde{\mathbf{q}}_R - \mathbf{q}_R\| = O(\epsilon^3)$. To prove this, we note that $\tilde{\mathbf{q}}_R \in \mathcal{R}_k(\mathbf{q}_L)$ implies

$$\psi_k^m(\tilde{\mathbf{q}}_R) = \psi_k^m(\mathbf{q}_L)\,, \quad m = 1, 2, \ldots, n\,, \quad m \neq k\,. \tag{6.30}$$

The change in the k-Riemann invariants from $\mathbf{q}_L$ to $\mathbf{q}_R$ is only $O(\epsilon^3)$. Therefore,

$$\psi_k^m(\tilde{\mathbf{q}}_R) = \psi_k^m(\mathbf{q}_R) + O(\epsilon^3)\,, \quad m = 1, 2, \ldots, n\,, \quad m \neq k\,. \tag{6.31a}$$

Equations (6.31) can be augmented with

$$\lambda_k(\tilde{\mathbf{q}}_R) = \lambda_k(\mathbf{q}_R)\,, \tag{6.31b}$$

to obtain n equations for $\tilde{\mathbf{q}}_R$. If the k-Riemann invariants have linearly independent derivatives with respect to $\mathbf{q}$, then $\operatorname{rank}(\partial_{\mathbf{q}}\psi_k^1, \ldots, \partial_{\mathbf{q}}\psi_k^n) = n - 1$. Moreover, because λ_k is linearly degenerate, $\partial_{\mathbf{q}}\lambda_k \notin \operatorname{span}(\partial_{\mathbf{q}}\psi_k^1, \ldots, \partial_{\mathbf{q}}\psi_k^n)$. Therefore, $(\partial_{\mathbf{q}}\psi_k^1, \ldots, \partial_{\mathbf{q}}\psi_k^n, \partial_{\mathbf{q}}\lambda_k)$ is nonsingular and, by the implicit function theorem, (6.31) is solvable. Taylor expansion of $\psi_k^m(\tilde{\mathbf{q}}_R)$ and $\lambda_k(\tilde{\mathbf{q}}_R)$ with center at $\mathbf{q}_R$ then yields that $\|\tilde{\mathbf{q}}_R - \mathbf{q}_R\| = O(\epsilon^3)$.

Summarizing, we find that the error in the intermediate states in the simple-waves-only approximation of the Riemann solution is at most

$$\sup_{l=1\ldots n} \Big(\big(\lambda_l(\mathbf{q}_{(l-1)/n}) - \lambda_l(\mathbf{q}_{l/n})\big)^3, 0 \Big)\,. \tag{6.32}$$

Although the computed intermediate states are accurate, even in the presence of (weak) shocks, the flux approximation is not necessarily so. By (6.22)–(6.23), if $\tilde{\mathbf{q}}_R \in \mathcal{R}_k(\mathbf{q}_L)$ and $\lambda_k(\mathbf{q}_L) > 0 > \lambda_k(\tilde{\mathbf{q}}_R)$, then

$$\begin{aligned}\mathbf{d}(\mathbf{q}_L, \tilde{\mathbf{q}}_R) = \int_{\mathbf{q}_L}^{\mathbf{q}^*} \mathbf{A}\big(\mathbf{w}(\xi)\big) \cdot \mathbf{r}_{k(l)}\big(\mathbf{w}(\xi)\big)\,\mathrm{d}\xi - \int_{\mathbf{q}^*}^{\tilde{\mathbf{q}}_R} \mathbf{A}\big(\mathbf{w}(\xi)\big) \cdot \mathbf{r}_{k(l)}\big(\mathbf{w}(\xi)\big)\,\mathrm{d}\xi \\ = 2\mathbf{f}(\mathbf{q}^*) - \mathbf{f}(\mathbf{q}_L) - \mathbf{f}(\tilde{\mathbf{q}}_R)\,,\end{aligned} \tag{6.33}$$

with $\mathbf{q}^* \in \mathcal{R}_k(\mathbf{q}_L)$ such that $\lambda_k(\mathbf{q}^*) = 0$. The Osher flux (6.20) then yields

$$\tilde{\mathbf{f}}(\mathbf{q}_L, \tilde{\mathbf{q}}_R) = \mathbf{f}(\mathbf{q}_L) + \mathbf{f}(\tilde{\mathbf{q}}_R) - \mathbf{f}(\mathbf{q}^*) \,. \tag{6.34}$$

In contrast, the Godunov flux corresponding to the k-shock is $\mathbf{f}(\mathbf{q}_L)$ if $s(\mathbf{q}_L; \mathbf{q}_R) > 0$ and $\mathbf{f}(\mathbf{q}_R)$ if $s(\mathbf{q}_L; \mathbf{q}_R) < 0$. Hence, ignoring terms of $O(\epsilon^3)$, the error in the flux approximation is

$$\tilde{\mathbf{f}}(\mathbf{q}_L, \mathbf{q}_R) - \mathbf{f}(\mathbf{q}_L, \mathbf{q}_R) = \begin{cases} \mathbf{f}(\mathbf{q}_R) - \mathbf{f}(\mathbf{q}^*) \,, & \text{if} \quad s(\mathbf{q}_L; \mathbf{q}_R) > 0 \,, \\ \mathbf{f}(\mathbf{q}_L) - \mathbf{f}(\mathbf{q}^*) \,, & \text{if} \quad s(\mathbf{q}_L; \mathbf{q}_R) < 0 \,. \end{cases} \tag{6.35}$$

To elaborate the error, we note that the states $\mathbf{q}_L$, $\mathbf{q}_R$ and $\mathbf{q}^*$ are interrelated by the k-Riemann invariants in the following manner:

$$\psi_k^m(\mathbf{q}^*) = \psi_k^m(\mathbf{q}_L) = \psi_k^m(\mathbf{q}_R) + O(\epsilon^3) \,, \quad m = 1, 2, \ldots, n \,, \quad m \neq k \,. \tag{6.36}$$

Moreover, because $\mathbf{q}_L$ and $\mathbf{q}_R$ are connected by a shock with strength ϵ,

$$\lambda_k(\mathbf{q}_L) = O(\epsilon) \,, \qquad \lambda_k(\mathbf{q}_R) = O(\epsilon) \,, \tag{6.37a}$$

and, by definition,

$$\lambda_k(\mathbf{q}^*) = 0 \,. \tag{6.37b}$$

From (6.36)–(6.37) it follows that

$$\|\mathbf{q}_{L/R} - \mathbf{q}^*\| = O(\epsilon) \,, \tag{6.38}$$

where $\mathbf{q}_{L/R}$ is either $\mathbf{q}_L$ or $\mathbf{q}_R$. Taylor expansion of $\mathbf{f}(\mathbf{q}_{L/R})$ with center at $\mathbf{q}^*$ then yields

$$\|\mathbf{f}(\mathbf{q}_{L/R}) - \mathbf{f}(\mathbf{q}^*)\| = O(\epsilon) \,. \tag{6.39}$$

Hence, by (6.35), the error in Osher's flux approximation in the instance of a slow shock ($\lambda_k(\mathbf{q}_R) < 0 < \lambda_k(\mathbf{q}_R)$) with strength ϵ is of $O(\epsilon)$. This failure of Osher's scheme is exemplified by means of the Burgers equation in [41].

6.3.3 Modified Scheme

To avoid the aforementioned deficiency of Osher's scheme, we propose a modification of the scheme. The simple-waves-only approximation of the Riemann solution is maintained. However, the overturned-simple-wave representation of shocks in the approximate Riemann solution is replaced.

We propose to extract the intermediate states in the approximate Riemann solution from

$$\psi_l^m(\tilde{\mathbf{q}}_{(l-1)/n}) = \psi_l^m(\tilde{\mathbf{q}}_{l/n}) \,, \qquad l, m = 1, 2, \ldots, n \,, \quad m \neq l \,, \tag{6.40}$$

with $\tilde{\mathbf{q}}_0 = \mathbf{q}_L$ and $\tilde{\mathbf{q}}_1 = \mathbf{q}_R$. This is in fact equivalent to (6.26) with a presumed P-variant ordering of the subpaths.

The intermediate states from (6.40) are subsequently used to construct the approximate Riemann solution:

$$\tilde{\mathbf{h}}(x/t;\mathbf{q}_L,\mathbf{q}_R) = \begin{cases} \tilde{\mathbf{q}}_0\,, & \text{if} \quad x/t < \tilde{\sigma}_0^+\,, \\ \tilde{\mathbf{q}}_{l/n}\,, & \text{if} \quad \tilde{\sigma}_l^- < x/t < \tilde{\sigma}_l^+\,, \qquad l = 1,\ldots,n-1\,, \\ \mathbf{h}_l(x/t)\,, & \text{if} \quad \tilde{\sigma}_{l-1}^+ < x/t < \tilde{\sigma}_l^-\,, \qquad l = 1,\ldots,n-1\,, \\ \tilde{\mathbf{q}}_R\,, & \text{if} \quad x/t > \tilde{\sigma}_n^-\,, \end{cases} \tag{6.41a}$$

with the approximate contact speeds $\tilde{\sigma}_l^{\pm}$,

$$\tilde{\sigma}_l^+ = \begin{cases} \lambda_{l+1}(\tilde{\mathbf{q}}_{l/n})\,, & \text{if} \quad \lambda_{l+1}(\tilde{\mathbf{q}}_{l/n}) \le \lambda_{l+1}(\tilde{\mathbf{q}}_{(l+1)/n})\,, \\ \tilde{s}_{l+1}\,, & \text{otherwise}\,, \end{cases} \tag{6.41b}$$

$$\tilde{\sigma}_l^- = \begin{cases} \lambda_l(\tilde{\mathbf{q}}_{l/n})\,, & \text{if} \quad \lambda_l(\tilde{\mathbf{q}}_{l/n}) \ge \lambda_l(\tilde{\mathbf{q}}_{(l-1)/n})\,, \\ \tilde{s}_l\,, & \text{otherwise}\,, \end{cases} \tag{6.41c}$$

and

$$\tilde{s}_l = \frac{1}{2}\lambda_l(\tilde{\mathbf{q}}_{(l-1)/n}) + \frac{1}{2}\lambda_l(\tilde{\mathbf{q}}_{l/n})\,. \tag{6.41d}$$

In (6.41a), $\mathbf{h}_l(x/t)$ represents the simple-wave solution between $\tilde{\mathbf{q}}_{(l-1)/n}$ and $\tilde{\mathbf{q}}_{l/n}$. Recall that $\tilde{\mathbf{q}}_{(l-1)/n}$ and $\tilde{\mathbf{q}}_{l/n}$ can indeed be connected by a simple wave due to the choice of the subpaths.

Comparison of the approximate Riemann solution (6.41) with the exact Riemann solution (6.18) shows that $\tilde{s}_l$ approximates the shock speed. In Ref. [60] it is proved that if $\mathbf{q}_R \in \mathcal{S}_k(\mathbf{q}_L)$ and $\epsilon := \lambda_k(\mathbf{q}_L) - \lambda_k(\mathbf{q}_R) > 0$, then the k-shock speed satisfies

$$s(\mathbf{q}_L;\mathbf{q}_R) = \frac{1}{2}\lambda_k(\mathbf{q}_L) + \frac{1}{2}\lambda_k(\mathbf{q}_R) + O(\epsilon^2)\,, \tag{6.42}$$

as $\epsilon \to 0$. Hence, the shock-speed approximation (6.41d) is $O(\epsilon^2)$ accurate. However, because the objective is to obtain an approximation to the Godunov flux, it is the sign of the shock speed that is of primary interest. The sign of the shock speed is correctly predicted by (6.41d), provided that

$$\left|\frac{1}{2}\lambda_l(\tilde{\mathbf{q}}_{(l-1)/n}) + \frac{1}{2}\lambda_l(\tilde{\mathbf{q}}_{l/n})\right| \gg \left(\lambda_l(\tilde{\mathbf{q}}_{(l-1)/n}) - \lambda_l(\tilde{\mathbf{q}}_{l/n})\right)^2\,. \tag{6.43}$$

Otherwise, the sign of the shock speed depends on the $O(\epsilon^2)$ remainder and becomes ambiguous. This occurs for strong, slow shocks.

The approximation of the Godunov flux, corresponding to the approximate Riemann solution (6.41), is $\tilde{\mathbf{f}}(\mathbf{q}_L,\mathbf{q}_R) = \mathbf{f}(\tilde{\mathbf{h}}(0;\mathbf{q}_L,\mathbf{q}_R))$, with

$$\tilde{\mathbf{h}}(0;\mathbf{q}_L,\mathbf{q}_R) = \begin{cases} \tilde{\mathbf{q}}_0, & \text{if} \quad \tilde{\sigma}_0^+ > 0, \\ \tilde{\mathbf{q}}_{l/n}, & \text{if} \quad \tilde{\sigma}_l^- < 0 < \tilde{\sigma}_l^+, \quad l \in \{1,\ldots,n-1\}, \\ \tilde{\mathbf{q}}^*, & \text{if} \quad \tilde{\sigma}_{l-1}^+ < 0 < \tilde{\sigma}_l^-, \quad l \in \{1,\ldots,n-1\}, \\ \tilde{\mathbf{q}}_1, & \text{if} \quad \sigma_n^- < 0, \end{cases} \tag{6.44}$$

where $\tilde{\mathbf{q}}^* \in \mathcal{R}_l(\tilde{\mathbf{q}}_{(l-1)/n})$ such that $\lambda_l(\tilde{\mathbf{q}}^*) = 0$, in case of a centered rarefaction wave.

6.4 Two-Fluid Flow Application

Inviscid, compressible two-fluid flows can be modeled by hyperbolic conservation laws. The interface between the contiguous fluids then appears as a discontinuity in the solution. In this section we consider the application of the modified Osher's scheme to two-fluid flows.

6.4.1 Two-Fluid Euler Equations

We consider the flow of two inviscid immiscible fluids. The fluids occupy a domain $\mathcal{V} \subset \mathbb{R}^d$ $(d = 2, 3)$. Positions in $\mathcal{V}$ are identified by $\mathbf{x} := x_1\mathbf{e}_1 + \ldots + x_d\mathbf{e}_d$. Time is denoted by $t \geq 0$. In both fluids, the flow is characterized by the state variables $\rho(\mathbf{x}, t)$, $p(\mathbf{x}, t)$ and $\mathbf{v}(\mathbf{x}, t)$, which represent density, pressure and velocity, respectively. The Cartesian components of the velocity are denoted by $v_j(\mathbf{x}, t) := \mathbf{e}_j \cdot \mathbf{v}(\mathbf{x}, t)$, $j = 1, \ldots, d$.

The fluids are separated by an interface, which we identify by the level set

$$\mathcal{S} := \{\mathbf{x} \in \mathcal{V} : \theta(\mathbf{x}, t) = 0\} . \tag{6.45}$$

The following kinematic condition ensures the immiscibility of the fluids:

$$\theta_t + \mathbf{v} \cdot \boldsymbol{\nabla}\theta = 0 , \qquad \mathbf{x} \in \mathcal{V}, t > 0 . \tag{6.46}$$

To distinguish the fluids, we arbitrarily designate one of the fluids as the primary fluid and the other as the secondary fluid. We assume that $\theta(\mathbf{x}, t)$ is positive in the primary fluid and negative in the secondary fluid.

In both fluids, the flow is governed by the Euler equations. Because our interest is in discontinuous solutions, we consider the weak formulation of the equations. To present the equations in weak formulation, we denote by Ω any arbitrary bounded subset of $\overline{\mathcal{V}} \times [0, \infty)$, by Θ its boundary and by $(\mathbf{n}, \gamma) := n_1\mathbf{e}_1 + \ldots + n_d\mathbf{e}_d + \gamma\mathbf{e}_{d+1}$ the outward unit normal vector to Θ; see the illustration in Figure 6.3 on the following page. The weak formulation of the Euler equations reads

$$\oint_\Theta a\,(\rho\gamma + \rho\mathbf{v}\cdot\mathbf{n})\,\mathrm{d}\Theta - \int_\Omega \rho\,(a_t + \mathbf{v}\cdot\boldsymbol{\nabla}a)\,\mathrm{d}\Omega = 0 , \tag{6.47a}$$

$$\oint_\Theta b\,(\rho v_j\gamma + \rho v_j\mathbf{v}\cdot\mathbf{n} + pn_j)\,\mathrm{d}\Theta - \int_\Omega \rho v_j\,(b_t + \mathbf{v}\cdot\boldsymbol{\nabla}b) + p\frac{\partial b}{\partial x_j}\,\mathrm{d}\Omega = 0 , \tag{6.47b}$$

with $j = 1, \ldots, d$, for all subsets Ω and all continuously differentiable functions a, b. The equations (6.47a) and (6.47b) express conservation of mass and conservation of momentum, respectively.

The kinematic condition (6.46) is not in conservation form. This renders (6.46)–(6.47) unsuitable for treatment by Godunov's method. However, under the conditions imposed by (6.47a), we can replace (6.46) by

$$\oint_\Theta c\,(\rho g(\theta)\,\gamma + \rho g(\theta)\,\mathbf{v}\cdot\mathbf{n})\,\mathrm{d}\Theta - \int_\Omega \rho g(\theta)\,(c_t + \mathbf{v}\cdot\boldsymbol{\nabla}c)\,\mathrm{d}\Omega = 0 , \tag{6.48}$$

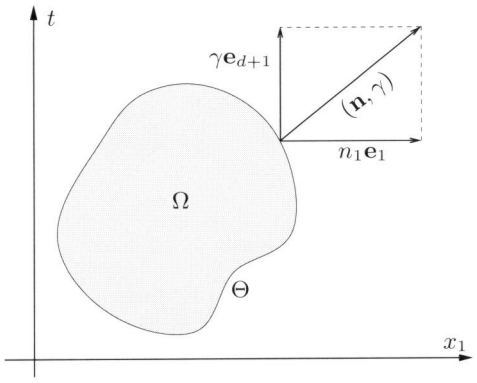

Figure 6.3: A bounded subset Ω in the $(\mathbf{x}, t)$ domain, with boundary Θ and outward unit normal $(\mathbf{n}, \gamma)$.

for all subsets Ω and all continuously differentiable functions c, with $g : \mathbb{R} \mapsto \mathbb{R}$ any strictly monotone continuously differentiable function. Equation (6.48) is in weak conservation form. To prove that (6.47a) and (6.48) imply (6.46), we note that the sum of (6.47a) and (6.48) yields:

$$\oint_{\Theta} \rho \left(cg(\theta)+a\right)\left(\gamma+\mathbf{v}\cdot\mathbf{n}\right) \mathrm{d}\Theta - \int_{\Omega} \rho \left(a_t+\mathbf{v}\cdot\boldsymbol{\nabla} a\right)+\rho g(\theta)\left(c_t+\mathbf{v}\cdot\boldsymbol{\nabla} c\right) \mathrm{d}\Omega = 0\,, \quad (6.49)$$

which holds for all continuously differentiable a, c and all subsets Ω. If we choose $a = -cg(\theta)$, then the boundary integrals cancel and we obtain

$$\int_{\Omega} \rho \Big([cg(\theta)]_t + \mathbf{v}\cdot\boldsymbol{\nabla}[cg(\theta)] - g(\theta)\left(c_t + \mathbf{v}\cdot\boldsymbol{\nabla} c\right)\Big) \mathrm{d}\Omega = 0\,. \quad (6.50)$$

Partial differentiation yields

$$\int_{\Omega} c\rho \left(g(\theta)_t + \mathbf{v}\cdot\boldsymbol{\nabla} g(\theta)\right) \mathrm{d}\Omega = 0\,, \quad (6.51)$$

or, equivalently,

$$\int_{\Omega} c\rho g_\theta \big(\theta_t + \mathbf{v}\cdot\boldsymbol{\nabla}\theta\big) \mathrm{d}\Omega = 0\,, \quad (6.52)$$

for all continuously differentiable c and all subsets Ω. Equation (6.52) implies (6.46) weakly. Therefore, (6.47a) and (6.48) imply (6.46) weakly.

To identify the associated Riemann problem, we collect (6.47)–(6.48) in:

$$\oint_{\Theta} a \left(q_j\gamma + \sum_{i=1}^{d} f_j^i(\mathbf{q}) n_i \right) \mathrm{d}\Theta - \int_{\Omega} \left(q_j a_t + \sum_{i=1}^{d} f_j^i(\mathbf{q}) \frac{\partial a}{\partial x_i} \right) \mathrm{d}\Omega = 0\,, \quad (6.53a)$$

$j = 1, \ldots, d+2$, for all continuously differentiable a and all subsets Ω, with

$$\mathbf{q} = \begin{pmatrix} \rho v_1 \\ \rho v_2 \\ \rho v_3 \\ \rho g(\theta) \\ \rho \end{pmatrix}, \mathbf{f}^1 = \begin{pmatrix} q_1^2/q_5 + p \\ q_2 q_1/q_5 \\ q_3 q_1/q_5 \\ q_4 q_1/q_5 \\ q_1 \end{pmatrix}, \mathbf{f}^2 = \begin{pmatrix} q_1 q_2/q_5 \\ q_2^2/q_5 + p \\ q_3 q_2/q_5 \\ q_4 q_2/q_5 \\ q_2 \end{pmatrix}, \mathbf{f}^3 = \begin{pmatrix} q_1 q_3/q_5 \\ q_2 q_3/q_5 \\ q_3^2/q_5 + p \\ q_4 q_3/q_5 \\ q_3 \end{pmatrix}, \tag{6.53b}$$

for $d = 3$. The case $d = 2$ can be treated as a special case of $d = 3$, with q_3 and $\mathbf{f}^3$ set to 0, and will therefore not be considered separately. Integrating (6.53) by parts, we obtain

$$\int_\Omega a \left(\frac{\partial q_j}{\partial t} + \sum_{i=1}^{d} \frac{\partial f_j^i(\mathbf{q})}{\partial x_i} \right) \mathrm{d}\Omega = 0 \,, \tag{6.54}$$

which implies the following strong form of the equations:

$$\frac{\partial \mathbf{q}}{\partial t} + \frac{\partial \mathbf{f}^1(\mathbf{q})}{\partial x_1} + \cdots + \frac{\partial \mathbf{f}^d(\mathbf{q})}{\partial x_d} = 0 \,. \tag{6.55}$$

To obtain the Riemann problem associated with the two-fluid Euler equations, we stipulate $\partial \mathbf{f}^i / \partial x_i = 0$ for $i = 2, \ldots, d$ and we prescribe discontinuous initial conditions conform (6.1b).

6.4.2 Equation of State

Closure of the two-fluid Euler equations requires an equation of state which interrelates p, ρ, $\mathbf{v}$ and θ. We consider fluids that separately satisfy a barotropic equation of state:

$$p := p_{\mathrm{p/s}}(\rho) \,, \quad \text{or} \quad \rho := \rho_{\mathrm{p/s}}(p) \,. \tag{6.56}$$

with $p_{\mathrm{p/s}} : (0, \infty) \mapsto \mathbb{R}$ and $\rho_{\mathrm{p/s}} : \mathbb{R} \mapsto (0, \infty)$ mutually inverse functions, i.e.,

$$p_{\mathrm{p/s}}(\rho_{\mathrm{p/s}}(p)) = p \,, \quad \text{and} \quad \rho_{\mathrm{p/s}}(p_{\mathrm{p/s}}(\rho)) = \rho \,, \tag{6.57}$$

for all $p \in \mathbb{R}$ and all $\rho \in (0, \infty)$. The subscripts p and s distinguish the primary and secondary fluid.

A relevant example of an equation of state conform (6.56) is Tait's equation of state (see, e.g., [71]):

$$p(\rho) = p_0 \left((1 + \eta_1) \left(\frac{\rho}{\rho_0} \right)^{\eta_2} - \eta_1 \right) , \tag{6.58}$$

with p_0 an appropriate reference pressure, e.g., the atmospheric pressure, ρ_0 the corresponding density of the fluid and η_1 and η_2 fluid-specific constants. Equation (6.58) can be used to describe the behavior of air in homentropic flow and of

Table 6.1: Constants in Tait's equation of state (6.58) for water and for air in homentropic flow.

	η_1	η_2
water	3000	7
air	0	7/5

water. The corresponding constants are listed in Table 6.1. Appropriate constants for other fluids are given in [71].

In order to construct an equation of state for the two-fluid compound, we consider a domain Ω which is occupied by the two co-existing fluids. If the fluids are separated, then the primary and the secondary fluid occupy domains Ω_p and Ω_s, respectively; see the illustration in Figure 6.4. Denoting by $|\Omega|$ the volume of Ω, we define the primary *volume fraction* by

$$\alpha := \frac{|\Omega_\mathrm{p}|}{|\Omega_\mathrm{p}| + |\Omega_\mathrm{s}|} \,. \tag{6.59}$$

If the pressure is constant in Ω, then the compound density reads:

$$\rho(p, \alpha) := \alpha\, \rho_\mathrm{p}(p) + (1 - \alpha)\, \rho_\mathrm{s}(p) \,. \tag{6.60}$$

Equation (6.60) specifies the equation of state for the two-fluid compound. The compound equation of state is illustrated in Figure 6.5 on the next page. An equation of state of the form $p(\rho, \theta)$ is obtained by introducing a mapping $\theta \mapsto \alpha(\theta)$.

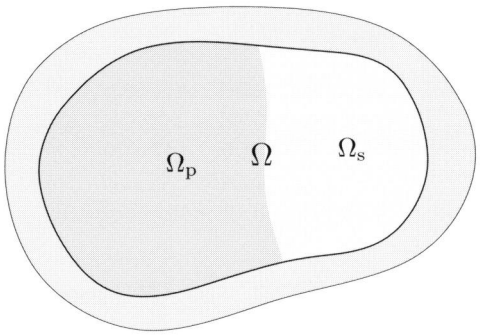

Figure 6.4: Separation of the fluids in a volume Ω. The primary and secondary fluid occupy Ω_p and Ω_s, respectively.

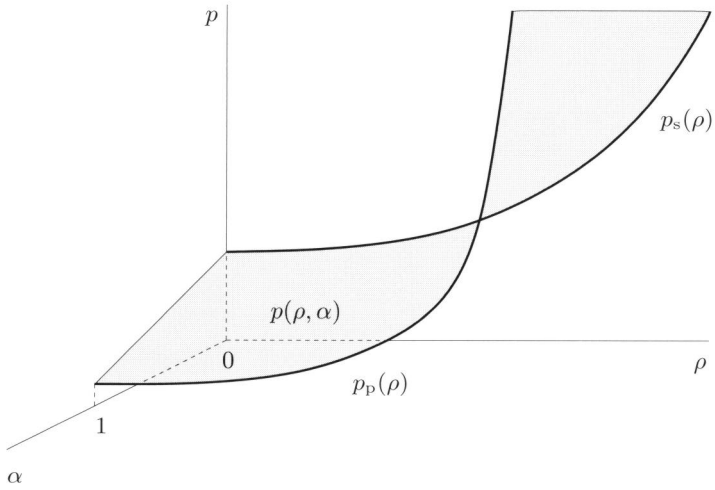

Figure 6.5: Compound equation of state for two barotropic fluids according to (6.60).

6.4.3 Riemann Invariants

We consider the flux function $\mathbf{f}^1$ according to (6.53b) with an equation of state of the general form $p := p(\rho, \theta)$. To facilitate the derivation of the associated Riemann invariants, we introduce the notation:

$$c_\rho(\rho, \theta) := \sqrt{\frac{\partial p(\rho, \theta)}{\partial \rho}}\,, \tag{6.61a}$$

$$c_\theta(\rho, \theta) := \sqrt{\frac{\partial p(\rho, \theta)}{\partial \theta}}\,. \tag{6.61b}$$

The Jacobian of the flux function then reads

$$\mathbf{A}(\mathbf{q}) = \begin{pmatrix} 2\,q_1/q_5 & 0 & 0 & c_\theta^2/q_5 & -(q_1^2 + c_\theta^2 q_4)/q_5^2 + c_\rho^2 \\ q_2/q_5 & q_1/q_5 & 0 & 0 & -q_2 q_1/q_5^2 \\ q_3/q_5 & 0 & q_1/q_5 & 0 & -q_3 q_1/q_5^2 \\ q_4/q_5 & 0 & 0 & q_1/q_5 & -q_4 q_1/q_5^2 \\ 1 & 0 & 0 & 0 & 0 \end{pmatrix}, \tag{6.62}$$

and its eigenvalues and the corresponding eigenvectors are

$$\lambda_1 = q_1/q_5 - c_\rho\,, \quad \lambda_{2,3,4} = q_1/q_5\,, \quad \lambda_5 = q_1/q_5 + c_\rho\,. \tag{6.63a}$$

and

$$\mathbf{r}_1 = \begin{pmatrix} q_1/q_5 - c_\rho \\ q_2/q_5 \\ q_3/q_5 \\ q_4/q_5 \\ 1 \end{pmatrix}, \qquad \mathbf{r}_2 = \begin{pmatrix} 0 \\ 1 \\ 0 \\ 0 \\ 0 \end{pmatrix}, \qquad \mathbf{r}_3 = \begin{pmatrix} 0 \\ 0 \\ 1 \\ 0 \\ 0 \end{pmatrix},$$
$$\mathbf{r}_4 = \begin{pmatrix} q_1 \\ 0 \\ 0 \\ -(c_\rho/c_\theta)^2 q_5^2 + q_4 \\ q_5 \end{pmatrix}, \qquad \mathbf{r}_5 = \begin{pmatrix} q_1/q_5 + c_\rho \\ q_2/q_5 \\ q_3/q_5 \\ q_4/q_5 \\ 1 \end{pmatrix}. \tag{6.63b}$$

The eigenpairs $(\lambda_k, \mathbf{r}_k)$ are genuinely nonlinear for $k = 1, 5$ and linearly degenerate for $k = 2, 3, 4$.

To derive the 1-Riemann invariants, we first solve the following system of ordinary differential equations:

$$\mathbf{h}'(\xi) = \mathbf{r}_k(\mathbf{h}(\xi)), \qquad \xi \in \mathbb{R}, \tag{6.64a}$$
$$\mathbf{h}(0) = \mathbf{h}^0, \tag{6.64b}$$

for $k = 1$. Trivially,

$$h_5(\xi) = \xi + h_5^0. \tag{6.65}$$

Hence, for $j = 2, 3, 4$, $h_j(\xi)$ is determined by

$$h_j'(\xi) = h_j(\xi)/(\xi + h_5^0), \quad h_j(0) = h_j^0, \tag{6.66}$$

which yields

$$h_j(\xi) = (h_j^0/h_5^0)\,\xi + h_j^0, \qquad j = 2, 3, 4. \tag{6.67}$$

Furthermore, $h_1(\xi)$ is governed by

$$h_1'(\xi) = h_1(\xi)/(\xi + h_5^0) - c_\rho(\xi), \quad h_1(0) = h_1^0, \tag{6.68}$$

with $c_\rho(\xi) := c_\rho\big(h_5(\xi), h_4(\xi)/h_5(\xi)\big)$. The solution to (6.68) is

$$h_1(\xi) = (\xi + h_5^0)\left(\frac{h_1^0}{h_5^0} - \int_{h_5^0}^{\xi + h_5^0} \frac{c_\rho(\omega)}{\omega}\,\mathrm{d}\omega\right). \tag{6.69}$$

To obtain 1-Riemann invariants, we construct ξ-independent functions of $h_j(\xi)$, $j = 1, \ldots, 5$. By (6.65) and (6.67),

$$\frac{h_j(\xi)}{h_5(\xi)} = \frac{(h_j^0/h_5^0)\,\xi + h_j^0}{\xi + h_5^0} = \frac{h_j^0}{h_5^0}, \qquad j = 2, 3, 4. \tag{6.70}$$

Therefore, q_j/q_5, $j = 2, 3, 4$ are 1-Riemann invariants. Moreover,

$$\frac{h_1(\xi)}{h_5(\xi)} + \int_{h_5^0}^{h_5(\xi)} \frac{c_\rho(\omega)}{\omega}\,\mathrm{d}\omega = \left(\frac{h_1^0}{h_5^0} - \int_{h_5^0}^{h_5(\xi)} \frac{c_\rho(\omega)}{\omega}\,\mathrm{d}\omega\right) + \int_{h_5^0}^{h_5(\xi)} \frac{c_\rho(\omega)}{\omega}\,\mathrm{d}\omega = \frac{h_1^0}{h_5^0}\,. \tag{6.71}$$

Hence, for an arbitrary constant $q_5^0 \in (0, \infty)$,

$$\frac{q_1}{q_5} + \int_{q_5^0}^{q_5} \frac{c_\rho(\omega)}{\omega}\,\mathrm{d}\omega\,, \tag{6.72}$$

is also a 1-Riemann invariant.

Due to the simple structure of the eigenvectors $\mathbf{r}_k$ for $k = 2, 3$, the corresponding Riemann invariants can be determined by inspection. Moreover, by (6.63), the 5-Riemann invariants are identical to the 1-Riemann invariants, with c_ρ replaced by $-c_\rho$.

To derive the 4-Riemann invariants, we solve (6.64) for $k = 4$. Obviously,

$$h_1(\xi) = h_1^0 \mathrm{e}^{\xi}\,, \quad h_2(\xi) = h_2^0\,, \quad h_3(\xi) = h_3^0\,, \quad h_5(\xi) = h_5^0 \mathrm{e}^{\xi}\,. \tag{6.73}$$

To facilitate the determination of $h_4(\xi)$, we recall that c_ρ and c_θ are defined by Eq. (6.61) and that h_5 and h_4 are defined by ρ and $\rho\theta$, respectively. Therefore,

$$h_4'(\xi) = -\frac{c_\rho^2}{c_\theta^2}\big(h_5(\xi)\big)^2 + h_4(\xi) \quad \Leftrightarrow \quad \frac{\partial p}{\partial \theta}\left(\theta\frac{\mathrm{d}\rho}{\mathrm{d}\xi} + \rho\frac{\mathrm{d}\theta}{\mathrm{d}\xi}\right) = -\frac{\partial p}{\partial \rho}\rho^2 + \frac{\partial p}{\partial \theta}\rho\theta\,. \tag{6.74}$$

From (6.73) it follows that $\rho = \rho'(\xi)$ and, hence,

$$\frac{\partial p}{\partial \theta}\frac{\mathrm{d}\theta}{\mathrm{d}\xi} + \frac{\partial p}{\partial \rho}\frac{\mathrm{d}\rho}{\mathrm{d}\xi} = \frac{\mathrm{d}p}{\mathrm{d}\xi} = 0\,. \tag{6.75}$$

This implies that $h_4(\xi)$ is implicitly given by

$$p\big(h_5(\xi), h_4(\xi)/h_5(\xi)\big) = p\big(h_5^0, h_4^0/h_5^0\big)\,. \tag{6.76}$$

Summarizing, by (6.73)–(6.76), 4-Riemann invariants are:

$$q_1/q_5\,, \quad q_2\,, \quad q_3\,, \quad p\,. \tag{6.77}$$

In conclusion, we can associate the following Riemann invariants with the flux function $\mathbf{f}^1$ according to (6.53b), with an equation of state of the form $p := p(\rho, \theta)$:

$$\psi_1^2 = v_1 + \Psi(\rho,\theta)\,, \quad \psi_1^3 = v_2\,, \quad \psi_1^4 = v_3\,, \quad \psi_1^5 = \theta\,, \tag{6.78a}$$
$$\psi_2^1 = v_1\,, \quad \psi_2^3 = \rho v_3\,, \quad \psi_2^4 = \rho\theta\,, \quad \psi_2^5 = p(\rho,\theta)\,, \tag{6.78b}$$
$$\psi_3^1 = v_1\,, \quad \psi_3^2 = \rho v_2\,, \quad \psi_3^4 = \rho\theta\,, \quad \psi_3^5 = p(\rho,\theta)\,, \tag{6.78c}$$
$$\psi_4^1 = v_1\,, \quad \psi_4^2 = \rho v_2\,, \quad \psi_4^3 = \rho v_3\,, \quad \psi_4^5 = p(\rho,\theta)\,, \tag{6.78d}$$
$$\psi_5^1 = v_1 - \Psi(\rho,\theta)\,, \quad \psi_5^2 = v_2\,, \quad \psi_5^3 = v_3\,, \quad \psi_5^4 = \theta\,, \tag{6.78e}$$

with

$$\Psi(\rho, \theta) := \int_{\rho^0}^{\rho} \frac{c_\rho(\omega, \theta)}{\omega} \, \mathrm{d}\omega \,, \tag{6.78f}$$

and ρ^0 an arbitrary constant in $(0, \infty)$.

6.4.4 Approximate Two-Fluid Solution

The Riemann invariants (6.78) can be used to extract from (6.40) the intermediate states in the simple-waves-only approximation to the solution of the two-fluid Riemann problem. Because the linearly degenerate eigenvalue v_1 has algebraic multiplicity $m = 3$, only two intermediate states have to be distinguished; see Sect. 6.3.1. These intermediate states are connected by a contact discontinuity. The eigenvalues $v_1 \pm \Psi$ are genuinely nonlinear. This implies that simple waves connect the intermediate states to the left and right states. In particular, the structure of the approximate Riemann solution is as follows: The left state $\tilde{\mathbf{q}}_0 := \mathbf{q}_L$ is connected to the intermediate state $\tilde{\mathbf{q}}_{1/3}$ by a simple wave. The intermediate states $\tilde{\mathbf{q}}_{1/3}$ and $\tilde{\mathbf{q}}_{2/3}$ are connected by a contact discontinuity. A simple wave connects the intermediate state $\tilde{\mathbf{q}}_{2/3}$ to the right state $\tilde{\mathbf{q}}_1 := \mathbf{q}_R$. The approximate solution of the two-fluid Riemann problem is illustrated in Figure 6.6.

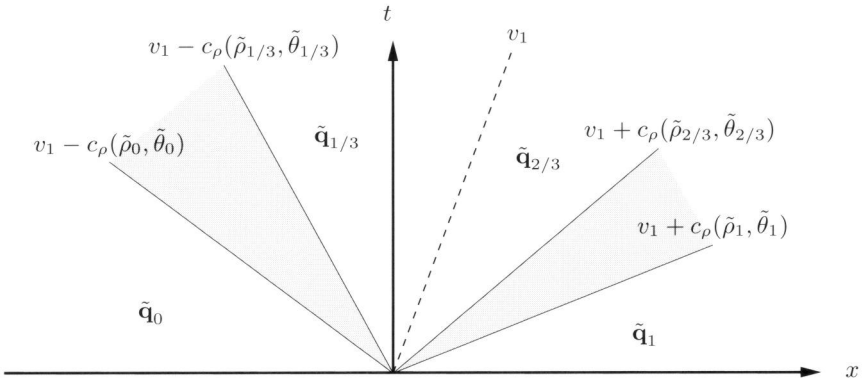

Figure 6.6: Approximate solution of the two-fluid Riemann problem. Simple waves (*shaded*) connect the left and right states to the intermediate states. The intermediate states are connected by a contact discontinuity (*dashed*).

It is important to note that θ is a k-Riemann invariant for $k = 1, 5$. Hence, a fluid transition can only occur across the contact discontinuity. Moreover, both v_1 and p are k-Riemann invariants for $k = 2, 3, 4$. Hence, v_1 and p are continuous across any contact discontinuity. In particular, v_1 and p are continuous across the interface. This implies that the kinematic and dynamic interface conditions are fulfilled. The interface between the fluids can therefore be construed as a particular instance of a contact discontinuity.

From (6.40) and (6.78) it follows that

$$\begin{pmatrix} \tilde{v}_2 \\ \tilde{v}_3 \\ \tilde{\theta} \end{pmatrix}_{1/3} = \begin{pmatrix} \tilde{v}_2 \\ \tilde{v}_3 \\ \tilde{\theta} \end{pmatrix}_0 , \qquad \begin{pmatrix} \tilde{v}_2 \\ \tilde{v}_3 \\ \tilde{\theta} \end{pmatrix}_{2/3} = \begin{pmatrix} \tilde{v}_2 \\ \tilde{v}_3 \\ \tilde{\theta} \end{pmatrix}_1 , \tag{6.79a}$$

and

$$(\tilde{v}_1)_{1/3} = (\tilde{v}_1)_{2/3} := (\tilde{v}_1)_{1/2} . \tag{6.79b}$$

Furthermore, $(\tilde{v}_1)_{1/2}$, $\tilde{\rho}_{1/3}$ and $\tilde{\rho}_{2/3}$ are determined by

$$(\tilde{v}_1)_{1/2} + \int_{\tilde{\rho}_0}^{\tilde{\rho}_{1/3}} \frac{c_\rho(\rho, \theta_0)}{\rho} \, \mathrm{d}\rho = (\tilde{v}_1)_0 , \tag{6.80a}$$

$$(\tilde{v}_1)_{1/2} - \int_{\tilde{\rho}_1}^{\tilde{\rho}_{2/3}} \frac{c_\rho(\rho, \theta_1)}{\rho} \, \mathrm{d}\rho = (\tilde{v}_1)_1 , \tag{6.80b}$$

$$p(\tilde{\rho}_{1/3}, \tilde{\theta}_0) = p(\tilde{\rho}_{2/3}, \tilde{\theta}_1) . \tag{6.80c}$$

In some cases the intermediate states can be explicitly extracted from (6.79)–(6.80). Otherwise, the intermediate states have to be determined by numerical approximation.

If the equation of state is of the form $\rho := \rho(p, \theta)$, or can be cast in this form, then the conditions for the intermediate states can be formulated in a convenient form. To derive this formulation, we note that

$$\int_{\rho_a}^{\rho_b} \frac{c_\rho(\rho, \theta)}{\rho} \, \mathrm{d}\rho = \int_{\rho_a}^{\rho_b} \frac{1}{\rho} \sqrt{\frac{\partial p(\rho, \theta)}{\partial \rho}} \, \mathrm{d}\rho = \int_{p_a}^{p_b} \frac{1}{\rho(p, \theta)} \sqrt{\frac{\partial \rho(p, \theta)}{\partial p}} \, \mathrm{d}p , \tag{6.81}$$

for certain integration limits ρ_a and ρ_b. The latter identity follows from the transformation $\rho := \rho(p, \theta)$. From (6.80)–(6.81) it follows that

$$\int_{\tilde{p}_0}^{\tilde{p}_{1/2}} \frac{1}{\rho(p, \tilde{\theta}_0)} \sqrt{\frac{\partial \rho(p, \tilde{\theta}_0)}{\partial p}} \, \mathrm{d}p + \int_{\tilde{p}_1}^{\tilde{p}_{1/2}} \frac{1}{\rho(p, \tilde{\theta}_1)} \sqrt{\frac{\partial \rho(p, \tilde{\theta}_1)}{\partial p}} \, \mathrm{d}p = (\tilde{v}_1)_0 - (\tilde{v}_1)_1 , \tag{6.82}$$

with $\tilde{p}_{1/2} := p(\tilde{\rho}_{1/3}, \tilde{\theta}_0) = p(\tilde{\rho}_{2/3}, \tilde{\theta}_1)$, conform (6.80c). Equation (6.82) presents a concise condition for the intermediate pressure $\tilde{p}_{1/2}$.

It is important to note that (6.82) is well suited to treatment by numerical approximation techniques. In particular, the derivatives of the integrals with respect to $\tilde{p}_{1/2}$, which are required in Newton's method, are simply the integrands evaluated at $\tilde{p}_{1/2}$. Moreover, for a given approximation to $\tilde{p}_{1/2}$, the integrals can be evaluated by a numerical integration method (see, e.g., Ref. [30]).

Once the intermediate pressure has been extracted from (6.82), the intermediate densities follow immediately from the equation of state:

$$\tilde{\rho}_{1/3} = \rho(\tilde{p}_{1/2}, \theta_0) , \quad \text{and} \quad \tilde{\rho}_{2/3} = \rho(\tilde{p}_{1/2}, \theta_1) . \tag{6.83}$$

We recall that once the intermediate states have been obtained, the modified Osher flux follows by straightforward computation; cf. Section 6.3.3.

6.5 Pressure Oscillations

A common objection to interface capturing is the occurrence of *pressure oscillations*. These pressure oscillations expose the loss of certain invariance properties of the continuum problem under discretization. Below, we exemplify the pressure oscillations and we derive a pressure-invariance condition for discrete approximations to two-fluid flow problems. Furthermore, we construct a non-oscillatory conservative discretization for two-fluid flow problems.

6.5.1 Exemplification

To exemplify the pressure oscillations that are generally incurred by conservative discretizations of two-fluid flow problems, we consider

$$\mathbf{q}_t + (\mathbf{f}(\mathbf{q}))_x = 0\,, \qquad x \in \mathcal{L}, t \geq 0\,, \tag{6.84a}$$

with

$$\mathbf{q} = \begin{pmatrix} \rho v \\ \rho\alpha \\ \rho \end{pmatrix}\,, \quad \text{and} \quad \mathbf{f}(\mathbf{q}) = \begin{pmatrix} \rho v^2 + p(\rho,\alpha) \\ \rho\alpha v \\ \rho v \end{pmatrix}\,, \tag{6.84b}$$

or its weak formulation, if appropriate. The considered equation of state is

$$\rho(p,\alpha) = \alpha\rho_{\mathrm{p}}(p) + (1-\alpha)\rho_{\mathrm{s}}(p)\,, \tag{6.84c}$$

with $\rho_{\mathrm{p}}(p)$ and $\rho_{\mathrm{s}}(p)$ given equations of state for the primary and secondary fluid. The interval $\mathcal{L}$ is subdivided into intervals (x_j, x_{j+1}) and (6.84) is supplemented with the initial conditions

$$\rho(x,0) = \rho_j^0\,, \quad v(x,0) = V\,, \quad \alpha(x,0) = \alpha_j^0\,, \quad \text{if } x \in (x_j, x_{j+1})\,, \tag{6.85a}$$

with V an arbitrary positive constant and ρ_j^0 and α_j^0 constants such that

$$\rho_j^0 = \alpha_j^0\,\rho_{\mathrm{p}}(P) + (1-\alpha_j^0)\,\rho_{\mathrm{s}}(P)\,, \tag{6.85b}$$

for some constant P. The equations (6.84)–(6.85) represent a two-fluid flow in which the velocity v is uniform and in which the density ρ and the (primary) volume fraction α are such that the pressure p is uniform as well.

The solution to (6.84)–(6.85) reads

$$\mathbf{q}(x,t) = \mathbf{q}(x - Vt, 0)\,. \tag{6.86}$$

The pressure $p(x,t)$ corresponding to (6.86) follows from the equation of state:

$$\rho(x,t) = \alpha(x,t)\,\rho_{\mathrm{p}}(p(x,t)) + \big(1-\alpha(x,t)\big)\,\rho_{\mathrm{s}}(p(x,t))\,. \tag{6.87}$$

By (6.86)–(6.87),

$$\rho(x-Vt,0) = \alpha(x-Vt,0)\,\rho_{\mathrm{p}}(p(x,t)) + \big(1-\alpha(x-Vt,0)\big)\,\rho_{\mathrm{s}}(p(x,t))\,, \tag{6.88}$$

which implies that $p(x,t) = P$, i.e., the pressure is invariant. Hence, if the initial velocity and pressure are uniform, then the pressure is invariant under (6.84).

Next, we consider the first order forward Euler discretization to (6.84)–(6.85) on the grid $\{(x_j, t_n) : j \in \mathbb{Z}, n \in \mathbb{N}\}$, with $t_0 = 0$ and $t_n < t_{n+1}$:

$$\frac{\mathbf{q}_j^{n+1} - \mathbf{q}_j^n}{t_{n+1} - t_n} + \frac{\mathbf{f}\big(\mathbf{q}_j^n, \mathbf{q}_{j+1}^n\big) - \mathbf{f}\big(\mathbf{q}_{j-1}^n, \mathbf{q}_j^n\big)}{x_{j+1} - x_j} = 0\,, \qquad n = 0, 1, \ldots, \tag{6.89}$$

with the initial conditions

$$\mathbf{q}_j^0 = \begin{pmatrix} \rho_j^0 V \\ \rho_j^0 \alpha_j^0 \\ \rho_j^0 \end{pmatrix}\,, \tag{6.90}$$

conform (6.85). The grid function $\mathbf{q}_j^n$ approximates $\mathbf{q}(x, t_n)$ according to (6.86) in the interval (x_j, x_{j-1}).

The states $\mathbf{q}_j^0$ and $\mathbf{q}_{j+1}^0$ are connected by a contact discontinuity with velocity V. The corresponding Godunov flux reads:

$$\mathbf{f}(\mathbf{q}_j^0, \mathbf{q}_{j+1}^0) = V \begin{pmatrix} \rho_j^0 V \\ \rho_j^0 \alpha_j^0 \\ \rho_j^0 \end{pmatrix} + \begin{pmatrix} P \\ 0 \\ 0 \end{pmatrix}\,. \tag{6.91}$$

Because shocks are absent, expression (6.91) is also valid for the (modified) Osher scheme. By (6.89),

$$\mathbf{q}_j^1 = \mathbf{q}_j^0 - C\big(\mathbf{q}_j^0 - \mathbf{q}_{j-1}^0\big)\,, \tag{6.92a}$$

with

$$C := V(t_1 - t_0)/(x_{j+1} - x_j)\,, \tag{6.92b}$$

the *CFL-number*. In conjunction with (6.85b), equation (6.92) implies

$$\rho_j^1 = \alpha_j^*\, \rho_p(P) + \big(1 - \alpha_j^*\big)\, \rho_{\mathrm{s}}(P)\,, \tag{6.93a}$$

with

$$\alpha_j^* := \alpha_j^0 - C\big(\alpha_j^0 - \alpha_{j-1}^0\big)\,. \tag{6.93b}$$

From (6.93) it follows that a necessary and sufficient condition for pressure invariance of the discrete approximation is $\alpha_j^1 = \alpha_j^*$. However, from (6.85b) and (6.92) we obtain

$$\alpha_j^1 = \frac{\big((1-C)(\alpha_j^0)^2 + C(\alpha_{j-1}^0)^2\big)\rho_{\mathrm{p}} + \big((1-C)\alpha_j^0(1-\alpha_j^0) + C\alpha_{j-1}^0(1-\alpha_{j-1}^0)\big)\rho_{\mathrm{s}}}{\big(\alpha_j^0 - C(\alpha_j^0 - \alpha_{j-1}^0)\big)\rho_{\mathrm{p}} + \Big(1 - \big(\alpha_j^0 - C(\alpha_j^0 - \alpha_{j-1}^0)\big)\Big)\rho_{\mathrm{s}}}\,, \tag{6.94}$$

with $\rho_{\mathrm{p/s}} := \rho_{\mathrm{p/s}}(P)$. In general, $\alpha_j^1 \neq \alpha_j^*$ and, hence, the discrete approximation (6.89) lacks the pressure-invariance property of the continuum equations (6.84).

Specific exceptions are:

$$C = 0 \quad \Rightarrow \quad \mathbf{q}_j^1 = \mathbf{q}_j^0 \,, \tag{6.95a}$$

$$C = 1 \quad \Rightarrow \quad \mathbf{q}_j^1 = \mathbf{q}_{j-1}^0 \,, \tag{6.95b}$$

$$\alpha_j^0 = \alpha_{j-1}^0 \quad \Rightarrow \quad \mathbf{q}_j^0 = \mathbf{q}_{j-1}^0 \,, \tag{6.95c}$$

$$\rho_\mathrm{p} = \rho_\mathrm{s} \quad \Rightarrow \quad \text{single-fluid flow} \,. \tag{6.95d}$$

Exceptions (6.95a)–(6.95c) are trivial. Exception (6.95d) confirms that the loss of the pressure-invariance property is special for two-fluid flows.

It is noteworthy that if $(\rho\alpha)_t + (\rho\alpha v)_x = 0$ in (6.84) is replaced by

$$\alpha_t + v\alpha_x = 0 \,, \qquad x \in \mathcal{L}, t \geq 0 \,, \tag{6.96}$$

then, subject to the initial conditions (6.90), the first order forward Euler discretization yields

$$\alpha_j^1 = \alpha_j^0 - C(\alpha_j^0 - \alpha_{j-1}^0) \,. \tag{6.97}$$

Hence, $\alpha_j^1 = \alpha_j^*$, and pressure invariance is ensured. Equation (6.96) is, however, in non-conservation form. Hence, the pressure invariance is in this case accomplished at the expense of the conservation form of the equations.

6.5.2 Pressure-Invariance Condition

The implications of the above exemplification are restricted: The analysis does not imply that pressure oscillations are inherent to conservative discretizations of two-fluid flow problems. It merely implies that discrete approximations to two-fluid flow problems do not obviously inherit the pressure-invariance property of the continuum equations.

To avoid pressure oscillations, it is necessary that a discrete approximation to a two-fluid flow problem complies with a *pressure-invariance condition*. We formulate this pressure-invariance condition for discrete approximations of

$$\mathbf{q}_t + (\mathbf{f}(\mathbf{q}))_x = 0 \,, \qquad x \in \mathcal{L}, t \geq 0 \,, \tag{6.98a}$$

or its weak formulation, with

$$\mathbf{q} = \begin{pmatrix} \rho v \\ \rho\beta(\theta) \\ \rho \end{pmatrix} \,, \qquad \mathbf{f}(\mathbf{q}) = \begin{pmatrix} \rho v^2 + p(\rho, \theta) \\ \rho\beta(\theta) v \\ \rho v \end{pmatrix} \,, \tag{6.98b}$$

and $p(\rho, \theta)$ a given equation of state, e.g., $p(\rho, \theta) = p(\rho, \alpha(\theta))$, with $p(\rho, \alpha)$ implicitly defined by (6.84c). We do not yet attach a specific connotation to β. For instance, β can be a continuously differentiable strictly monotone function, so that $\theta_t + v\theta_x = 0$ is implied (cf. §6.4.1), or β can be the primary volume fraction α. Note that θ only serves as an intermediary between β and p. Hence, it is not necessary that θ appears explicitly in the formulation.

We consider a discretization of (6.98) on a grid $\{(x_j, t_n) : j \in \mathbb{Z}, n \in \mathbb{N}\}$, with $t_0 = 0$ and $t_n < t_{n+1}$. We denote by $\mathbf{q}_j^n$ the discrete approximation to $\mathbf{q}(x, t_n)$ in the interval (x_j, x_{j+1}). In particular, $\mathbf{q}_j^0$ is the discrete representation of the initial data. The discretization of (6.98) is characterized by the mapping $\{\mathbf{q}_j^n\} \mapsto \{\mathbf{q}_j^{n+1}\}$. The pressure-invariance condition for discretizations $\{\mathbf{q}_j^n\} \mapsto \{\mathbf{q}_j^{n+1}\}$ of (6.98) reads: If $v_j^n = V$, with V a constant, and ρ_j^n and θ_j^n satisfy

$$p(\rho_j^n, \theta_j^n) = P\,, \tag{6.99a}$$

for some constant P, then

$$p\big(\rho_j^{n+1}, \theta_j^{n+1}\big) = P\,. \tag{6.99b}$$

For instance, for an equation of state of the form (6.84c), the pressure-invariance condition reads: If $v_j^n = V$ and

$$\rho_j^n = \alpha(\theta_j^n)\,\rho_{\mathrm{p}}(P) + (1 - \alpha(\theta_j^n))\,\rho_{\mathrm{s}}(P)\,, \tag{6.100a}$$

then

$$\rho_j^{n+1} = \alpha(\theta_j^{n+1})\,\rho_{\mathrm{p}}(P) + \big(1 - \alpha(\theta_j^{n+1})\big)\,\rho_{\mathrm{s}}(P)\,. \tag{6.100b}$$

6.5.3 A Non-Oscillatory Conservative Scheme

In order to construct a pressure-invariant discretization for two-fluid flow problems, we define the partial primary and secondary densities by:

$$\rho'_{\mathrm{p}} := \alpha\rho_{\mathrm{p}}\,, \quad \text{and} \quad \rho'_{\mathrm{s}} := (1 - \alpha)\rho_{\mathrm{s}}\,, \tag{6.101}$$

where α is the primary volume fraction conform (6.59) and ρ_{p} and ρ_{s} denote the densities of the primary and secondary fluids, respectively. In one spatial dimension, conservation of mass of the primary and secondary fluid stipulates

$$(\rho'_{\mathrm{p}})_t + (\rho'_{\mathrm{p}} v)_x = 0\,, \tag{6.102a}$$

$$(\rho'_{\mathrm{s}})_t + (\rho'_{\mathrm{s}} v)_x = 0\,. \tag{6.102b}$$

The compound density is defined by

$$\rho := \alpha\rho_{\mathrm{p}} + (1 - \alpha)\rho_{\mathrm{s}} = \rho'_{\mathrm{p}} + \rho'_{\mathrm{s}}\,. \tag{6.103}$$

Hence, if β denotes the primary *mass fraction*,

$$\beta := \rho'_{\mathrm{p}}/\rho\,, \tag{6.104}$$

then conservation of mass, of both the primary and the secondary fluid, and of momentum is described by:

$$\mathbf{q}_t + (\mathbf{f}(\mathbf{q}))_x = 0\,, \qquad x \in \mathcal{L}, t \geq 0\,, \tag{6.105a}$$

or its weak formulation, with

$$\mathbf{q} = \begin{pmatrix} \rho v \\ \rho\beta \\ \rho \end{pmatrix}, \qquad \mathbf{f}(\mathbf{q}) = \begin{pmatrix} \rho v^2 + p(\rho,\beta) \\ \rho\beta v \\ \rho v \end{pmatrix}. \tag{6.105b}$$

Moreover, if the primary and secondary fluid are equipped with barotropic equations of state $\rho_{\mathrm{p/s}}(p)$ and the compound equation of state is given by (6.84c), then $p(\rho,\beta)$ in (6.105) is implicitly given by

$$\rho\beta = \alpha\rho_{\mathrm{p}}(p)\,, \tag{6.106a}$$
$$\rho - \rho\beta = (1-\alpha)\rho_{\mathrm{s}}(p)\,, \tag{6.106b}$$

or, by eliminating α,

$$\frac{1}{\rho} = \frac{1-\beta}{\rho_{\mathrm{s}}(p)} + \frac{\beta}{\rho_{\mathrm{p}}(p)}\,. \tag{6.107}$$

We consider the first order forward Euler discretization of (6.105)–(6.106) on a grid $\{(x_j,t_n) : j \in \mathbb{Z}, n \in \mathbb{N}\}$, conform (6.89). If $v_j^n = V$, with V a positive constant, and

$$(\rho\beta)_j^n = \alpha_j^n \rho_{\mathrm{p}}(P)\,, \tag{6.108a}$$
$$\rho_j^n - (\rho\beta)_j^n = (1-\alpha_j^n)\rho_{\mathrm{s}}(P)\,, \tag{6.108b}$$

for all $j \in \mathbb{Z}$, with P a constant, then the first order forward Euler discretization yields

$$\rho_j^{n+1} = \rho_j^n - C\big(\rho_j^n - \rho_{j-1}^n\big)\,, \tag{6.109a}$$
$$(\rho\beta)_j^{n+1} = (\rho\beta)_j^n - C\big((\rho\beta)_j^n - (\rho\beta)_{j-1}^n\big)\,, \tag{6.109b}$$

with C according to (6.92b). From (6.108)–(6.109) it follows that

$$(\rho\beta)_j^{n+1} = \alpha_j^{n+1}\rho_{\mathrm{p}}(P)\,, \tag{6.110a}$$
$$\rho_j^{n+1} - (\rho\beta)_j^{n+1} = (1-\alpha_j^{n+1})\rho_{\mathrm{s}}(P)\,, \tag{6.110b}$$

with

$$\alpha_j^{n+1} := \alpha_j^n - C\big(\alpha_j^n - \alpha_{j-1}^n\big)\,. \tag{6.110c}$$

Therefore, $p(\rho_j^{n+1},\beta_j^{n+1}) = P$, which implies that the first order forward Euler discretization of (6.105)–(6.106) complies with the pressure-invariance condition.

Chapter 7
Conclusions

Motivated by the demand for efficient computational methods for steady viscous free-surface flow problems in practical applications such as ship hydrodynamics, in this thesis we concerned ourselves with numerical techniques for the Navier–Stokes equations with a free boundary.

An investigation of the free-surface Navier–Stokes equations in primitive variables was presented. We analyzed the generic problem of perturbations of a uniform flow, by means of perturbation methods and Fourier techniques. The analysis clarifies the characteristic features of viscous free-surface flows, such as the dispersive behavior of surface gravity waves, the asymptotic temporal behavior of wave groups and the structure of the free-surface boundary layer. Moreover, by virtue of the formulation in primitive variables, the analysis can serve in the assessment of numerical methods, if the differential operators in the continuum equations are replaced by their difference approximation.

We showed that the usual time-integration method for solving the steady free-surface Navier–Stokes equations is often inefficient as a result of the specific transient behavior of surface gravity waves and a stability restriction on the admissible time step. We then proposed a new iterative solution method, based on a so-called quasi free-surface condition. To establish the efficiency of the method, we showed that its asymptotic computational complexity deteriorates only moderately with decreasing mesh width. Moreover, mesh width independence of the computational complexity can be accomplished by nested iteration. Numerical results were presented for a two-dimensional model problem. The numerical experiments confirm that the convergence behavior of the method is asymptotically independent of the mesh width. We believe that the proposed method can be useful in ship hydrodynamics and other fields of application in which the efficient computation of steady free-surface flows at high Reynolds number is required.

In addition, we investigated the numerical solution of steady-free surface flows by means of the adjoint optimal shape design method. To obtain an indication of the properties of the method, we considered its application to the steady free-surface potential flow equations. The adjoint shape optimization method is equally applicable to the free-surface Navier–Stokes equations, but the specifics of the method are much more involved in that case. We showed that the optimal shape design problem displays the usual characteristic behavior of steady free-surface flows. We determined the convergence behavior of the adjoint method for the generic problem of perturbations of a uniform flow. The method yields exponential convergence (i.e., $O(\zeta)^n$), $0 < \zeta < 1$) for 2D supercritical flows and algebraic convergence (typically, $1/\sqrt{n}$ in 2D and $1/n$ in 3D) in all other cases. The deteriorated convergence behavior for 3D and 2D subcritical flows can be attributed to the occurrence of critical modes. We showed that preconditioning is imperative to avoid mesh-width dependence of the convergence behavior and we presented a suitable preconditioner for the steady free-surface flow problem. Numerical results were presented for two-dimensional flow over an obstacle in a channel. The observed convergence behavior confirms the asymptotic estimates.

Free-surface flows being a special case of two-fluid flow, we presented a preliminary investigation of the interface capturing method for two-fluid flows. We constructed an Osher-type approximate Riemann solver. Details were presented for fluids with a barotropic equation of state. We showed that fluid transitions can only occur across contact discontinuities, which implies that the kinematic and dynamic interface conditions are satisfied. The spurious pressure oscillations that are commonly incurred by conservative discretizations of two-fluid flows were identified as a result of the loss of invariance properties under discretization. We formulated a pressure-invariance condition for discrete approximations to two-fluid flow problems and constructed a non-oscillatory discretization. The implementation of the interface capturing approach with efficient techniques for steady problems is deferred to future research.

Chapter 8
Recommendations

This thesis presents an investigation into numerical methods for the steady free-surface Navier–Stokes equations. Based on the results of the investigation, below we phrase several recommendations for future research and for applications.

The analysis presented in Chapter 3 shows that for free-surface flows with vanishing viscosity, the asymptotic transient behavior is $O(1/\sqrt{t})$ in 2D and $O(1/t)$ in 3D. This algebraic convergence behavior renders time-integration methods inefficient for solving steady free-surface flows at high Reynolds numbers. However, since the algebraic convergence behavior is exclusively attributable to surface gravity waves of which the group velocity equals the flow velocity, it appears possible to restore efficiency by removing these waves by other means. In particular, nested iteration could prove useful, e.g., a Krylov-subspace accelerated time-integration method, or a combination of adjoint shape optimization with time integration. An investigation of such nested iteration methods is recommended.

Based on (3.36), it is anticipated that the usual time-integration method performs well for steady free-surface flows at low Reynolds numbers. However, we emphasize that the exponential temporal decay due to viscosity was derived in the limit of vanishing viscosity. Therefore, a re-investigation of the roots of the dispersion relation (3.33) is required to establish the convergence behavior of time-integration methods for low Reynolds number applications.

We believe that the quasi-free-surface-condition (QFSC) method presented in Chapter 4 is useful for solving steady ship waves and other steady free-surface Navier–Stokes flows at high Reynolds numbers. This thesis presents an application of the method to a two-dimensional model problem. The method is in principle equally applicable to three-dimensional problems. However, the extension to actual 3D ship wave computations introduces several pertinent complications:

(1) A surface-penetrating object is inserted, which introduces an intersection between the free-surface and a no-slip boundary. Although the QFSC method

does not suffer from the usual contact line problem of time-integration methods because the quasi free-surface condition is identically satisfied at the intersection, further investigation is required.

(2) In actual ship wave computations, singularities occur near the bow and stern. If the singularities compromise the solution process, simple ad hoc correctives can be used, because the continuum equations do not correctly represent the physical behavior in the neighborhood of the singularities anyway: collapsing waves and splashing occur, and entirely different physical phenomena play a critical role. An example of a possible corrective is a smooth transition from the quasi-free-surface condition to the usual free-slip condition near the singularities.

(3) Two and three-dimensional free-surface flows exhibit essentially different behavior, due to diverging waves which are only present in the three-dimensional case. An investigation of the implications for the numerical treatment of the 3D steady free-surface flow problem is appropriate.

(4) In practical computations, infinite spatial domains must be truncated. It is expected that the treatment of the artificial lateral boundaries that occur as a result of the truncation, is more complicated in 3D than in 2D. Absorbing boundary conditions for artificial boundaries have received much attention in the context of transient problems. In contrast, few efforts have been made to investigate absorbing boundary conditions for iterative solution methods for boundary value problems. Evidently, the boundary conditions and their treatment play a crucial part in the convergence behavior of an iterative method, and an investigation of absorbing boundary conditions for iterative solution methods is therefore warranted.

It is important to note that the QFSC method transfers the complexity of the steady free-surface flow problem to the sub-problems, i.e., the boundary value problems that must be solved in each iteration cycle. Efficient solution of the sub-problems is therefore important. To construct an efficient solution method for the sub-problems in ship wave computations, the aforementioned issues must be addressed.

The adjoint optimal shape design method is in general inefficient for solving steady free-surface flows, due to the algebraic convergence of critical modes. However, efficiency can be restored by eliminating these modes by other means. In particular, because the retarded modes of the adjoint shape optimization method and the time-integration method are different, we anticipate that an efficient method can be constructed by combining these methods. The advantage of such a nested method over the QFSC method of Chapter 4, is that the underlying sub-problems have straightforward boundary conditions at the free surface: the time-integration method requires stress-free boundary conditions and the adjoint optimal shape design method requires free-slip boundary conditions. We recommend that such a

nested method is implemented and assessed for the steady free-surface potential-flow equations.

The interface capturing approach is still in its infancy and it is not clear whether it can eventually provide a useful alternative for surface fitting methods for (steady) problems with smooth free surfaces. To assess the suitability of the interface capturing approach for steady free-surface flows, the following issues have to be addressed; (1) treatment of source terms, in order to include the gravitational force, (2) resolution near the interface, (3) implementation of the interface capturing method with efficient numerical solution methods for steady hyperbolic problems.

The correctives presented in the literature (see Section 6.1) to avoid pressure oscillations, sacrifice the conservation form of the equations in the vicinity of the interface. Because the conservation form is imperative for a correct representation of shock waves, it is anticipated that these methods fail if the interface interacts with a shock wave. We propose a comparative study of the conservative non-oscillatory method of Chapter 6 and contemporary numerical methods for two-fluid flow, applied to a discriminating test case, e.g., a shock wave passing the interface.

Bibliography

[1] R. Abgrall, *How to prevent pressure oscillations in multicomponent flow calculations: A quasi conservative approach*, J. Comput. Phys. **125** (1996), 150–160.

[2] R. Abgrall and S. Karni, *Computations of compressible multifluids*, J. Comput. Phys. **169** (2001), 594–623.

[3] B. Alessandrini and G. Delhommeau, *Simulation of three-dimensional unsteady viscous free surface flow around a ship model*, Int. J. Num. Meth. Fluids **19** (1994), 321–342.

[4] R. Aris, *Vectors, tensors and the basic equations of fluid mechanics*, Prentice-Hall, Englewood Cliffs, N.J., 1962.

[5] G.K. Batchelor, *An introduction to fluid dynamics*, Cambridge University Press, Cambridge, 1967.

[6] R. Becker, *An optimal control approach to a-posteriori error estimation for finite element discretizations of the Navier–Stokes equations*, Tech. Report IWR/SFB-Preprints 2000-34, Ruprecht-Karls-Universität Heidelberg, 2000, Available at `http://www.iwr.uni-heidelberg.de/sfb359/PP/Preprint2000-34.ps.gz`.

[7] R. Becker, M. Braack, and R. Rannacher, *Adaptive finite element methods for flow problems*, Tech. Report IWR/SFB-Preprints 2000-20, Ruprecht-Karls-Universität Heidelberg, 2000, Available at `http://www.iwr.uni-heidelberg.de/sfb359/PP/Preprint2000-20.ps.gz`.

[8] A. Brandt, *Multigrid techniques: 1984 guide with applications to fluid dynamics*, Tech. report, GMD, 1984.

[9] E.H. van Brummelen, *Numerical solution of steady free-surface Navier–Stokes flow*, Tech. Report MAS-R0018, ISSN 1386-3703, CWI, 2000, Available at `http://www.cwi.nl/ftp/CWIreports/MAS/MAS-R0018.ps.Z`.

[10] E.H. van Brummelen, H.C. Raven, and B. Koren, *Efficient numerical solution of steady free-surface Navier–Stokes flow*, J. Comput. Phys. **174** (2001), 120–137.

[11] J. Cahouet, *Etude numérique et experimentale du problème bidimensionnel de la résistance de vagues non-linéaire*, Ph.D. thesis, ENSTA, Paris, 1984, (In French).

[12] E. Campana, A. Di Mascio, P.G. Esposito, and F. Lalli, *Viscous-inviscid coupling in free surface ship flows*, Int. J. Num. Meth. Fluids **21** (1995), 699–722.

[13] T. Cebeci and A.M.O. Smith, *Analysis of turbulent boundary layers*, Academic Press, New York, 1974.

[14] Y.C. Chang, T.Y. Hou, B. Merriman, and S. Osher, *A level set formulation of Eulerian interface capturing methods for incompressible fluid flows*, J. Comput. Phys. **124** (1996), 449–464.

[15] U.T. Ehrenmark, *On viscous wave motion over a plane beach*, SIAM J. Appl. Math. **51** (1991), 1–19.

[16] B. Engquist and A. Majda, *Absorbing boundary conditions for the numerical simulation of waves*, Math. Comp. **31** (1977), 629–651.

[17] J. Farmer, L. Martinelli, and A. Jameson, *A fast multigrid method for solving the nonlinear ship wave problem with a free surface*, Proceedings of the 6th International Conference on Numerical Ship Hydrodynamics (Iowa, 1993) (W. Patel and F. Stern, eds.), National Academy Press, Washington D.C., 1994, pp. 155–172.

[18] R.P Fedkiw, T. Aslam, B. Merriman, and S. Osher, *A non-oscillatory Eulerian approach to interfaces in multimaterial flows (the ghostfluid method)*, J. Comput. Phys. **152** (1999), 457–492.

[19] C.A.J. Fletcher, *Computational techniques for fluid dynamics 2*, Springer, Berlin, 1988.

[20] A.V. Fursikov, M.D. Gunzburger, and L.S. Hou, *Boundary value problems and optimal boundary control for the Navier–Stokes system: the two-dimensional case*, SIAM J. Control Optim. **36** (1998), no. 3, 852–894.

[21] M.B. Giles and N.A. Pierce, *Adjoint equations in CFD: Duality, boundary conditions and solution behaviour*, AIAA **97-1850** (1997).

[22] S.K. Godunov, *Finite difference method for numerical computation of discontinuous solutions of the equations of fluid dynamics*, Mat. Sbornik **47** (1959), 271–306, (In Russian).

[23] M.D. Gunzburger and H. Kim, *Existence of an optimal solution of a shape control problem for the stationary Navier–Stokes equations*, SIAM J. Control Optim. **36** (1998), no. 3, 895–909.

[24] M.D. Gunzburger and H.K. Lee, *An optimization-based domain decomposition method for the Navier–Stokes equations*, SIAM J. Numer. Anal. **37** (2000), no. 5, 1455–1480.

[25] B. Gustafsson, H.-O. Kreiss, and J. Oliger, *Time dependent problems and difference methods*, Pure and Applied Mathematics, Wiley, New York, 1995.

[26] W.J. Harrison, *The influence of viscosity on the oscillations of superposed fluids*, Proc. Lond. Math. Soc. **6** (1908).

[27] R. Hartmann and P. Houston, *Adaptive discontinuous Galerkin finite element methods for nonlinear hyperbolic conservation laws*, Tech. Report IWR/SFB-Preprints 2001-20, Ruprecht-Karls-Universität Heidelberg, 2001, Available at `http://www.iwr.uni-heidelberg.de/sfb359/PP/Preprint2001-20.ps.gz`.

[28] P.W. Hemker and S.P. Spekreijse, *Multiple grid and Osher's scheme for the efficient solution of the steady Euler equations*, Appl. Num. Math. **2** (1986), 475–493.

[29] M. Hoekstra, *Numerical simulation of ship stern flows with a space-marching Navier–Stokes method*, Ph.D. thesis, Delft University of Technology, Netherlands, 1999.

[30] E. Isaacson and H.B. Keller, *Analysis of numerical methods*, Wiley, New York, 1966.

[31] P. Jenny, B. Müller, and H. Thomann, *Correction of conservative Euler solvers for gas mixtures*, J. Comput. Phys. **132** (1997), 91–107.

[32] S. Karni, *Multicomponent flow calculations by a consistent primitive algorithm*, J. Comput. Phys. **112** (1994), 31–43.

[33] ———, *Hybrid multifluid algorithms*, SIAM J. Sci. Comput. **17** (1996), 1019–1039.

[34] F.J. Kelecy and R.H. Pletcher, *The development of a free surface capturing approach for multidimensional free surface flows in closed containers*, J. Comput. Phys. **138** (1997), 939–980.

[35] J. Kevorkian and J.D. Cole, *Perturbation methods in applied mathematics*, Applied Mathematical Sciences, no. 34, Springer, Berlin, 1981.

[36] H.-O. Kreiss, *Initial boundary value problems for hyperbolic systems*, Comm. Pure Appl. Math. **23** (1970), 277–298.

[37] H. Lamb, *Hydrodynamics*, 6th ed., Dover, New York, 1945.

[38] P.D. Lax, *Hyperbolic systems of conservation laws II*, Comm. Pure Appl. Math. **10** (1957), 537–566.

[39] ———, *Hyperbolic systems of conservation laws and the mathematical theory of shock waves*, Regional Conference Series in Applied Mathematics, vol. 11, SIAM, Philadelphia, 1973.

[40] B. van Leer, *Flux vector splitting for the Euler equations*, Proceedings of the 8th International Conference on Numerical Methods in Fluid Dynamics (Aachen, Germany, 1982) (E. Krause, ed.), Lecture Notes in Physics, vol. 170, Springer, Berlin, 1982, pp. 507–512.

[41] ———, *On the relation between the upwind-differencing schemes of Godunov, Engquist-Osher and Roe*, SIAM J. Sci. Stat. Comput. **5** (1984), 1–20.

[42] R.J. LeVeque, *Numerical methods for conservation laws*, Lectures in Mathematics, Birkhäuser, Basel, 1990.

[43] M.J. Lighthill, *Introduction to Fourier analysis and generalised functions*, Cambridge University Press, Cambridge, 1958.

[44] ———, *Waves in fluids*, Cambridge University Press, Cambridge, 1978.

[45] H. Miyata, T. Sato, and N. Babo, *Difference solution of a viscous flow with free-surface wave about an advancing ship*, J. Comput. Phys. **72** (1987), 393–421.

[46] W. Mulder, S. Osher, and J.A. Sethian, *Computing interface motion in compressible gas dynamics*, J. Comput. Phys. **100** (1992), 209–228.

[47] O.A. Oleinik, *Discontinuous solutions of nonlinear differential equations*, Uspekhi Mat. Nauk **12** (1957), 3–73, Amer. Math. Soc. Transl. Ser. 2, 26, pp. 95-172.

[48] S. Osher and S. Chakravarthy, *Upwind schemes and boundary conditions with applications to Euler equations in general geometries*, J. Comput. Phys. **50** (1983), 447–481.

[49] S. Osher and F. Solomon, *Upwind difference schemes for hyperbolic conservation laws*, Math. Comput. **38** (1982), 339–374.

[50] O. Pironneau, *Optimal shape design for elliptic systems*, Computational Physics, Springer, Berlin, 1984.

[51] H.C. Raven, *A solution method for the nonlinear ship wave resistance problem*, Ph.D. thesis, Delft University of Technology, Netherlands, 1996.

[52] R.D Richtmyer and K.W. Morton, *Difference methods for initial-value problems*, 2nd ed., Pure and Applied Mathematics, no. 4, Wiley, New York, 1967.

[53] P.L. Roe, *Approximate Riemann solvers, parameter vectors, and difference schemes*, J. Comput. Phys. **43** (1981), 357–372.

[54] P.A. Sackinger, P.R. Schuck, and R.R. Rao, *A Newton-Raphson pseudo-solid domain mapping technique for free and moving boundary problems: A finite element implementation*, J. Comput. Phys. **125** (1996), 83–103.

[55] H. Saito and L.E. Scriven, *Study of coating flow by the finite element method*, J. Comput. Phys. **42** (1981), 53–76.

[56] R. Saurel and R. Abgrall, *A multiphase Godunov method for compressible multifluid and multiphase flows*, J. Comput. Phys. **150** (1999), 425–467.

[57] L.E. Scriven, *Dynamics of a fluid interface*, Chem. Eng. Sc. **12** (1960), 98–108.

[58] W.J. Silliman and L.E. Scriven, *Separating flow near a static contact line: Slip at a wall and shape of a free surface*, J. Comput. Phys. **34** (1980), 287–313.

[59] J. Simon, *Nonhomogeneous viscous incompressible fluids: Existence of velocity, density and pressure*, SIAM J. Math. Anal. **20** (1990), 1093–1117.

[60] J. Smoller, *Shock waves and reaction-diffusion equations*, Grundlehren der mathematischen Wissenschaften, Springer, New York, 1983.

[61] S. Spekreijse, *Multigrid solution of monotone second-order discretizations of hyperbolic conservation laws*, Math. Comput. **49** (1987), 135–155.

[62] J.L. Steger and R.F. Warming, *Flux vector splitting of the inviscid gasdynamic equations with application to finite-difference methods*, J. Comput. Phys. **40** (1981), 263–293.

[63] J.J. Stoker, *Water waves: the mathematical theory with applications*, Pure and Applied Mathematics, Wiley, New York, 1992.

[64] E. Süli, P. Houston, and B. Senior, *hp-discontinuous Galerkin finite element methods for hyperbolic problems: error analysis and adaptivit*, Numerical Methods for Fluid Dynamics VII (Oxford, U.K., 16-19 March 2001) (M.J. Baines, ed.), ICFD, 2001, To appear.

[65] P.K. Sweby, *High resolution schemes using flux limiters for hyperbolic conservation laws*, SIAM J. Numer. Anal. **21** (1984), 995–1011.

[66] S. Ta'asan, *Infinite dimensional preconditioners for optimal design problems*, Inverse Design and Optimization Methods (R.A. van den Braembussche and M. Manna, eds.), VKI Lecture Series, vol. 5, Von Karman Institute for Fluid Dynamics, 1997.

[67] ———, *Multigrid one-shot methods and design strategy*, Inverse Design and Optimization Methods (R.A. van den Braembussche and M. Manna, eds.), VKI Lecture Series, vol. 5, Von Karman Institute for Fluid Dynamics, 1997.

[68] ———, *Theoretical tools for problem setup*, Inverse Design and Optimization Methods (R.A. van den Braembussche and M. Manna, eds.), VKI Lecture Series, vol. 5, Von Karman Institute for Fluid Dynamics, 1997.

[69] R. Témam, *Navier–Stokes equations : theory and numerical analysis*, Studies in mathematics and its applications, vol. 2, North-Holland, Amsterdam, 1977.

[70] ———, *Navier–Stokes equations and nonlinear functional analysis*, CBMS Regional Conference Series in Applied Mathematics, vol. 41, SIAM, Philadelphia, 1983.

[71] P.A. Thompson, *Compressible fluid dynamics*, Advanced Engineering Series, McGraw-Hill, New York, 1972.

[72] E.C. Titchmarsh, *Introduction to Fourier integrals*, Oxford University Press, Oxford, 1937.

[73] E.F. Toro, *Riemann solvers and numerical methods for fluid dynamics*, Springer, Berlin, 1997.

[74] W. Tsai and D.K.P. Yue, *Computation of nonlinear free-surface flows*, Annual Rev. Fluid. Mech. **28** (1996), 249–278.

[75] G.D. Tzabiras, *A numerical investigation of 2D steady free surface flows*, Int. J. Num. Meth. Fluids **25** (1997), 567–598.

[76] M. Vogt, *A numerical investigation of the level set method for computing free-surface waves*, Tech. Report CHA/NAV/R-98/0054, ISSN 1101-0614, Chalmers University of Technology, 1998.

[77] P. Wesseling, *Principles of computational fluid dynamics*, Springer Series in Computational Mathematics, vol. 29, Springer, Berlin, 2001.

[78] G.B. Whitham, *Linear and nonlinear waves*, Pure and Applied Mathematics, Wiley, New York, 1974.

[79] E. Zauderer, *Partial differential equations of applied mathematics*, 2nd ed., Pure and Applied Mathematics, Wiley, Chichester, 1989.

[80] S. Zhu and Y. Zhang, *On nonlinear transient free-surface flows over a bottom obstruction*, Phys. Fluids **9** (1997), no. 9, 2598–2604.

Appendix A
Abstract

Flows that are partly bounded by a freely moving boundary occur in many physical systems and engineering applications. Accurate prediction of the behavior of such free-surface flows is therefore of fundamental importance, for instance, in the design and evaluation of immersed structures and vessels. Numerical methods play an important role in the solution of free-surface flow problems. Most practical computational methods for solving free-surface flows around a surface-penetrating body are presently based on a potential flow model. However, to advance the aforementioned engineering applications, it is imperative to progress to a more sophisticated flow model, viz., the Navier–Stokes equations.

An important class of free-surface flow problems for which efficient numerical techniques for the Navier–Stokes equations are still unavailable, are *steady* free-surface flows. Concurrent computational methods for the steady free-surface Navier–Stokes equations generally resort to a straightforward time-integration method. However, the particular transient behavior of free-surface flows often abates the efficiency of this method. Alternative solution methods exist, but the performance of these methods usually depends sensitively on the parameters in the problem, or their applicability is too restricted. An investigation into numerical methods for the steady free-surface Navier–Stokes equations is therefore warranted.

Following the formulation of the free-surface flow problem, we present an analysis of the free-surface Navier–Stokes equations in primitive variables, by means of perturbation methods and Fourier techniques. The analysis elucidates the characteristic features of viscous free-surface flows. Results concern the occurrence of surface gravity waves and their dispersive behavior, the asymptotic temporal behavior of wave groups and the structure of the free-surface boundary layer. Moreover, by virtue of the formulation in primitive variables, the analysis can serve in the assessment of numerical methods, by replacing the differential

operators by their difference approximation conform the considered discretization.

We prove that the usual time-integration method is generally inefficient for solving steady free-surface flows at high Reynolds numbers, due to the asymptotic temporal behavior of surface-gravity-wave groups, and a stability restriction on the admissible time step. We propose a novel iterative method, based on a so-called quasi free-surface condition. To demonstrate the efficiency of the method, we show that its computational complexity is mesh-width independent. Numerical results are presented for a two-dimensional model problem. The results confirm the mesh-width independence of the convergence behavior. Comparison of the numerical results with measurements shows good agreement.

Next, we investigate the numerical solution of steady free-surface flows by the adjoint optimal shape design method. To obtain an indication of the properties of the method, we investigate its application to the steady free-surface potential-flow equations. The method can be extended to the Navier–Stokes equations, but the details are much more involved in that case. The free-surface flow problem is reformulated as an optimal shape design problem. By means of perturbation methods and Fourier analysis we show that the design problem displays the usual characteristic features of steady free-surface flows. We determine the asymptotic convergence behavior of the method. Moreover, we show that preconditioning is essential to avoid mesh-width dependence of the convergence behavior and we present a preconditioner for the optimal shape design problem. Numerical results are presented for a two-dimensional model problem. The observed convergence behavior confirms the asymptotic estimates.

Free surface flows being a special case of two-fluid flow, we finally explore the interface capturing approach to solving two-fluid flow problems. In the absence of viscosity, two-fluid flows are described by a system of hyperbolic conservation laws. We consider Godunov's method for discretizing hyperbolic systems. To reduce the computational cost of the flux evaluation in Godunov's method, an Osher-type approximate Riemann solver is constructed. Details are presented for two fluids with a barotropic equation of state. The pressure oscillations that are commonly incurred by conservative discretizations of two-fluid flows are addressed. A pressure-invariance condition is formulated and a non-oscillatory conservative discretization for two-fluid flows is presented. The implementation of the interface capturing approach with efficient solution methods for steady hyperbolic systems is deferred to future research.

Appendix B
Samenvatting

In veel fysische systemen en technische toepassingen treden stromingen op die gedeeltelijk begrensd worden door een vrij bewegend oppervlak. Het nauwkeurig voorspellen van het gedrag van dergelijke vrije-rand stromingen is daarom van groot belang, bijvoorbeeld, voor het ontwerpen en valideren van omstroomde constructies en vaartuigen. Numerieke methoden spelen een belangrijke rol bij het oplossen van vrije-rand stromingsproblemen. De meeste praktische methoden voor het oplossen van stromingen om een object dat het vrije oppervlak doorsnijdt, zijn gebaseerd op een potentiaal-stroming model. Om vooruitgang te kunnen boeken in de voornoemde technische toepassingen, is het echter noodzakelijk over te gaan op een nauwkeuriger model, namelijk, de Navier–Stokes-vergelijkingen.

Een belangrijke klasse van vrije-rand stromingsproblemen, waarvoor efficiënte numerieke methoden voor de Navier–Stokes-vergelijkingen niet beschikbaar zijn, zijn stationaire vrije-rand stromingen. De huidige rekenmethoden voor de stationaire vrije-rand Navier–Stokes-vergelijkingen vallen in het algemeen terug op een eenvoudige tijdsintegratiemethode. Echter, de efficiëntie van deze methode is vaak slecht, tengevolge van het specifieke tijdsafhankelijke gedrag van vrije-rand stromingen. Er bestaan alternatieve oplosmethoden, maar de prestaties van deze methoden zijn veelal gevoelig voor parameters in het probleem, of de toepasbaarheid is te beperkt. Een onderzoek naar numerieke methoden voor de stationaire vrije-rand Navier–Stokes-vergelijkingen is daarom gerechtvaardigd.

Na het formuleren van het vrije-rand strominsprobleem, presenteren we een analyse van de vrije-rand Navier–Stokes-vergelijkingen in primitieve variabelen, middels storingsrekening en Fourier technieken. Deze analyse geeft inzicht in de karakteristieke eigenschappen van viskeuze vrije-rand stromingen. De resultaten betreffen het optreden van oppervlakte golven en hun dispersief karakter, het asymptotisch tijdsgedrag van golf groepen, en de vorm van de grenslaag bij de vrije rand. Door de formulering in primitieve variabelen kan de analyse bovendien

gebruikt worden voor het valideren van numerieke methoden voor het vrije-rand probleem, als de differentiaaloperatoren worden vervangen door hun differentiebenadering.

We bewijzen dat de gebruikelijke tijdsintegratiemethode in het algemeen inefficiënt is voor het oplossen van stationaire vrije-rand-stromingen bij hoge Reynoldsgetallen, tengevolge van het asymptotisch tijdsgedrag van oppervlakte-golf-groepen en een stabiliteitsrestrictie op de toelaatbare tijdstap. We stellen een nieuwe iteratieve methode voor, die gebaseerd is op een zogenaamde quasi-vrije-randvoorwaarde. Om de efficiëntie van de methode te tonen, bewijzen we dat de rekencomplexiteit onafhankelijk van de maaswijdte is. We tonen numerieke resultaten voor een twee-dimensionaal modelprobleem. Deze resultaten bevestigen de maaswijdte-onafhankelijkheid van het convergentiegedrag. Een vergelijking van de numerieke resultaten met metingen toont een goede overeenstemming.

Vervolgens onderzoeken we het numeriek oplossen van stationaire vrije-randstromingen door middel van de *adjoint-optimal-shape-design* methode. Teneinde een indicatie van de eigenschappen van de methode te krijgen, onderzoeken we de toepassing op de stationaire vrije-rand potentiaalvergelijkingen. De methode kan uitgebreid worden naar de Navier–Stokes-vergelijkingen, maar de details zijn in dat geval veel ingewikkelder. We herformuleren het vrije-randprobleem als een *optimal-shape-design* probleem. Met behulp van storingsrekening en Fourieranalyse tonen we aan dat het *design* probleem de gebruikelijke karakteristieken van stationaire vrije-rand stromingen heeft. We bepalen het asymptotisch convergentiegedrag van de methode. Bovendien tonen we aan dat preconditionering essentieel is om maaswijdte-afhankelijkheid van het convergentie gedrag te vermijden, en presenteren we een preconditionering voor het *optimal-shape-design* probleem. Numerieke resultaten worden gepresenteerd voor een twee-dimensionaal modelprobleem. Het waargenomen convergentiegedrag bevestigt de asymptotische schattingen.

Omdat vrije-rand stromingen een bijzonder geval zijn van twee-fase stromingen, onderzoeken we tenslotte de *interface-capturing*-methode voor het oplossen van twee-fase-stromingen. In de afwezigheid van viscositeit, kunnen twee-fase stromingen beschreven worden door middel van hyperbolische behoudswetten. We beschouwen Godunov's methode voor het discretiseren van hyperbolische systemen. Teneinde de rekenkosten van de flux-evaluaties in de methode te reduceren, construeren we een benaderende Riemann-oplosser van het Osher-type. Details worden gepresenteerd voor fluïda met een barotropische toestandsvergelijking. Tevens behandelen we de druk-oscillaties die in het algemeen optreden in behoudende discretisaties van twee-fase-stromingen. We formuleren een druk-invariantie-voorwaarde. Bovendien presenteren we een oscillatie-vrije, behoudende discretisatie voor twee-fase-stromingen. De implementatie van de *interface-capturing*-methode met efficiënte oplostechnieken voor stationaire hyperbolische systemen wordt uitgesteld tot vervolgonderzoek.

Author Index

Subject Index

Stellingen

bij het proefschrift

"Numerical Methods for Steady Viscous Free-Surface Flows"

door E.H. van Brummelen

1. De gebruikelijke tijdsintegratiemethode is inefficiënt voor het oplossen van stationaire vrije-rand stromingen met hoge Reynoldsgetallen, als stationaire gravitatie golven optreden.

2. De *adjoint-shape-optimization* methode is inefficiënt voor het oplossen van stationaire vrije-rand stromingen, in dezelfde gevallen waarin ook de gebruikelijke tijdsintegratiemethode inefficiënt is.

3. Stationaire vrije-rand stromingen kunnen efficiënt opgelost worden met behulp van quasi vrije-rand voorwaarden.

4. Er bestaan drukoscillatie-vrije, conservatieve discretisaties voor twee-fluïda stromingsproblemen.

5. Exacte wetenschap is een creatief vak.

6. Eén van de belangrijkste bijdragen van de informatietechnologie aan de wetenschap is de eenvoudige hanteerbaarheid van de *copy* en de *paste* functie.

7. Onenigheid is een voorwaarde voor vruchtbare samenwerking

8. Uit het toekennen van subsidies aan kunstenaars op grond van bezoekers aantallen en het toekennen van subsidies aan wetenschappers op grond van aantallen publicaties, blijkt dat subsidieverstrekkende instanties vaak onvoldoende kennis van zaken hebben om inhoudelijke criteria toe te passen.